Aalborg Universitet

AALBORG UNIVERSITY

Coordinated Control and Stability Enhancement of Direct Current Shipboard Microgrids

Jin, Zheming

DOI (link to publication from Publisher):
10.54337/aau301506731

Publication date:
2018

Document Version
Publisher's PDF, also known as Version of record

Link to publication from Aalborg University

Citation for published version (APA):
Jin, Z. (2018). *Coordinated Control and Stability Enhancement of Direct Current Shipboard Microgrids*.
https://doi.org/10.54337/aau301506731

General rights
Copyright and moral rights for the publications made accessible in the public portal are retained by the authors and/or other copyright owners and it is a condition of accessing publications that users recognise and abide by the legal requirements associated with these rights.

- Users may download and print one copy of any publication from the public portal for the purpose of private study or research.
- You may not further distribute the material or use it for any profit-making activity or commercial gain
- You may freely distribute the URL identifying the publication in the public portal -

Take down policy
If you believe that this document breaches copyright please contact us at vbn@aub.aau.dk providing details, and we will remove access to the work immediately and investigate your claim.

Downloaded from vbn.aau.dk on: December 05, 2025

COORDINATED CONTROL AND STABILITY ENHANCEMENT OF DIRECT CURRENT SHIPBOARD MICROGRIDS

BY
ZHEMING JIN

DISSERTATION SUBMITTED 2018

AALBORG UNIVERSITY
DENMARK

COORDINATED CONTROL AND STABILITY ENHANCEMENT OF DIRECT CURRENT SHIPBOARD MICROGRIDS

PH.D. Dissertation

by

Zheming Jin

Department of Energy Technology

Aalborg University, Denmark

AALBORG UNIVERSITY
DENMARK

Dissertation submitted in 2018

.

Dissertation submitted:	September 11th, 2018
PhD supervisor:	Prof. Josep M. Guerrero, Aalborg University
Assistant PhD supervisor:	Associate Prof. Juan C. Vasquez, Aalborg University
PhD committee:	Professor Remus Teodorescu (chairman) Aalborg University
	Prof.Dr. eng. Pavol Bauer Delft University of Technology
	Professor Manuela Sechilariu Université de Technologie de Compiègne (UTC)
PhD Series:	Faculty of Engineering and Science, Aalborg University
Department:	Department of Energy Technology

ISSN (online): 2446-1636
ISBN (online): 978-87-7210-322-8

Published by:
Aalborg University Press
Langagervej 2
DK – 9220 Aalborg Ø
Phone: +45 99407140
aauf@forlag.aau.dk
forlag.aau.dk

© Copyright: Zheming Jin

Printed in Denmark by Rosendahls, 2018

Mandatory page in PhD theses:

1. Thesis title.

Coordinated Control and Stability Enhancement of Direct Current Shipboard Microgrid

2. Name of PhD student.

Zheming Jin

3. Name and title of supervisor and any other supervisors.

Supervisor: Josep M. Guerrero, Professor;

Co-supervisor: Juan C. Vásquez, Associate Professor.

4. List of published papers.

1st Authored Journal Publications:

- Z. Jin, L. Meng, J. M. Guerrero and R. Han, "Hierarchical Control Design for a Shipboard Power System with DC Distribution and Energy Storage Aboard Future More-Electric Ships," in *IEEE Transactions on Industrial Informatics*, vol. 14, no. 2, pp. 703-714, Feb. 2018.
- Z. Jin, G. Sulligoi, R. Cuzner, L. Meng, J. C. Vasquez and J. M. Guerrero, "Next-Generation Shipboard DC Power System: Introduction Smart Grid and dc Microgrid Technologies into Maritime Electrical Networks," in *IEEE Electrification Magazine*, vol. 4, no. 2, pp. 45-57, June 2016.

1st Authored Conference Publications:

- Zheming Jin, M. Savaghebi, J. C. Vasquez, Lexuan Meng and J. M. Guerrero, "Maritime DC microgrids - a combination of microgrid technologies and maritime onboard power system for future ships," *2016 IEEE 8th International Power Electronics and Motion Control Conference (IPEMC-ECCE Asia)*, Hefei, 2016, pp. 179-184.
- Z. Jin, L. Meng, J. C. Vasquez and J. M. Guerrero, "Frequency-division power sharing and hierarchical control design for DC shipboard microgrids with hybrid energy storage systems," *2017 IEEE Applied Power Electronics Conference and Exposition (APEC)*, Tampa, FL, 2017, pp. 3661-3668.
- Z. Jin, L. Meng and J. M. Guerrero, "Comparative admittance-based analysis for different droop control approaches in DC microgrids," *2017 IEEE Second*

International Conference on DC Microgrids (ICDCM), Nuremburg, 2017, pp. 515-522.

- Z. Jin, L. Meng, R. Han, J. M. Guerrero and J. C. Vasquez, "Admittance-type RC-mode droop control to introduce virtual inertia in DC microgrids," *2017 IEEE Energy Conversion Congress and Exposition (ECCE)*, Cincinnati, OH, 2017, pp. 4107-4112.
- Z. Jin, L. Meng and J. M. Guerrero, "Constant power load instability mitigation in DC shipboard power systems using negative series virtual inductor method," *IECON 2017 - 43rd Annual Conference of the IEEE Industrial Electronics Society*, Beijing, 2017, pp. 6789-6794.
- Z. Jin, L. Meng, J. C. Vasquez and J. M. Guerrero, "Specialized hierarchical control strategy for DC distribution based shipboard microgrids: A combination of emerging DC shipboard power systems and microgrid technologies," *IECON 2017 - 43rd Annual Conference of the IEEE Industrial Electronics Society*, Beijing, 2017, pp. 6820-6825.
- Z. Jin and J. M. Guerrero, "Two-degree-of-freedom admittance-type droop control for plug-and-play DC microgrid," *2018 IEEE Applied Power Electronics Conference and Exposition (APEC)*, San Antonio, TX, 2018, pp. 3326-3332.
- Z. Jin, J. M. Guerrero and M. Li, "An Alternative Realization of Droop Control and Virtual Impedance for Paralleled Converters in DC Microgrid," *2018 IEEE Energy Conversion Congress and Exposition (ECCE)*, Portland, OR, 2018.

Selected co-authored Publications:

- M. Nasir, Z. Jin, H. Khan, N. Zaffar, J. Vasquez and J. M. Guerrero, "A Decentralized Control Architecture applied to DC Nanogrid Clusters for Rural Electrification in Developing Regions," in *IEEE Transactions on Power Electronics*. (Early Access)
- S. G. Jayasinghe, L. Meegahapola, N. Fernando, Z. Jin, and J. M. Guerrero. "Review of Ship Microgrids: System Architectures, Storage Technologies and Power Quality Aspects." *Inventions* 2 no. 1 (2017): 4-23.
- M. D. A. Al-Falahi, T. Tarasiuk, S. G. Jayasinghe, Z. Jin, H. Enshaei, and J. M. Guerrero. "AC Ship Microgrids: Control and Power Management Optimization." *Energies* 11 no. 6 (2018): 1458-1478.
- R. Han, H. Wang, Z. Jin, L. Meng and J. M. Guerrero, "Containment-based distributed coordination control to achieve both bounded voltage and precise current sharing in reverse-droop-based DC microgrid," *2017 IEEE Energy Conversion Congress and Exposition (ECCE)*, Cincinnati, OH, 2017, pp. 4121-4127.
- M. Li, Y. Gui, Z. Jin, Y. Guan, and J. M. Guerrero, "A Synchronous-Reference-Frame I-V Droop Control Method for Parallel-Connected Inverters" *2018 IEEE International Power Electronics Conference, IPEC-Niigata 2018-ECCE Asia*, Niigata, 2018.

CV

Zheming Jin received the B.Sc in electrical engineering from Beijing Jiaotong University, China, in 2013, and M.Sc degree in power electrics and drive from Beijing Jiaotong University, China, in 2015.

He is currently working towards his Ph.D. degree in the Department of Energy Technology at Aalborg University, Aalborg East, Denmark. His research interests include power electronics, modeling, control and integration of energy storages in DC Microgrids and electrified transportation.

ENGLISH SUMMARY

In recent years, direct current (DC) distribution technology based solution has become an emerging choice for shipboard power system (SPS), especially for those where electric propulsion is needed. By using DC distribution, the fuel efficiency could be greatly improved by enabling variable-speed operation of diesel engines. At the same time, emerging power sources such as fuel cell and energy storages (e.g. batteries, supercapacitors, flywheels, etc.) can be easily installed. In this context, DC SPS become a perfect example of DC microgrid in the real-world engineering. This project is to introduce and to investigate suitable control methods for DC shipboard microgrid onboard future electric marine vessel.

According to the classification societies' prediction, driven by the ever-stricter emission regulation rules and the deployment of new emission control areas, low-emission power source will play a much more important role in the future ships, nevertheless, conventional diesel engine will still be widely installed. Therefore, the new SPSs will be more complicated which require proper coordinated control strategy for multiple power sources. In addition to that, due to the unique fuel efficiency characteristic of diesel-electric generation, the commonly used droop based proportional power sharing strategy of land-based microgrids may not offer good fuel efficiency. To meet these challenges, a re-designed hierarchical control strategy for DC shipboard microgrid is proposed. In the new proposal, the power sharing of diverse power sources onboard a ship is according to their different characteristic instead of their power rating. On the basis of the proposed power sharing methods, technical solutions to achieve fuel efficiency management and system-level voltage restoration are also discussed, thus forming a comprehensive coordinated control solution for DC shipboard microgrid with improved fuel efficiency.

In addition, the stability of DC distribution system is a huge challenge. Due to the fact that a majority of power generated onboard an electric ship will be consumed by the vessel's propulsion system, the high-power non-linear active load may interact with the controllers of source-side power electronic converters and cause instability issues. Therefore, additional stability analysis and control method is needed. In order to analyze the impact of using different control methods on system stability margin, comparative admittance-based analysis among different voltage control strategies is conducted. The two categories of control methods used: (1) impedance-type control (including the most commonly used dual-loop voltage control and the conventional droop method using virtual impedance loop); (2) admittance-type control (i.e. current-based droop control) are modeled and compared.

Inspired by this modeling work, control methods for enhancing stability of DC shipboard microgrid is proposed. First, a stability enhancement that can be adopted by both dual-loop voltage controller and conventional voltage droop controller is

proposed, in which specially designed negative series virtual inductor (NSVI) is introduced to cancel part of the instinct impedance of the dual-loop voltage controller. With properly designed NSVI, the output impedance of source-side converter can be modified, thus improving its capability feeding high-power nonlinear active load. The design procedure of NSVI is also discussed.

In addition, control method that can improve the performance and stability margin of admittance-type droop controller is also investigated. Due to its different nature compared to impedance-type control method and its inherent convenience to achieve parallel structure, virtual capacitor that connected in parallel to virtual resistor is proposed as a second degree-of-freedom. By adding virtual capacitor accordingly to conventional virtual resistor, the output impedance and the system-level inertia could be modified at the same time. As a result, due to the virtual inertia injection function of the proposed method, both transient response and stability margin of the system can be modified.

To validate the effectiveness and performance of proposed methods, simulations and experiments are carried out using multi-converter DC microgrid setup. The results demonstrate the effectiveness of proposed control methods in real-world applications.

DANSK RESUME

I de senere år er DC-distributionsteknologibaseret løsning blevet et fremtrædende valg til skibsbrændselssystem (SPS), især for dem, hvor der kræves elektrisk fremdrift. Ved at anvende DC-distribution kan brændstofeffektiviteten forbedres betydeligt ved at muliggøre dieselmotorer med variabel hastighed. Samtidig kan nye kraftkilder såsom brændselscelle og energilager (f.eks. Batterier, superkapacitorer, flyhjul osv.) Nemt installeres. I denne sammenhæng bliver DC SPS et perfekt eksempel på DC-mikrogrid i real-world engineering. Dette projekt er at introducere og undersøge passende kontrolmetoder for DC-ombord mikrogrid ombord fremtidige elektriske marinefartøjer.

Ifølge klassifikationsselskabernes forudsigelse, der er drevet af de strengere regler for emissionsregulering og udbredelsen af nye emissionskontrolområder, vil en lavemissions-kraftkilde spille en meget vigtigere rolle i de fremtidige skibe, men konventionel dieselmotor vil ikke desto mindre være bredt installeret. Derfor vil de nye SPS'er være mere komplicerede, hvilket kræver en korrekt koordineret kontrolstrategi for flere strømkilder. Ud over det skyldes den almindeligt anvendte droopbaserede proportional kraftdelingsstrategi for landbaserede mikrogrider på grund af den unikke brændstofeffektivitet, der er karakteristisk for diesel-elektrisk produktion, ikke en god brændstofeffektivitet. For at imødekomme disse udfordringer foreslås en genudformet hierarkisk kontrolstrategi for DC-skibsmikrogrid. I det nye forslag er strømfordeling af forskellige strømkilder ombord på et skib afhængig af deres forskellige karakteristika i stedet for deres effektbedømmelse. På baggrund af de foreslåede effektdelingsmetoder diskuteres også tekniske løsninger til opnåelse af brændstofeffektivitetsstyring og systemniveau spændingsgendannelse, hvilket danner en samlet koordineret kontrolløsning til DC-skibsmikrogrid med forbedret brændstofeffektivitet.

Desuden er stabiliteten af DC distributionssystemet en enorm udfordring. På grund af det faktum, at et flertal af strømmen, der genereres ombord, vil et elektrisk skib forbruges af fartøjets fremdrivningssystem, kan den højeffektive ikke-lineære aktive belastning interagere med controllerne af strømforsyningsomformere i kilden og forårsage ustabilitetsproblemer. Derfor er der behov for yderligere stabilitetsanalyser og kontrolmetoder. For at analysere virkningen af at anvende forskellige kontrolmetoder på systemstabilitetsmarginen udføres sammenlignende adgangsbaseret analyse blandt forskellige spændingsstyringsstrategier. De to kategorier af kontrolmetoder, der anvendes: (1) impedans-type kontrol (inklusiv den mest anvendte dual-loop spændingskontrol og den konventionelle droopmetode ved anvendelse af virtuel impedanssløjfe); (2) indgangstype kontrol (dvs. strømbaseret droop control) modelleres og sammenlignes.

Inspireret af dette modelleringsarbejde foreslås kontrolmetoder til forbedring af stabiliteten af DC-skibsmikrogrid. For det første foreslås en stabilitetsforbedring, der kan vedtages af både dual-loop spændingsstyring og konventionel spændingsdrejningsregulator, hvori specielt konstrueret negativ serie virtuel induktor (NSVI) introduceres for at annullere en del af instinktimpedansen af dual-loop spændingen controller. Med korrekt udformet NSVI kan output-impedansen af kildekonverter konverteres, hvilket forbedrer dets evne til at fodre kraftig, ikke-lineær aktiv belastning. NSVI's designprocedure diskuteres også.

Derudover undersøges også kontrolmetoden, som kan forbedre præstations- og stabilitetsmarginen for adgangsreguleringsmodulet. På grund af sin forskellige natur sammenlignet med impedans-typen kontrolmetode og dens iboende bekvemmelighed for at opnå parallel struktur, foreslås den virtuelle kondensator, der er forbundet parallelt med virtuel modstand, som en anden grad af frihed. Ved at tilføje virtuel kondensator i overensstemmelse hermed til konventionel virtuel modstand, kan outputimpedansen og systemniveau inertien modificeres på samme tid. Som et resultat kan både transient respons og stabilitetsmargin på systemet på grund af den inaktive injektionsfunktion af den foreslåede metode modificeres.

For at validere effektiviteten og ydeevnen af foreslåede metoder udføres simuleringer og eksperimenter ved hjælp af multi-converter DC microgrid setup. Resultaterne viser effektiviteten af foreslåede kontrolmetoder i virkelige applikationer.

ACKNOWLEDGEMENTS

The Ph.D. study, entitled 'Coordinated Control and Stability Enhancement of Direct Current Shipboard Microgrids', is carried out from November 15th, 2015 till November 13th, 2018, under the supervision of Prof. Josep M. Guerrero from the Department of Energy Technology, Aalborg University, Denmark. I would like to thank China Scholarship Council (CSC) for the financial support during my Ph.D. study in Aalborg.

Firstly, I would like to express my appreciation to my supervisor Prof. Josep M. Guerrero and co-supervisor Associate Prof. Juan C. Vasquez. Thanks for providing me such a good chance to conduct Ph.D. study in Aalborg. I would like to express my sincere appreciation to your supervision, encouragements, support, and time spent during my Ph.D. study.

Also, I would give my special thanks to Prof. Pavol Bauer, Dr. Zi'an Qin, and all the DCE&S team members. I really appreciate your help during my studying in Delft University of Technology and my stay in the Netherlands, where I learned a lot of different things from discussion with them.

I would sincerely appreciate the committee members Prof. Remus Teodorescu, Prof. Pavol Bauer, and Prof Manuela Sechilariu. Thanks a lot for paying your time reading my thesis and coming to attend my Ph.D. defense.

To the microgrid team people, Lexuan Meng, Dan Wu, Yajuan Guan, Wei Feng, Baoze Wei, Chi Zhang, Xin Zhao, Bo Sun, Renke Han, Wenzhao Liu, Mingshen Li, Jinghang Lv and all others. It was a pleasure to me to stay with you. It was the fate brought us together. We have been working, talking, joking, partying and traveling together. As a team member, I am always happy to be with you. It was a really joyful research team.

I am also grateful to have colleagues and roommates from other research groups in Aalborg University: Hao Yi, Shunliang Wang, Yilin Ji, Yongheng Yang, Huai Wang, Xiongfei Wang, Dong Liu, Zhijian Yin, Yanfeng Shen, Haoran Wang, Qian Wang, and all, for their help on my study and daily life.

I hope to send my gratitude to all staffs and friends who are with the Department of Energy Technology or were once with us. My time at Aalborg was enjoyable because of your help during the past three years.

Finally, I hope to say "thank you" to my parents Dr. Minghua Zhao and Mr. Xuerun Jin, and all my families. It was your continuous encouragement, unreserved support, and endless love provides me the chance to become who I am today.

It was always rememberable days in this world's happiest city. To all, hope you will smile every day.

Zheming Jin

金哲铭

Aalborg University

Aalborg, Denmark

September 3rd, 2018

TABLE OF CONTENTS

TABLE OF FIGURES

CHAPTER 1. INTRODUCTION

1.1. BACKGROUND AND MOTIVATION

Electrical power has been introduced onboard marine vessels for more than 100 years, from the earliest record of DC arc lighting system in 1880s to the latest all-electric ships [1]-[2]. In 1984, the *Cunard Line* re-equipped the *Queen Elizabeth II* with the new electric propulsion system, which gives an annual fuel saving of 35% and starts the era of modern electric ship [2]. In addition to the fuel saving, electric propulsion also grants new opportunities. In off-shore vessels such as platform supply vessels (PSV) and drilling vessels, dynamic positioning (DP) systems have been widely adopted [3]. The DP system is to control vessel's position on sea surface by combining electric propulsion and sophisticated motion control systems. With its help, several specialized operations are enabled, however, it will also lead to fast-changing load.

On the commercial side, the two most critical issues facing ship owners and builders are the fuel efficiency and the increasingly stricter regulation rules for emissions. According to estimation of *International Maritime Organization* (IMO), in 2012, 2.6% of global greenhouse emission, 15% of nitrogen oxides, and 13% of the sulphur oxides are produced by marine vessels. Therefore, IMO has proposed *MARPOL Annex VI* regulation rules for air pollutant and energy efficiency [4]. Due to these stringent regulation rules, a lot of effort has been made by improving marine engines and, more importantly, introducing new technologies [2], [3].

In 2009, a 330 kW fuel cell system and a 442 kWh battery bank were installed onboard offshore support vessel *Viking Lady* and supply power to the electric propulsion system, thus making it the world's fuel cell powered ship [5], [6]. According to its 18500 hours' operation report, the annual fuel consumption is reduced by 20~30% through smoothing the operation of main engines. In 2015, the world's first fully electric passenger and car ferry, the *MF Ampere* was launched in Norway. It is equipped with battery bank up to 1 MW and is capable of accommodating 120 cars and 360 passengers for a 30-min trip [2], [3].

In 2016, the world's largest classification society *DNV GL* published their vision report for the future application of battery and hybrid power onboard future ships, entitled "the future is hybrid" [7]. At the same time, battery as power source is included in their classification rules for the first time [8]. From their point of view, *DNV GL* proposed that the price of battery has reach the breakthrough point, and, from 2015, they are economically viable to be used for shipboard applications. As a result of this, in the near future, hybrid power system that combines diverse power sources, as illustrated in Figure 1-1 [7], will become the more competitive solution for ship propulsion.

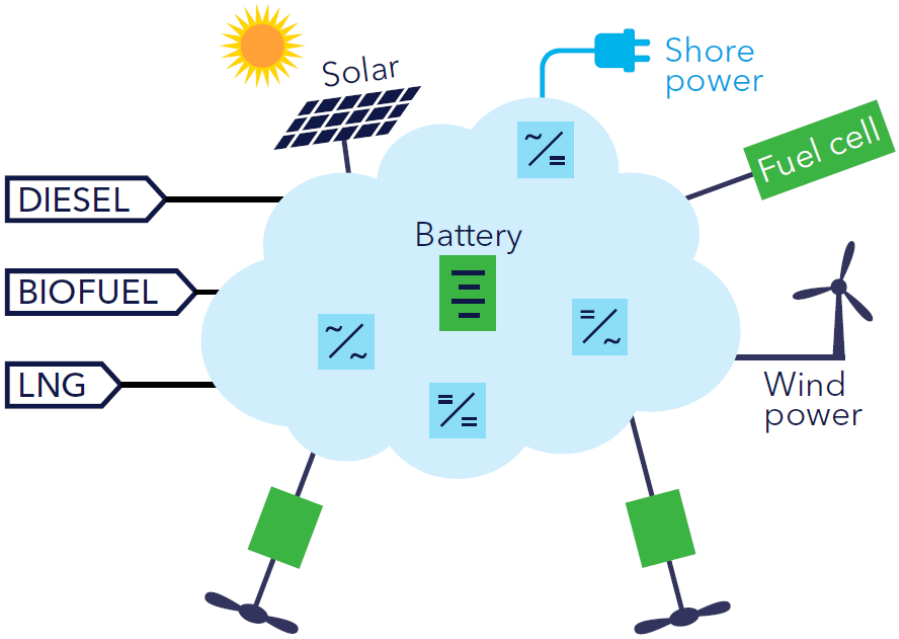

Figure 1-1 Concept Map of Future Ship Power from DNV GL's vision report [7].

1.1.1. SHIPBOARD POWER SYSTEMS AND MICROGRIDS

Microgrids are defined as geographically small power systems capable of operating when connected to, or islanded form, a macro grid (i.e. utility grid) [9]-[12]. When islanded from macro grid, the microgrid is required to maintain its energy independence and availability for an extended time period [13]-[14]. Marine vessel's shipboard power systems are perfect example of this definition. They are physically isolated (i.e. islanded) while at sea, and could become part of a terrestrial grid while docking at berth through shore to ship power connection (i.e. cold ironing equipment).

Technically speaking, shipboard power systems have a lot of common features and challenges with terrestrial microgrids, especially those are operating in stand-alone mode [15]-[19]. In the author's opinion, the most important commonality is that they share the same fundamental challenge, which is the mismatching issue between their power generation and power consumption. On the one hand, terrestrial stand-alone microgrids are focusing on maintain availability and continuity of power supply to its local power consumers, while its power generation are mostly coming from intermittent distributed renewables. On the other hand, shipboard microgrids are equipped with multiple diesel-electric generator sets (i.e. gensets) which are more efficient at certain operating points, while fast and dramatic load changes are inevitable due to the nature of shipboard application.

For abovementioned reason, many of the methods and equipment used are basically same or similar in these two application scenarios. In addition to that, many control strategies and design principles of terrestrial microgrids (e.g. control schemes, power sharing, protective functions, etc.) are possible to be adopted in shipboard power system, or vice versa [2], [3], [15]-[19]. At the same time, some of the major difference need to be taken into consideration, which are summarized as following:

1. *Mission-critical:* It differs from terrestrial microgrids that shipboard microgrids are highly mission-critical. For this reason, the major task of shipboard power system is to "deliver right amount of power to the right place at right time". In order to meet this design philosophy, the shipboard microgrid has high requirement on reliability, survivability and stability.

2. *"Pay-per-use" nature:* In terrestrial microgrids, renewable sources, i.e. solar and wind, could be the major energy source. As a result, the power generation can bring income to the system. However, it is not the case of the state-of-the-art shipboard microgrids, in which power generation results in cost and emission.

3. *Electrical distances:* In terrestrial microgrids, the electrical distance is a considerable issue. It will affect dynamic, voltage regulation and power sharing of the system. But in shipboard microgrids, the electrical distance will be intentionally designed to be short, and, therefore, trivializing the effect. However, the short electrical distance results in low impedance which will increase the coupling between different parts of the power system.

4. *Load profile:* Due to the inevitable uncertainty of sea, the power demand of electric propulsion systems is often rapidly changing. Moreover, the DP systems is mandatory for some certain types of vessels. The recent DP systems can act to ocean current within a second, which means seconds-level fast load changing need to be considered as potential load profile. Such a fast-changing load profile is hardly considered in terrestrial microgrids.

5. *Planning of generation:* In terrestrial microgrids, the power delivered by each generation unit could be scheduled by optimization, such as day-ahead scheduling. However, due to its rapidly changing load profile, load sharing methods (usually droop control method) and on/off control according to predefined look-up table is more frequently used in shipboard microgrids.

6. *System's scale:* Due to the shipboard power system's limited size and extent, a centralized control structure is possible. Hence, it is usually integrated together with the mandatory monitoring system of the vessel's power plant.

1.1.2. ONBOARD ENERGY STORAGE: BATTERY AND OTHER CHOICES

Driven by the tendency of electric vehicles, the performance of batteries, especially lithium-ion batteries, have been greatly improved. For example, in the past five years, batteries have dropped 50% in price and last much longer than what they did five years ago [7]. It is clearly predictable that ongoing and potentially transformative developments are taking place in the battery technology. In the near future, batteries with significantly increased cycle life, power and energy density are expected to be available on the market with lower costs.

Existing onboard battery systems are mostly based on the same or very similar large-format cells as those are used for electric vehicles and hybrid electric vehicles. However, due to the different power level, battery systems used in maritime sector are more related to the MWh-level systems that are designed and installed for utility grid applications [20]-[24], whereas additional safety requirement need to be met.

Although battery system can be optimized to have high energy-storage capacity or high instant power capability, one of the existing problems is that some applications, for example drilling vessel and naval vessel, will require a combination of both high energy and high power, which is currently neither technically easy nor economically efficient to be met by any single kind of battery [25]-[30]. For this reason, other energy storage media with higher power density, such as electrostatic double-layer capacitors (EDLCs or a.k.a. supercapacitors) and high-speed flywheels, have been considered for installation [3], [16], [25]-[33]. Both of them, as energy storage media, are optimized for short-term (including periodical or repetitive cases), power-intensive applications. In addition to that, the flywheel's unique inherent resistance to humid environment is also a noteworthy point due to safety requirement.

Regardless what kind of energy storage media is used, installing onboard energy storage system will always introduce a new degree-of-freedom in the control and management of shipboard power system [19]. It opens new possibility to actively optimize the fuel efficiency and/or emission of the onboard power generation. By cooperative control of onboard energy storage systems and generators, the optimization toward lowest fuel consumption and/or least emission, as well as the need to feed highly dynamic load demands, can be achieved simultaneously. In addition to that, the presence of energy storage also provides new choice for the mandatory reservation of power generation onboard a marine vessel, which is considerable in the ship design process.

1.1.3. AC VERSUS DC

The earliest shipboard power systems were using DC distribution, but it was replaced by AC distribution. One of major reasons for this change was that the early DC

shipboard power systems (without power electronics) had to use rotating devices to make power conversion between different voltage levels, which greatly limited the capability of the whole system. As a result, AC distribution based shipboard power system has been used in an overwhelming number of marine vessels [2], [3].

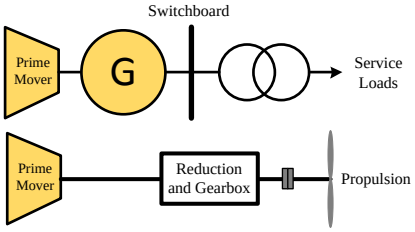

Figure 1-2 Configuration of power system in conventional ships.

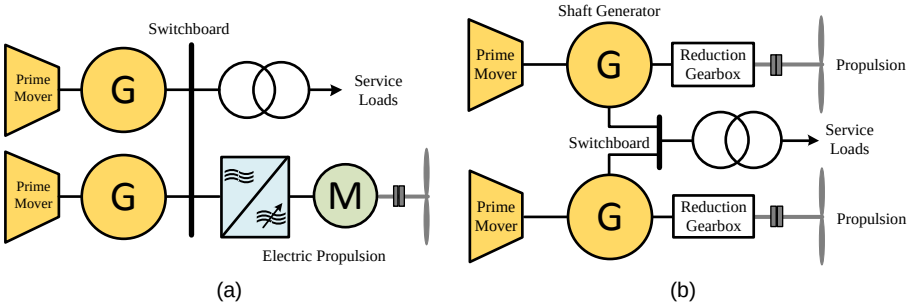

Figure 1-3 Major existing configuration of shipboard power systems using AC distribution. (a) AC integrated power system; (b)shaft generation design.

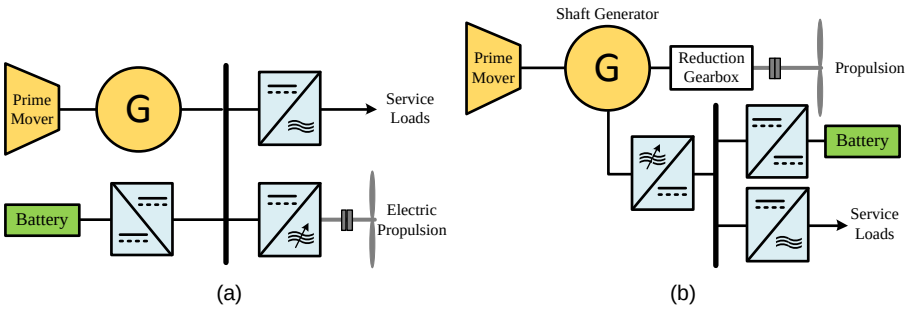

Figure 1-4 Major existing configuration of shipboard power systems using DC distribution. (a) DC integrated power system; (b) paralleled hybrid propulsion.

In the latest decades, with the advantage obtained from the introduction of modern power electronics and electric propulsion systems, DC distribution technology has

been recognized to have several considerable advantages over its more conventional AC counterparts, which are summarized and listed as following [3], [17]-[19]:

1. *Efficiency:* The most important advantage of DC shipboard power system design is its better overall efficiency. For power transmission purpose, using DC means cables do not experience skin effect, which will reduce ohmic resistance and improve the capability of conducting. At the same time, due to the lack of a fundament frequency, only ohmic resistance is needed to be considered, which further reduces the system's transmission losses. For power conversion, DC distribution will have at least same number of front-to-end power conversion stages for pure diesel-electric propulsion power-train and reduced number of power conversion stages for emerging power sources (i.e. fuel cell and battery). As a result, the conversion losses will be reduced.

2. *Variable-speed operation of prime mover:* In conventional AC shipboard power systems, the prime movers are limited to operate at a certain narrow speed range. But in DC systems, as there is no constraint of system frequency or phase angle synchronization, the prime movers are enabled to operates at their optimized speeds independently, thus saving considerable fuel. In addition to that, the lack of system frequency constraint also means higher-speed prime movers, typically the gas turbines, can be easily integrated into the system, which can save space and weight.

3. *Natural elimination of reactive power and harmonics:* In state-of-the-art shipboard applications, because of the wide use of passive rectifier (i.e. diode rectifier) in electric propulsion systems, both reactive power and harmonics are causing huge problem. But in DC systems, due to the lack of system frequency, neither reactive power nor harmonics will cause similar problem as they did in AC systems. It will possibly help saving space and weight (by reducing compensator), improving efficiency, and enhancing quality of service (QoS) indicator.

4. *Plug and play capability:* In DC systems, as there is no need for phase angle synchronization, power sources can be connected into the distribution system much faster and easier, when compared with AC systems. It makes "plug and play" operation much easier. At the same time, this feature also provides better support to power sources with slow dynamics, e.g. fuel cell and gas turbines, thus opening opportunities to exploit their better fuel efficiency. In addition to that, it also makes future upgrade and/or retrofit of the shipboard power system easier.

5. *Space saving and weight reduction:* By using DC distribution, the overall weight and space of the system can be reduced for at least two reasons: (1)

DC system require only two conductors while three conductors are needed in AC system; (2) more compact gen-set design can be allowed, for example, high-speed gas turbine can be coupled with permanent magnetic generator, thus forming a very compact power source.

6. *Efficient integration of energy storage:* When compared with AC systems, energy storage systems do not require additional AC/DC power conversion, which can reduce the size of the system, and providing better energy efficiency that helps reducing the cost of running energy storage systems.

In addition to these general advantages, new technological advances in new power electronics and solid-state protective equipment, especially those developed for medium voltage levels, are solving many of the current issues and challenges of DC shipboard microgrids.

1.1.4. STATE-OF-THE-ART CONTROL SOLUTIONS IN DC SHIPBOARD MICROGRIDS

1.1.4.1 Excitation based control

So far, the most cost-efficient solution for bus voltage regulation of DC shipboard microgrids is the traditional excitation-based control method, in which the current of exciter winding is controlled to regulate the DC bus voltage [34]-[36]. It is similar to the automatic voltage regulator (AVR) that is commonly used in AC power systems. In Figure 1-5, the control scheme is illustrated.

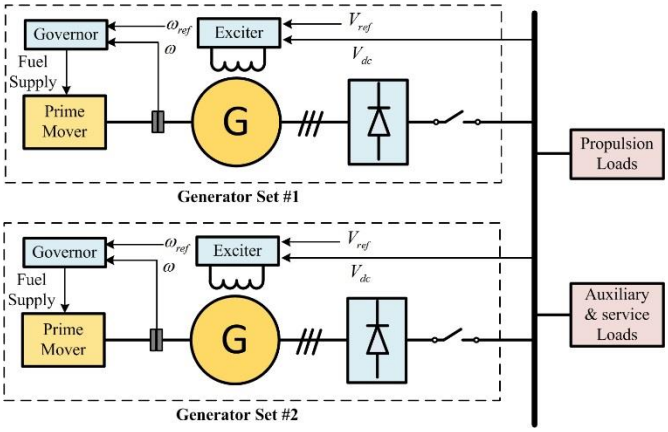

Figure 1-5 Excitation based control scheme [57].

The most important advantage of this control solution, also the major reason for its popularity, is that it requires well-proven synchornous generators (SGs) and simple

diode rectifier to perform voltage control, which will significantly reduce the cost and grant convincing reliability.

The principle of excitation based control scheme is quite simple. In the normal commutation mode operation of diode rectifier, the average value of output current and the DC bus voltage has an approximated linear relationship given as [37]-[39]:

$$V_{dc} = \frac{3\sqrt{3}}{\pi} V_m - \frac{3}{\pi} \omega_e L_{ac} I_{dc} \tag{1.1}$$

where V_m is the peak value of phase voltage, ω_e is the electrical angular speed, L_{ac} is the AC side inductance (i.e. synchronous inductance of SG), I_{dc} is the average value of output current. In the case of using SG, the peak phase voltage V_m is determined by:

$$\begin{cases} V_{qs} = R_{qs} I_{qs} + \omega_e L_{ds} I_{ds} + \omega_e L_m I_f \\ V_{ds} = R_{ds} I_{ds} - \omega_e L_{qs} I_{qs} \end{cases} \tag{1.2}$$

$$V_m = \sqrt{V_{ds}{}^2 + V_{qs}{}^2}\Big|_{I_{ds}=I_{qs}=0} = \omega_e L_m I_f = \omega_e \psi_f$$

where V_{ds}, V_{qs}, I_{ds}, I_{qs}, R_{ds}, R_{qs}, L_{ds}, L_{qs} are the stator voltage, current, resistance and inductance components in d-q reference frame, respectively; L_m is the magnetizing inductance of the SG; I_f is the excitation current; ψ_f is the excitation flux established by exciter.

Therefore, the bus voltage can be controlled by tuning ψ_f in (1.2) to compensate voltage drop shown in (1.1).

Although excitation control scheme is easy to implement in the real-world engineering, its drawbacks are also noteworthy:

1) The control bandwidth of this solution is limited, which is a considerable problem due to the highly dynamic load profiles of marine vessels.
2) The control solution can only be achieved by using SGs, when compared to more compact permanent magnetic generators (PMGs), the weight and volume will be larger.

1.1.4.2 Voltage droop control

Voltage droop control is a commonly used method to coordinate generators and energy storage systems in both terrestrial and shipboard microgrids [35], [40]. The control principle is to add intentional voltage drop in output voltage control of power sources as they are feeding loads. As a result, the steady-state power sharing will be show proportion to the droop coefficient design. In Figure 1-6, a typical droop pattern for DC shipboard microgrid is illustrated.

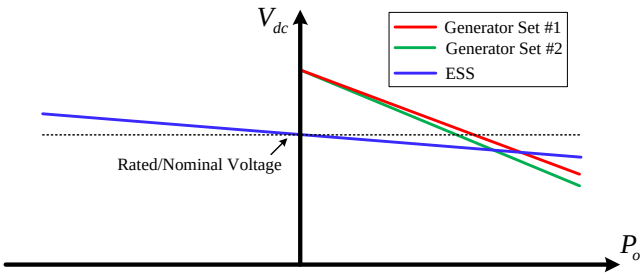

Figure 1-6 A typical voltage droop pattern for DC shipboard microgrid [57].

The major adavantage of adopting droop control is that the improper power sharing caused by measurement error among power sources can be effectively limited and proportional power sharing can be ensured.

However, it is also noteworthy that voltage droop control (for DC distribution) is firstly proposed as adaptive voltage positioning (AVP) technique [41] for modular power supplys for chips and communication devices, therefore, the cost of generation is not taken into consideration. When adopted in a DC shipboard microgrids, the fast-changing load profile of marine vessels will result in frequent change of loading condition of the gen-set, which significantly degrades fuel efficiency. Moreover, the frequent load changing will also result in mechnical issues.

1.1.5. STABILITY ISSUE OF DC SHIPBOARD MICROGRIDS

The constant power load (CPL) instability is a common issue for DC microgrids in both terrestrial [42]-[48] and shipboard applications [49]-[54], it is because of the nature of power electronics that their controllers tend to maintain certain variable in the output side to be constant, regardless changes in the input side. This feature is reported as a major cause of bus voltage instability of DC microgrids.

In DC shipboard microgrids, CPL instability is even more critical than terrestrial microgrids. It is because majority of power generated onboard a ship will be consumed by its propulsion system. The high-power electric propulsion system of electric ships will show strong CPL characteristic, which is a huge treat to the system stability of shipboard microgrid.

1.1.5.1 Mechanism of CPL instability

The voltage-current characteristic of an ideal CPL can be illustrated as shown in Figure 1-7 [59].

The incremental resistance of a constant power load can be presented by:

$$\frac{\partial V_{dc}}{\partial i_{Load}} = \frac{\partial}{\partial i_{Load}}\left(\frac{P_{Load}}{i_{Load}}\right) = -\frac{P_{Load}}{i_{Load}^2} = -\frac{V_{dc}^2}{P_{Load}} = R_{CPL} \tag{1.3}$$

It indicates that the CPLs, although still consuming power, are acting like negative incremental resistance in the system, which will unexpectedly reduce the system damping [41]-[54], [59].

A linearized equivalent circuit of a CPL can be derived from (1.3), which composed by the derived negative resistance and a controlled current source, as shown in Figure 1-8 [59].

In addition to that, the discussion above are satisfied within the control bandwidth of the load converter's control bandwidth. Beyond the control bandwidth, additional higher order impedance characteristic will appear.

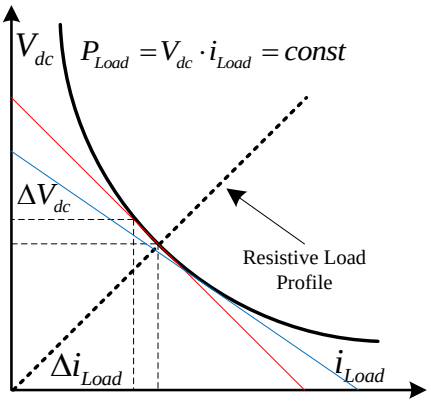

Figure 1-7 Voltage-current characteristic of an ideal constant power load [59].

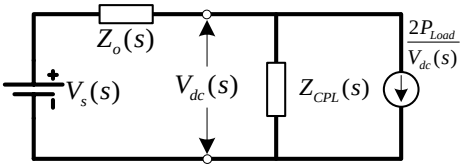

Figure 1-8 Analytical circuit for constant power load instability issue [59].

For the analytical circuit shown in Figure 1-8 [59], the stability of bus voltage will be determined by:

$$\begin{cases} V_{dc}(s) = \dfrac{V_s(s)Z_{CPL}(s)}{Z_o(s)+Z_{CPL}(s)} = V_s(s)T_m(s) \\ T_m(s) = \dfrac{1}{1+Z_o(s)/Z_{CPL}(s)} \end{cases} \tag{1.4}$$

where $V_s(s)$, $Z_o(s)$ and $Z_{CPL}(s)$ stand for source voltage, source-side output impedance and negative impedance of CPLs, all presented by frequency-domain transfer functions. $T_m(s)$ is defined as minor loop gain of the system, which is critical to the system stability analysis.

The sufficient condition of bus voltage stability is that all the dominant poles of $T_m(s)$ locate in the stable region. As an inference of this, the source-side output impedance $Z_o(s)$ shall always have smaller magnitude than the load-side input impedance $Z_{CPL}(s)$, or, at least, $Z_o(s)/Z_o(s)$ fulfill the marginal stable condition.

1.2. THESIS OBJECTIVE

The major idea of the project presented by this thesis is to introduce advanced and proven techniques from terrestrial microgrid research to the shipboard microgrids. In detail, the following specified objectives are considered.

Regarding the coordinated control of DC shipboard microgrids, the following research objectives are defined:

- The first objective is to adopt hierarchical control concept, which is well-proven in terrestrial microgrids, into DC shipboard microgrids.
- The second objective is to propose new control concept that can fully exploit the presence of onboard energy storages. The new proposal is expected to grant modified fuel efficiency.

Regarding the stability issue of DC shipboard microgrids, the following research objectives are defined:

- The first objective is to investigate and to compare the impact of using different control methods, including voltage control and droop control. The output immittance characteristic of each control method will be modeled and analyzed.
- The second objective is to propose stability enhancement methods for the analyzed control methods. The capability of feeding CPL is expected to be modified by applying proposed methods.
- The third objective is to study performance improvement methods aiming at the fast load changes in shipboard microgrids.

1.3. THESIS OUTLINE

The following parts of this thesis are organized as follows:

Chapter 2 presents the paper A in the Appendix. The contributions of this chapter focus on coordinated control solution of DC shipboard microgrid, in which different kinds of power sources (i.e. diesel gen-sets, energy storages, and fuel cells) are involved. The proposed method focuses on achieving characteristic-based power sharing among different kinds of power sources, thus optimizing fuel efficiency of the system under fast-changing load profile. In addition to that, control solutions to achieve individual operational optimization and system-level bus voltage restoration are also introduced, thus forming a re-designed hierarchical control architecture for DC shipboard microgrids.

Chapter 3 presents the paper B in the Appendix. The contributions of this chapter focus on modeling and comparison of different primary-level control solutions used in DC microgrids. The impedance-type control (i.e. conventional voltage/droop control method using dual-loop voltage controller and virtual impedance feedback loop) and admittance-type control (i.e. controllers that realize droop characteristic by its finite gain) are modeled and compared.

Chapter 4 presents the paper C in the Appendix. The contributions of this chapter focus on stability enhancement for impedance-type controllers, in which specially designed negative series virtual inductor (NSVI) is introduced to modify the output impedance of source-side converters. The mechanism and design rules of NSVI are also discussed.

Chapter 5 presents the paper D in the Appendix. The contributions of this chapter focus on improving performance of admittance-type control. In this chapter, RC-mode admittance-type control that introduce paralleled virtual resistor and virtual capacitor is proposed. By adding virtual capacitor, the output impedance will be modified, and, more importantly, the inertial behavior of the system is enhanced, thus providing smoother transient response compared to normal control solutions.

Chapter 6 concludes the contributions of this thesis and the potential future works.

CHAPTER 2. HIERARCHICAL CONTROL DESIGN FOR DC SHIPBOARD MICROGRIDS

In this chapter, a hierarhical control design for DC shipboard microgrids is presented. In the proposed method, power sources onboard the ship are coordinated according to their different characteristic in dynamic and fuel efficiency, thus providing a better fuel efficiency under fast-changing load profile of marine vessel.

2.1. PROPOSED POWER SHARING METHOD

2.1.1. COOPERATIVE INVERSE-DROOP CONTROL

2.1.1.1 Principle of cooperative Inverse-droop control

The control function of conventional voltage droop control method is commonly explained to be introducing virtual resistor to the system, which can be presented by:

$$V_{dc} = V_{ref}^{*} - R_{vr} I_o \tag{2.1}$$

By assuming the voltage drop is relatively small, it can be linearized into a voltage-power equation, which is also widely used as voltage-power droop [40]:

$$V_{dc} = V_{ref}^{*} - mP_o \quad m = R_{vr}/V_{nom} \quad \text{when} \quad V_{dc} \approx V_{nom} \tag{2.2}$$

where R_{vr} is the virtual resistor, I_o is the output current, P_o is the output power, V_{ref}^{*} is the voltage reference, V_{nom} is the nominal voltage, m is named as droop coefficient or power droop coefficient.

These two equations can be also reformulated as:

$$I_o = \frac{1}{R_{vr}}\left(V_{ref}^{*} - V_{dc}\right) \tag{2.3}$$

$$P_o = \frac{1}{m}\left(V_{ref}^{*} - V_{dc}\right) \tag{2.4}$$

These two equations reveal the physical nature of droop control — the power sources are controlled as Thevenin circuit instead of stiff voltage source. Therefore, it becomes possible to coordinate their output power by intentionally controlled voltage deviation, which is defined as inverse-droop control method.

The principle of inverse-droop control method can be defined as following: for a determined amount of output power P_{ref} from droop controlled sources, it will be achieved by intentional controlling the bus voltage according to:

$$V_{dc}^{*}=\frac{1}{2}\left(V_{ref}^{*}+\sqrt{V_{ref}^{*\,2}-4R_{vr}P_{ref}}\right) \tag{2.5}$$

$$V_{dc}^{*}=V_{ref}^{*}-mP_{ref} \tag{2.6}$$

where V_{dc}^{*} is the calculated reference.

For multiple converters, the control function can be re-written as:

$$V_{dc}^{*}=\frac{1}{2}\left(V_{ref}^{*}+\sqrt{V_{ref}^{*\,2}-4R_{eq}P_{ref}}\right)\quad R_{eq}=1\Big/\sum_{i=1}^{n}\left(\frac{1}{R_{vri}}\right) \tag{2.7}$$

$$V_{dc}^{*}=V_{ref}^{*}-m_{eq}P_{ref}\quad m_{eq}=1\Big/\sum_{i=1}^{n}\left(\frac{1}{m_{i}}\right) \tag{2.8}$$

where R_{vri} is the virtual resistor of the ith converter, m_i is the droop coefficient of the ith converter, R_{eq} is the equivalent resistance of the system, m_{eq} is the equivalent power droop coefficient of the system.

2.1.1.2 Advantages of cooperative Inverse-droop control in DC shipboard microgrids

In Figure 2-1 [57], the equivalent circuits of conventional droop method and proposed inverse-droop method are illustrated. The major difference between droop controlled system and inverse-droop controlled system is that inverse-droop controlled system contains a voltage controlled source in addition to the droop controlled sources. For both cases, the power sharing is proportional among all droop controlled sources, but in inverse-droop controlled system, additional asymmetrical power sharing will occur between the voltage controlled source and droop controlled sources.

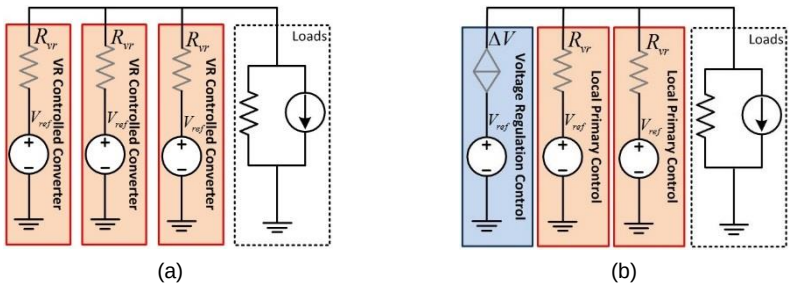

Figure 2-1 Equivalent steady-state circuit of droop and inverse-droop methods: (a) droop method; (b) proposed inverse-droop method [57].

As a result of this asymmetrical power sharing, the voltage controlled source will naturally absorb the load fluctuations, whereas droop controlled sources will work in controlled constant load condition. At the same time, voltage controlled source will automatically perform peak-shaving, and spinning reserve functions. It is noteworthy that these functions are exactly the same with the expected usage of energy storage in the shipboard microgrids. Therefore, the new proposal will be an effective solution to integrate energy storages into DC shipboard microgrids.

In addition to that, as shown in equation (1.1), the diode rectified generators (including both SG and PMG) will show an inherent voltage droop characteristic. This inherent behavior make it possible to use PMGs with simple diode rectifier as power source in the inverse-droop controlled system. In this way, the overall cost and volume of the onboard generating units can be reduced. Moreover, the uncontrollability problem of using diode rectifier can be overcome, thus providing complementary advantages of using controllable and uncontrollable power electronics.

2.1.2. FREQUENCY-DIVISION CONTROL FOR HYBRID ENERGY STORAGE SYSTEM

As mentioned previously, hybrid energy storage system (HESS) that composed by two or more types of energy storage media is a potential solution to meet the twofold requirement on power and energy densities for shipboard applications. But the control and real-time management of HESS will be challenging. To exploit complementary advantage from different storage media, advanced power sharing method that consist with characteristics of different storage media will be mandatory.

The asymmetrical power sharing of proposed inverse-droop control method can be considered as to divide the load profile into two different parts: (1) baseline power that is constant (i.e. $f=0$); (2) fluctuating power that is varying along with the time (i.e. $f>0$). The baseline power is shared among multiple droop controlled sources, whereas the fluctuating power is supplied by the voltage controlled source. As a result, the different characteristic of diesel generation and ESS are respected.

Similarly, the fluctuating power can be also subdivided into two parts, which are low-frequency fluctuation and high-frequency fluctuation. In DC applications, the high-frequency power fluctuation caused by load changes will attenuate rapidly, which means the total energy demand is very low. For this reason, it is efficient to absorb the high-frequency fluctuating power by power-intensive storages (i.e. EDLC and flywheel), while the other part is absorbed by battery. Therefore, power-intensive and energy-intensive storage media can be cooperative in the dynamic power sharing. The subdivision of power fluctuations can be easily implemented by inserting paired low-pass and high-pass filters into the inner-loop controllers, as shown in Figure 2-2 [57]. With the effective frequency-division design, the system can exploit the benefit of HESS without interventions of management-level control.

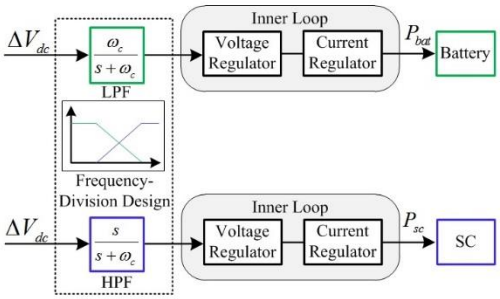

Figure 2-2 Frequency-division design for inverse-droop control with HESS [57].

2.2. HIGHER CONTROL LEVELS

2.2.1. OPERATION POINT MANAGMENT

In shipboard applications, the management of system operation typically includes two different kinds of activities, i.e. managing number of running gen-sets and optimizing operation point of gen-sets. With the presence of batteries in a shipboard microgrid, an effective choice for the on/off control is to act according to state-of-charge (SoC) of battery. Therefore, the discussion of management level control in this thesis is focused on the methods of realizing desired fuel efficiency.

The fuel efficiency of a genset is related to many different variables, including the load torque, engine speed, air temperature, coolant temperature, atmospheric pressure, etc. As an empirical conclusion, in a standard test environment, the optimal fuel efficiency will appear when the output is 80%-90% of the rated torque/load and it will vary according to the engine speed. In this thesis, operational data of a 360 kW diesel engine for power generation purpose is used for evaluation purpose.

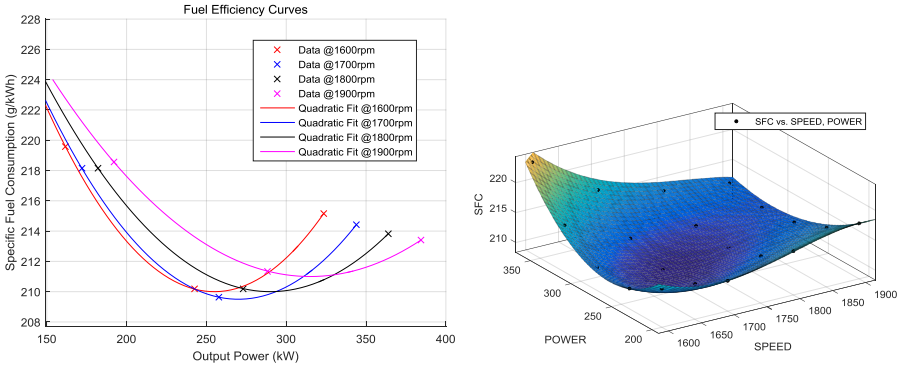

(a) (b)

Figure 2-3 Fuel efficiency model used in this thesis: (a) operational data; (b)specific fuel consumption map [57].

By using the proposed power sharing methods, the bus voltage will be intentionally controlled to coordinate operation of gen-sets. Therefore, the operational point can be selected by introducing an additional adjustable voltage deviation into the no-load voltage reference as secondary adjustment, thus it differentiates the output power of gen-sets. Such control function can be realized by simple PI controller.

2.2.2. SYSTEM-LEVEL BUS VOLTAGE RESTORATION

The system-level bus voltage restoration is referred as the second control layer or secondary control of terrestrial microgrids. However, similar control function has been hardly reported for shipboard microgrids. A major reason is that the equipment is required to tolerate the maximum voltage deviation introduced by primary power sharing control. Yet, this control level will be needed in the operating scenarios like when two zonal microgrids are to be connected (e.g. after DP operation).

To restore the bus voltage to a certain value, a global offset (usually generated by additional PI controller with relatively slow response) is needed to be inject to the original voltage reference. In this case, the power sharing will not be affected, and the optimized operational points of gen-sets are maintained.

Ultimately, the comprehensive control diagram of proposed hierarchical control design is shown in Figure 2-4 [57] and Figure 2-5[57].

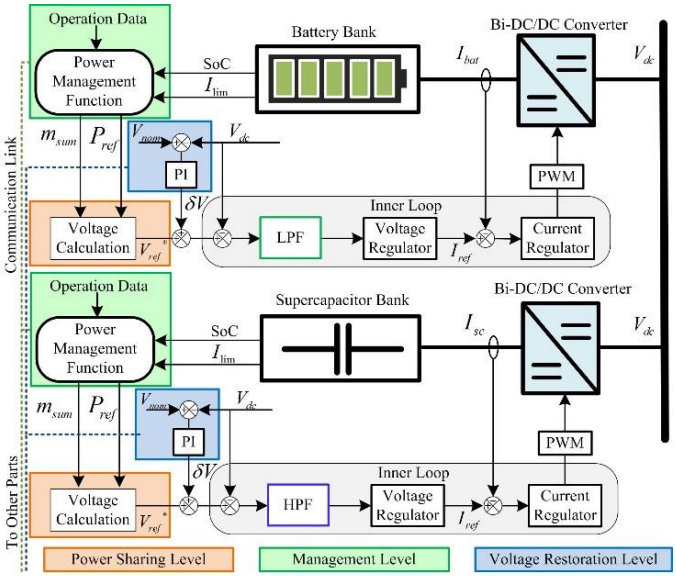

Figure 2-4 Implementation of proposed hierarchical control design in different controllers of HESS [57].

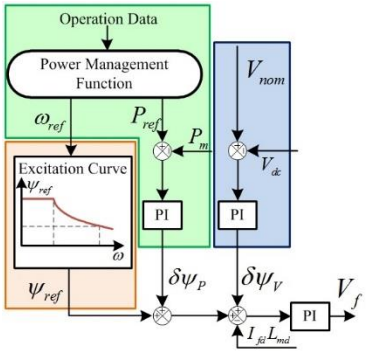

Figure 2-5 Implementation of proposed hierarchical control design in exciters [57].

2.3. SIMULATION VERIFICATION

To validate the methods presented in this paper, real-time simulations in detailed switching level are carried out with Opal-RT real-time simulator. Performance of using conventional droop control and proposed inverse-droop control are compared. The fuel consumption model shown in Figure 2-3 [57] is quantified and used during the simulation to evaluate their fuel consumption.

2.3.1. THE STUDY-CASE SHIPBOARD MICROGRIDS

A notional DC-SPS with the same configuration as shown in Figure 2-6 [57], is used as the study case. The parameters of each component are as shown in Table 2-1 [57], whereas control parameters are shown in Table 2-2 [57].

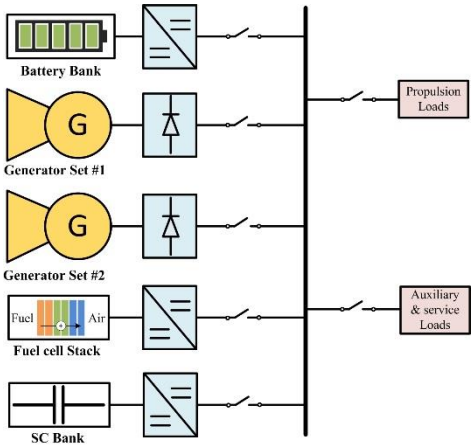

Figure 2-6 Configuration of study-case DC shipboard microgrid [57].

Category	Parameter	Value	Unit
DC Bus	Nominal voltage (range)	1500 (±10%)	V
Gensets	Nominal rotational speed	1800	rpm
	Rated power	330	kW
	Synchronous inductance	0.969	mH
	Rated line voltage (@1800rpm)	1215	Vrms
Battery	Rated capacity	265.2	kWh
	Maximum power (dis-/charge)	390/390	kW
	Switching frequency	1	kHz
SC	Rated capacitance	2200	F
	Rated voltage	288	V
	Maximum capacity	91	MJ
	Switching frequency	10	kHz
FC	Rated power	100	kW
Loads	Rated propulsion power	625	kW
	Auxiliary power	85	kW

Table 2-1 Parameters of the study-case shipboard microgrid [57].

Inner-loop Controllers	Battery voltage controller (P/I)	1/125	-
	Battery current controller (P/I)	0.0015/0.20	-
	SC voltage controller (P/I)	10/1000	-
	SC current controller (P/I)	0.0045/0.20	-
	Cut-off frequency of paired filters	5	Hz
Power Sharing Level	Base voltage	1640	V
	Base rotational speed	1800	rpm
	Base droop coefficient	0.5	V/kW
Management Level	Notional optimal operation point 1	300/1800	kW/rpm
	Notional optimal operation point 2	260/1700	kW/rpm
	Voltage deviation controller (P/I)	0.5/5	-
Voltage Restoration Level	Voltage restoration controller (P/I)	0.1/10	-
ESS Droop Control	Initial voltage reference	1500	V
	Droop coefficient	0.3	V/kW

Table 2-2 Control parameters of the study-case shipboard microgrid [57].

To validate the performance, especially the fuel efficiency of proposed methods, two operating scenarios are set:

(1) The full-load acceleration process, in which the propulsion load increased from 0 to 100%.

(2) The DP process, in which a fast periodical load change is emulated.

2.3.2. SCENARIO 1: FULL-LOAD ACCELERATION PROCESS

This simulation scenario is detailed as follows:

a) ***Stage 1 (0-t_1):*** This stage emulates the grid-forming process of the system. The genset #1 accelerates from idle speed to its rated speed and then connected into system. The bus voltage is regulated by energy storage.
b) ***Stage 2 (t_1-t_2):*** At t_1, genset #1 is connected to supply power and the propulsion load starts increasing to maximum. The proposed inverse-droop control method starts working at the same time, the power reference is set to be 280 kW. In the comparative simulation using conventional droop method, the droop coefficient is designed to load each genset equal to 85% of the rated power, which is also 280kW, at the full propulsion load.
c) ***Stage 3 (t_2-t_3):*** At t_2, the management level is activated, and gradually updating the power reference.
d) ***Stage 4 (t_3-t_4):*** At t_3, the SoC of battery triggers on/off control. Therefore genset #2 accelerates from idle speed and later connected into the system. The management level also optimized the operational point of genset #2 after reaching steady states.
e) ***Stage 5 (t_4-20s):*** At t_4, the proposed voltage restoration level control is activated, the DC bus voltage is gradually restored to its rated value (i.e. 1500V).

In Figure 2-7 [57], the simulation results of using conventional droop control as power sharing method are shown. In Figure 2-8 [57] and Figure 2-9 [57], the results using proposed method with centralized ESS and HESS are presented, respectively.

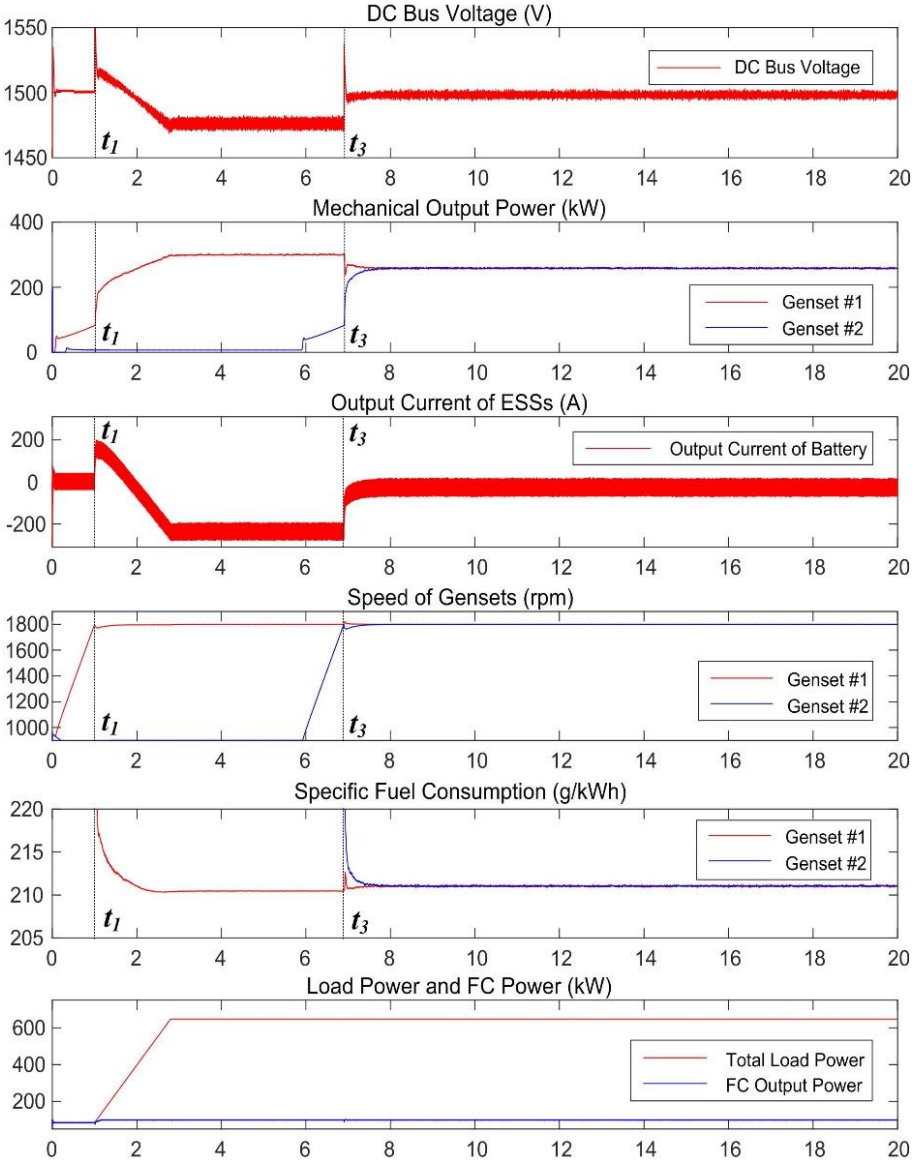

Figure 2-7 Simulation results of scenario 1 using conventional droop control method [57].

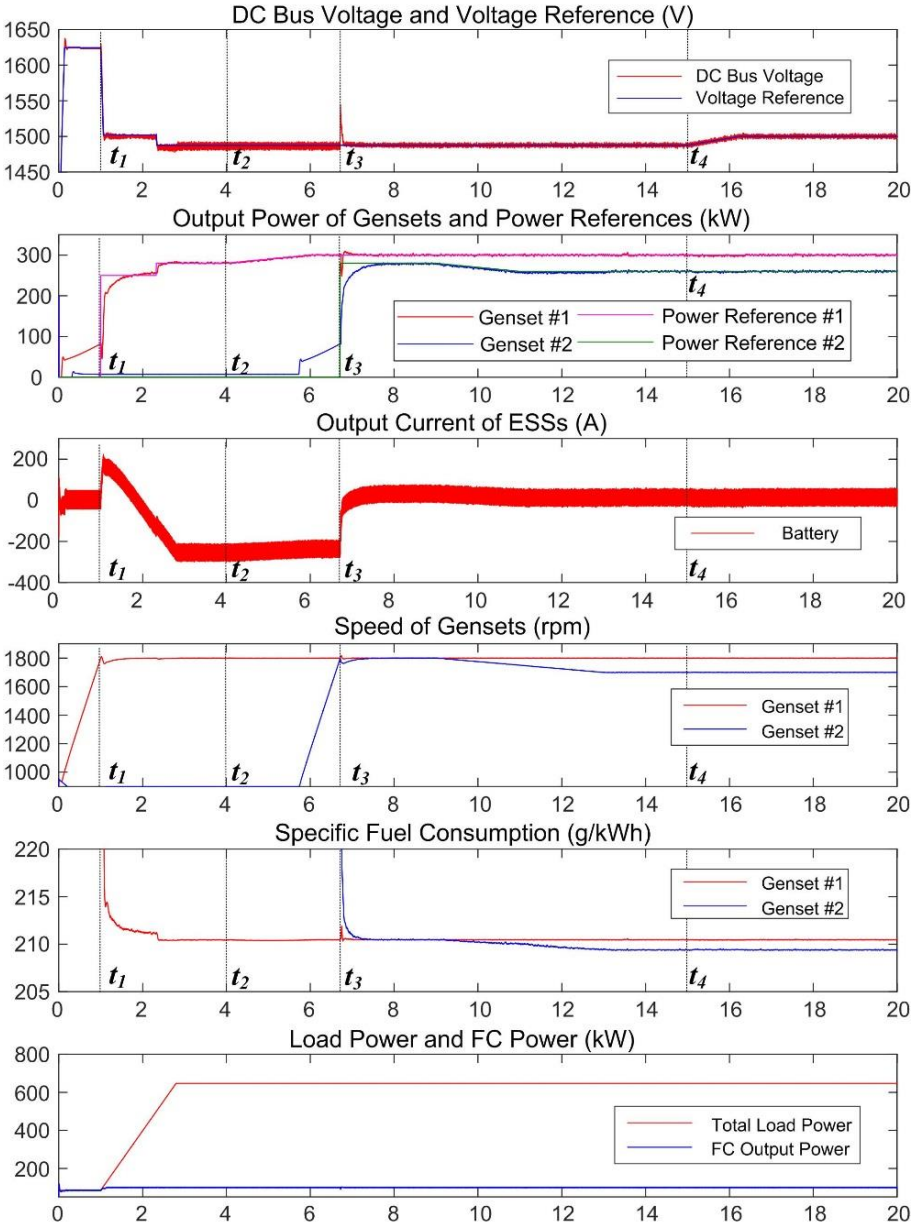

Figure 2-8 Simulation results of scenario 1 using proposed hierarchical control design with centralized ESS [57].

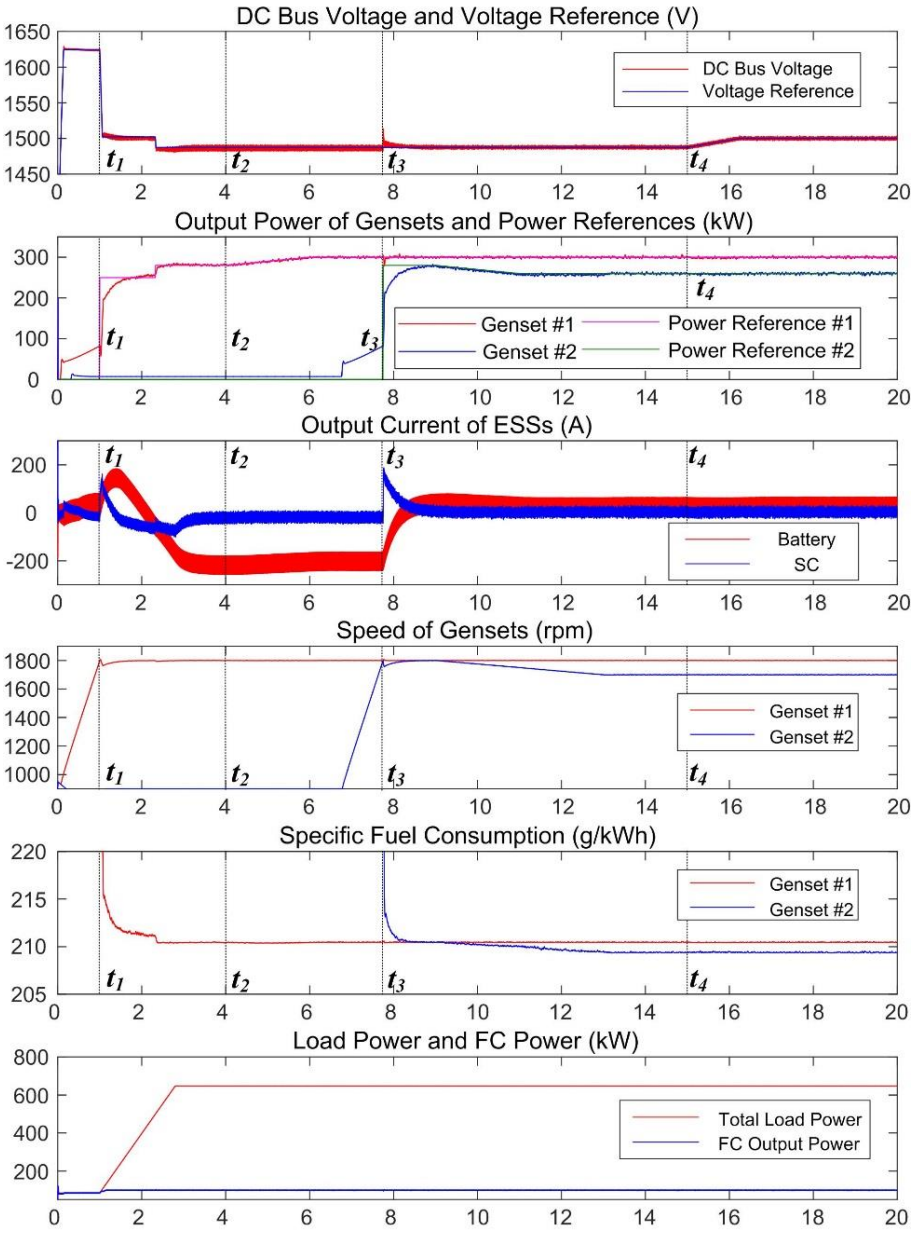

Figure 2-9 Simulation results of scenario 1 using proposed hierarchical control design with HESS and frequency-division method [57].

2.3.3. SCENARIO 2: DP PROCESS

In this simulation scenario, the propulsion load is set to be changing between 25% and 100% periodically, instead of being constant, to emulate the highly dynamic load behavior in a DP process. This simulation scenario is detailed as follows:

a) ***Stage 1 (0-t_1):*** This stage emulates the grid-forming process of the system. The genset #1 accelerates from idle speed to its rated speed and then connected into system. The bus voltage is regulated by energy storage.
b) ***Stage 2 (t_1-t_2):*** At t_1, genset #1 is connected to supply power and the propulsion load starts increasing to maximum. The proposed inverse-droop control method starts working at the same time, the power reference is set to be 280 kW. In the comparative simulation using conventional droop method, the droop coefficient is designed to load each genset equal to 85% of the rated power, which is also 280kW, at the full propulsion load. In this stage, the loads are supplied by genset #1 and ESSs, the peak-shaving function is performed.
c) ***Stage 3 (t_2-t_3):*** At t_2, the management level is activated, and gradually updating the power reference.
d) ***Stage 4 (t_3-t_4):*** At t_3, the on/off management is executed. Genset #2 is connected into the system after acceleration. Afterwards, the management level adjusted its operation point.
e) ***Stage 5 (t_4-20s):*** At t_4, the proposed voltage restoration level control is activated, the DC bus voltage is gradually restored to its rated value (i.e. 1500V).

The simulation results are shown in Figure 2-10 [57], 2-11 [57] and 2-12 [57]. The simulation results show that with proposed method the fuel consumption in dynamic load profile can be reduced and the gensets can work at optimal points continuously.

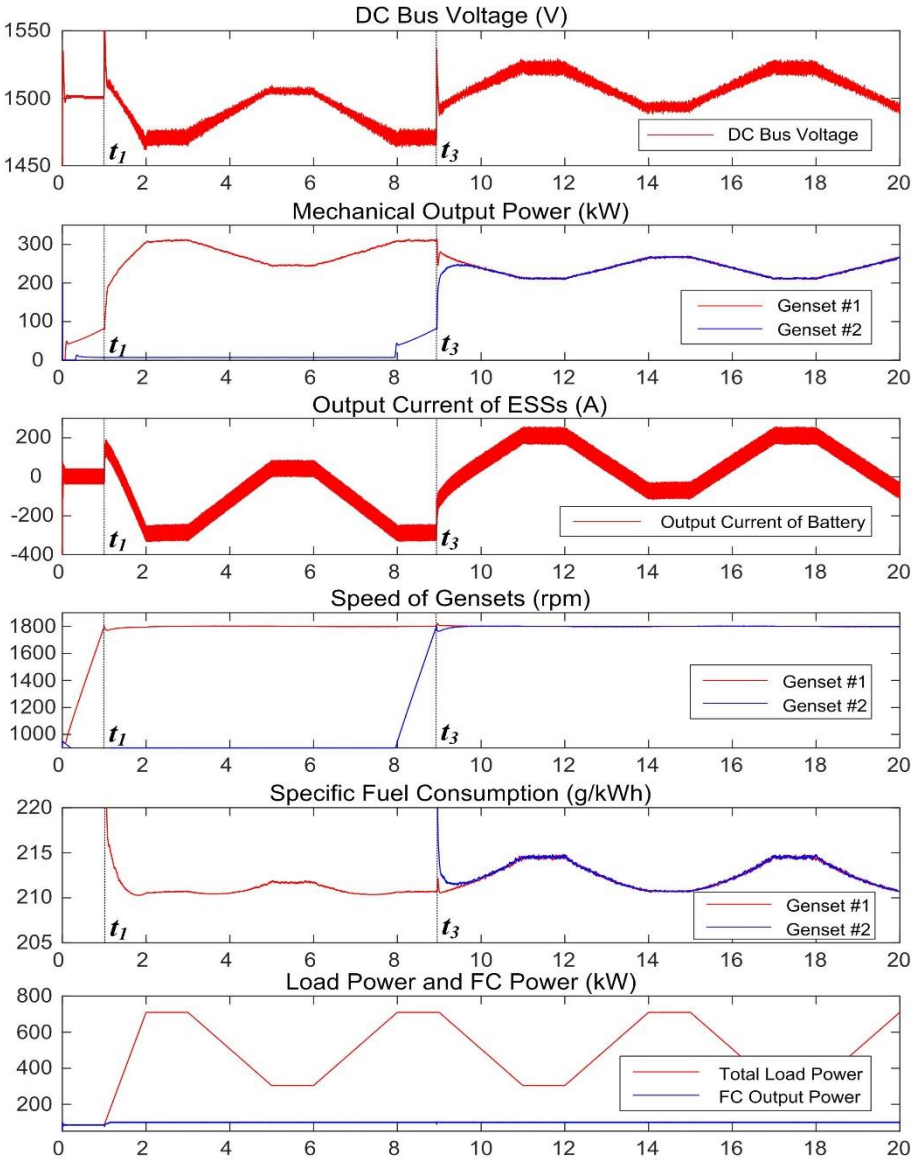

Figure 2-10 Simulation results of scenario 2 using conventional droop control method [57].

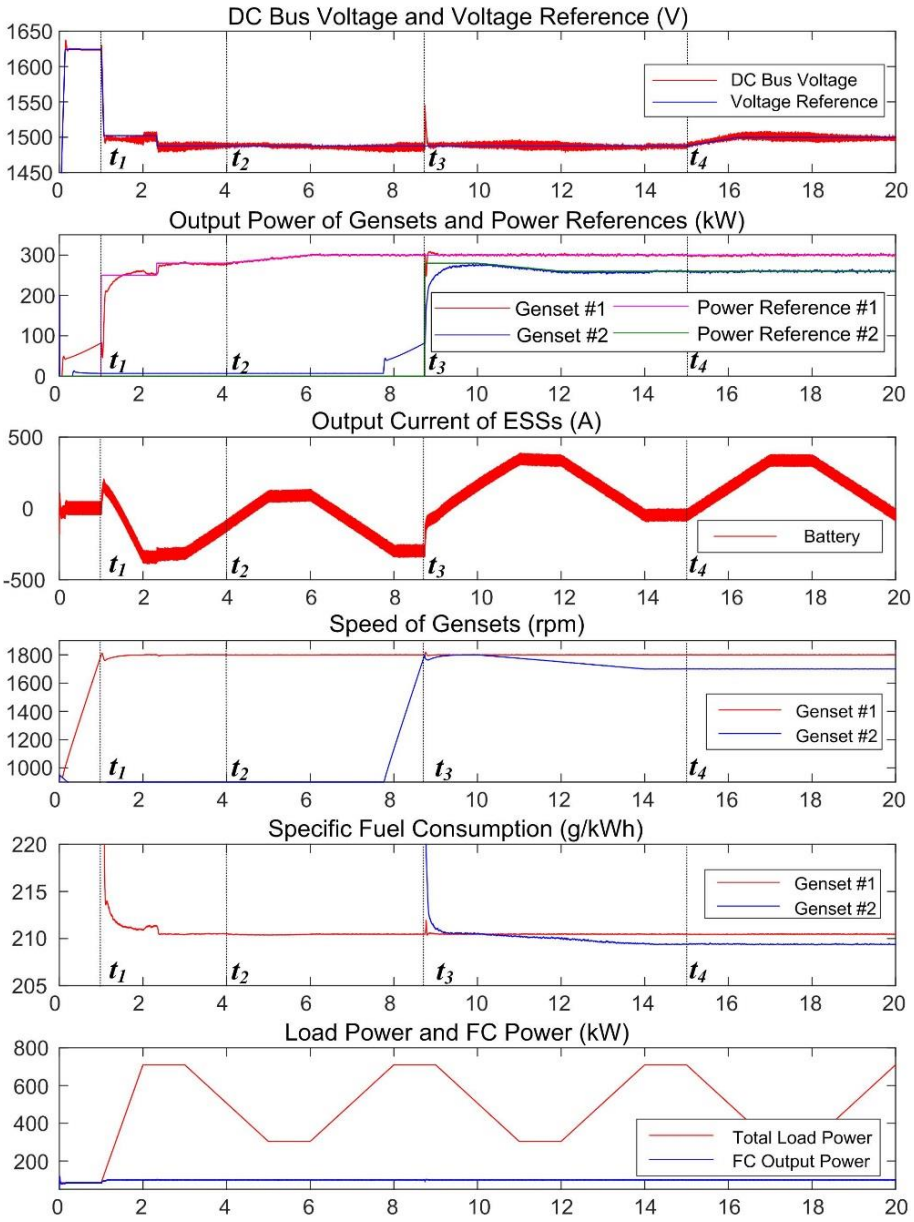

Figure 2-11 Simulation results of scenario 2 using proposed hierarchical control design with centralized ESS [57].

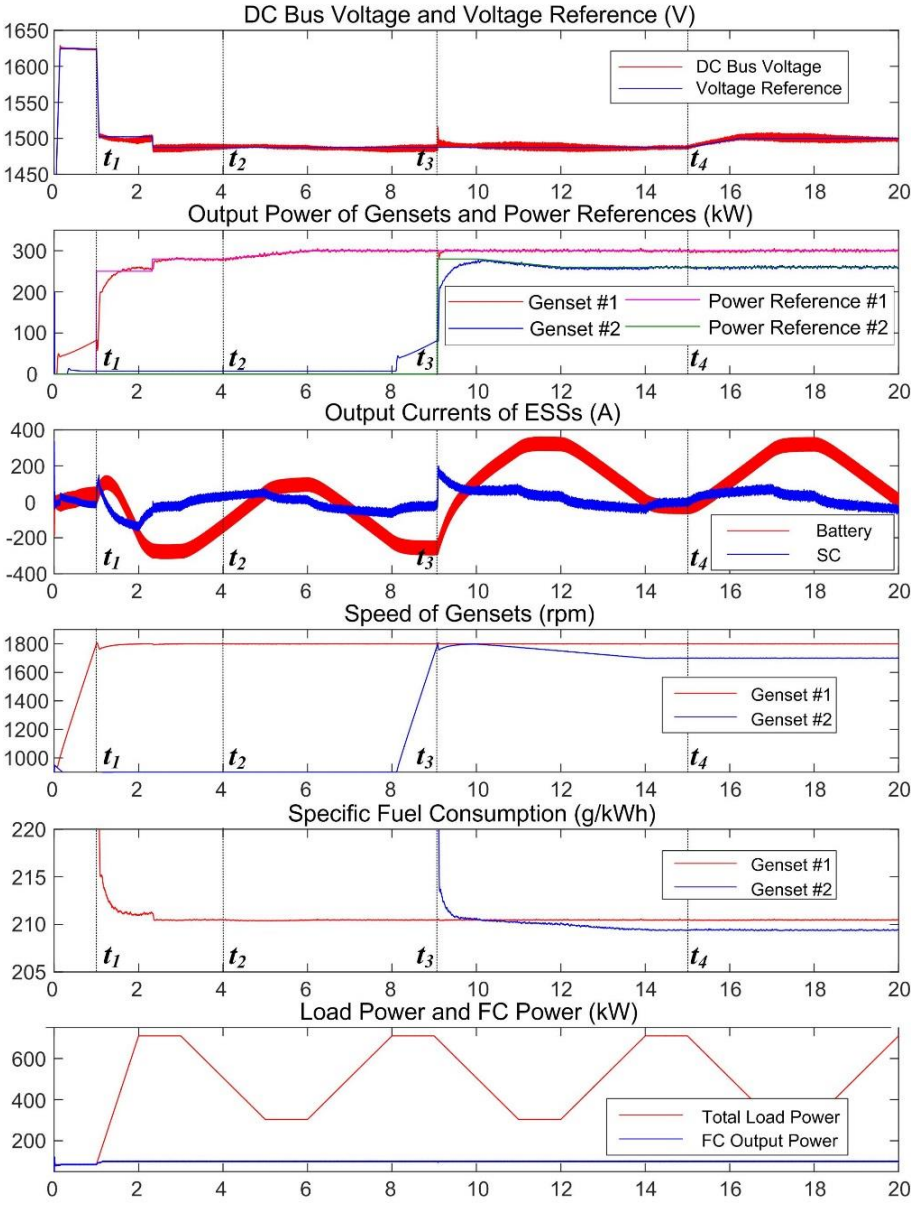

Figure 2-12 Simulation results of scenario 2 using proposed hierarchical control design with HESS and frequency-division method [57].

CHAPTER 3. MODELING, ANALYZING AND COMPARISON OF DIFFERENT DROOP CONTROL REALIZATIONS

In this chapter, the impact of using different control methods on system performance and stability margin is analyzed. In this thesis, the two major categories, which are impedance-type control, (i.e. the conventional dual-loop voltage control and droop control), and admittance-type control (as detailed below), are modeled, analyzed and compared.

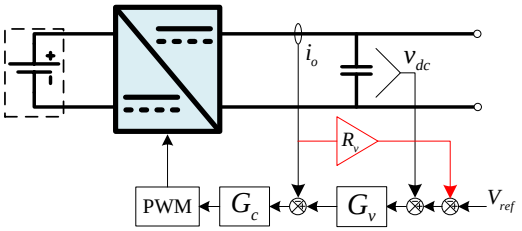

Figure 3-1 Control diagram of impedance-type realization of droop control [58].

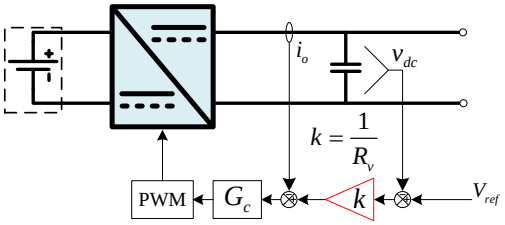

Figure 3-2 Control diagram of admittance-type realization of droop control[58].

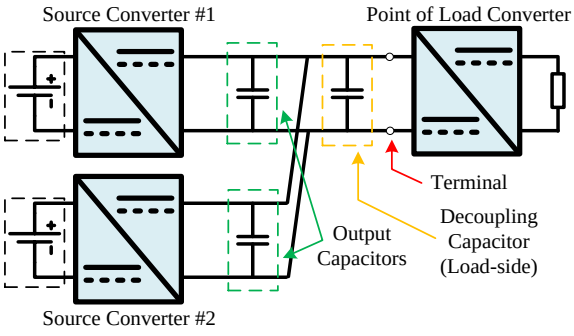

Figure 3-3 The study-case DC microgrid used in this chapter [58].

3.1. SCALABLE STATE-SPACE MODELING

3.1.1. STATE-SPACE BASED MODELING FOR IMPEDANCE-TYPE REALIZATION METHOD

For the *i*-th Buck converters, the increment of the average output current can be described by the differential equations as:

$$\begin{cases} L_i \dfrac{di_{oi}}{dt} = E_i d_i - u - r_i i_{oi} \\ C \dfrac{du}{dt} = \sum i_{oi} - i_{Load} \end{cases} \quad (i \in \{1,2\}) \tag{3.1}$$

where the subscript *i* represents the *i*-th converter, E_i, and d_i are the input voltage and the duty cycle, respectively. L_i, r_i and i_{oi} stands for the inductance, the stray resistance, the average current of the inductor, respectively. C, u, and i_{Load} are the total capacitance connected to the common DC bus, the voltage of common DC bus, and the load current.

When adopting conventional impedance-type controller, the duty cycle d_i is generated according to the following equations:

$$d_i = K_{pci}\left(i_{refi} - i_{oi}\right) + K_{ici}\int_0^t \left(i_{refi} - i_{oi}\right)dt \tag{3.2}$$

$$i_{refi} = K_{pvi}\left(V_{ref} - u - R_{vi} i_{oi}\right) + K_{ivi}\int_0^t \left(V_{ref} - u - R_{vi} i_{oi}\right)dt \tag{3.3}$$

where K_{pci}, K_{pvi} represents the proportional term of current and voltage PI controller, respectively. Similarly, K_{ici} and K_{ivi} are the integral term of current and voltage PI controller. R_{vi} is the virtual resistance of the droop control. V_{ref} is the global no-load voltage reference of the droop control.

Rewrite (3.2) and (3.3) as differential equations:

$$\frac{dd_i}{dt} = K_{pci}\frac{di_{refi}}{dt} - K_{pci}\frac{di_{oi}}{dt} + K_{ici} i_{refi} - K_{ici} i_{oi} \tag{3.4}$$

$$\frac{di_{refi}}{dt} = K_{pvi}\frac{dV_{ref}}{dt} - K_{pvi}\frac{du}{dt} - K_{pvi} R_{vi}\frac{di_{oi}}{dt} + K_{ivi}\left(V_{ref} - u - R_{vi} i_{oi}\right) \tag{3.5}$$

As V_{ref} is a time-invariant parameter, substitute (3.1) into (3.5), the equation will be:

$$\frac{di_{refi}}{dt} = K_{ivi}\left(V_{ref} - u - R_{vi} i_{oi}\right) - K_{pvi}\left(\sum \frac{i_{oi}}{C} - \frac{i_{Load}}{C}\right) - K_{pvi} R_{vi}\left(\frac{E_i}{L_i} d_i - \frac{u}{L_i} - \frac{r_i}{L_i} i_{oi}\right) \tag{3.6}$$

Substitute (3.6) into (3.4), the equation can be rewritten as:

$$\begin{aligned}\frac{dd_i}{dt} &= K_{pci}K_{ivi}\left(V_{ref}-u-R_{vi}i_{oi}\right)-K_{pci}K_{pvi}\left(\sum\frac{i_{oi}}{C}-\frac{i_{Load}}{C}\right)\\ &-\left(K_{pci}K_{pvi}R_{vi}+K_{pci}\right)\left(\frac{E_i}{L_i}d_i-\frac{u}{L_i}-\frac{r_i}{L_i}i_{oi}\right)+K_{ici}i_{refi}-K_{ici}i_{oi}\end{aligned} \tag{3.7}$$

By combining (3.1), (3.6) and (3.7), a scalable state-space model can be derived as following:

$$\dot{\boldsymbol{X}} = \boldsymbol{AX}+\boldsymbol{BU},\quad \boldsymbol{Y}=\boldsymbol{CX}, \tag{3.8}$$

$$\begin{gathered}\boldsymbol{X}=\left[x_1,\cdots,x_n,u\right]^T,\boldsymbol{U}=\left[V_{ref},i_{Load}\right]^T,\boldsymbol{x_i}=\left[i_{oi},i_{refi},d_i\right]\\ \boldsymbol{A}=\begin{bmatrix}\boldsymbol{J_1}&\boldsymbol{M_1}&\cdots&\boldsymbol{M_1}&\boldsymbol{F}_1\\ \boldsymbol{M_2}&\boldsymbol{J_2}&\cdots&\boldsymbol{M_2}&\boldsymbol{F_2}\\ \vdots&\vdots&\ddots&\vdots&\vdots\\ \boldsymbol{M_n}&\boldsymbol{M_n}&\cdots&\boldsymbol{J_n}&\boldsymbol{F_n}\\ \boldsymbol{C_1}&\boldsymbol{C_1}&\cdots&\boldsymbol{C_1}&0\end{bmatrix},\boldsymbol{B}=\begin{bmatrix}\boldsymbol{B_1}\\ \vdots\\ \boldsymbol{B_n}\\ \boldsymbol{C_2}\end{bmatrix},\boldsymbol{C}=\boldsymbol{I}_{(3n+1)\times(3n+1)}\end{gathered} \tag{3.9}$$

$$\begin{gathered}\boldsymbol{J_i}=\begin{bmatrix}-\frac{r_i}{L_i}&0&\frac{E_i}{L_i}\\ j_{i1}&0&\frac{K_{pvi}R_{vi}E_i}{L_i}\\ j_{i2}&K_{ici}&j_{i3}\end{bmatrix},\boldsymbol{M_i}=\begin{bmatrix}0&0&0\\ -\frac{K_{pvi}}{C}&0&0\\ -\frac{K_{pvi}K_{pci}}{C}&0&0\end{bmatrix},\\ \boldsymbol{F_i}=\begin{bmatrix}-\frac{1}{L_i}\\ f_{i1}\\ f_{i2}\end{bmatrix},\begin{matrix}\boldsymbol{C_1}=\left[\frac{1}{C},0,0\right]\\ \boldsymbol{C_2}=\left[0,-\frac{1}{C}\right]\end{matrix},\boldsymbol{B_i}=\begin{bmatrix}0&0\\ K_{ivi}&\frac{K_{pvi}}{C}\\ K_{pci}K_{ivi}&\frac{K_{pci}K_{pvi}}{C}\end{bmatrix}\end{gathered} \tag{3.10}$$

$$\begin{cases}j_{i1}=\dfrac{K_{pvi}R_{vi}r_i}{L_i}-\dfrac{K_{pvi}}{C}-K_{ivi}R_{vi},\\ j_{i2}=\dfrac{K_{pci}r_i\left(K_{pvi}R_{vi}+1\right)}{L_i}-\dfrac{K_{pci}K_{pvi}}{C}-K_{ici}-K_{pci}K_{ivi}R_{vi},\\ j_{i3}=-\dfrac{K_{pci}E_i(K_{pvi}R_{vi}+1)}{L_i},\end{cases}\begin{cases}f_{i1}=\dfrac{K_{pvi}R_{vi}}{L_i}-K_{ivi},\\ f_{i2}=\dfrac{K_{pci}\left(K_{pvi}R_{vi}+1\right)}{L_i}-K_{pci}K_{ivi},\end{cases} \tag{3.11}$$

where the component matrix $\boldsymbol{M_i}$ is related to coupling effect among paralleled converters, component matrix $\boldsymbol{J_i}$, $\boldsymbol{F_i}$, $\boldsymbol{B_i}$, $\boldsymbol{C_i}$ are related to the internal control.

3.1.2. STATE-SPACE BASED MODELING FOR ADMITTANCE-TYPE REALIZATION METHOD

When adopting admittance-type realization method, the output current of the *i*-th converters will follow the same equation as shown in (3.1). However, the current reference i_{refi} and the duty cycle d_i will be calculated by the following equations:

$$i_{refi} = k_i \left(V_{ref} - u \right) \tag{3.12}$$

$$d_i = K_{pci} \left(k_i V_{ref} - k_i u - i_{oi} \right) + K_{ici} \int_0^t \left(k_i V_{ref} - k_i u - i_{oi} \right) dt \tag{3.13}$$

$$\begin{cases} \dfrac{di_{refi}}{dt} = -k_i \dfrac{du}{dt} = k_i \dfrac{i_{Load}}{C} - k_i \sum \dfrac{i_{oi}}{C} \\ \dfrac{dd_i}{dt} = K_{ici} \left(k_i V_{ref} - k_i u - i_{oi} \right) + K_{pci} k_i \left(\dfrac{i_{Load}}{C} - \sum \dfrac{i_{oi}}{C} \right) - K_{pci} \left(\dfrac{E_i}{L_i} d_i - \dfrac{u}{L_i} - \dfrac{r_i}{L_i} i_{oi} \right) \end{cases} \tag{3.14}$$

where k_i=1/ R_{vi}, which represents conductance of the virtual resistor.

As a result, a new set of component matrixes can be obtained that can be used directly in the abovementioned scalable state-space model:

$$\begin{aligned} \boldsymbol{J}_i' &= \begin{bmatrix} -\dfrac{r_i}{L_i} & 0 & \dfrac{E_i}{L_i} \\ -\dfrac{k_i}{C} & 0 & 0 \\ j_i' & 0 & -\dfrac{K_{pci} E_i}{L_i} \end{bmatrix}, \boldsymbol{M}_i' = \begin{bmatrix} 0 & 0 & 0 \\ -\dfrac{k_i}{C} & 0 & 0 \\ -\dfrac{k_i K_{pci}}{C} & 0 & 0 \end{bmatrix}, \\ \boldsymbol{F}_i' &= \begin{bmatrix} -\dfrac{1}{L_i} \\ 0 \\ \dfrac{K_{pci}}{L_i} - k_i K_{ici} \end{bmatrix}, \begin{matrix} \boldsymbol{C_1} = \left[\dfrac{1}{C}, 0, 0 \right] \\ \boldsymbol{C_2} = \left[0, -\dfrac{1}{C} \right] \end{matrix}, \boldsymbol{B}_i' = \begin{bmatrix} 0 & 0 \\ 0 & \dfrac{k_i}{C} \\ k_i K_{ici} & \dfrac{k_i K_{pci}}{C} \end{bmatrix} \\ j_i' &= \frac{K_{pci} r_i}{L_i} - \frac{k_i K_{pci}}{C} - K_{ici} \end{aligned} \tag{3.15}$$

In addition to that, by correctly arranging component matrixes shown in (3.10) and (3.15), the proposed state-space model can also be used to describe dynamic behavior of DC microgrids controlled by a mixed combination of impedance-type controllers and admittance-type controllers.

3.1.3. SIMULATION VERIFICATION OF PROPOSED MODEL

To validate the derived state-space models, simulations of abovementioned study case are carried out using PLECS. In Figure 3-4 [58], the simulation results of two impedance-type controller are adopted, whereas the simulation results of admittance-type control are shown in Figure 3-5 [58].

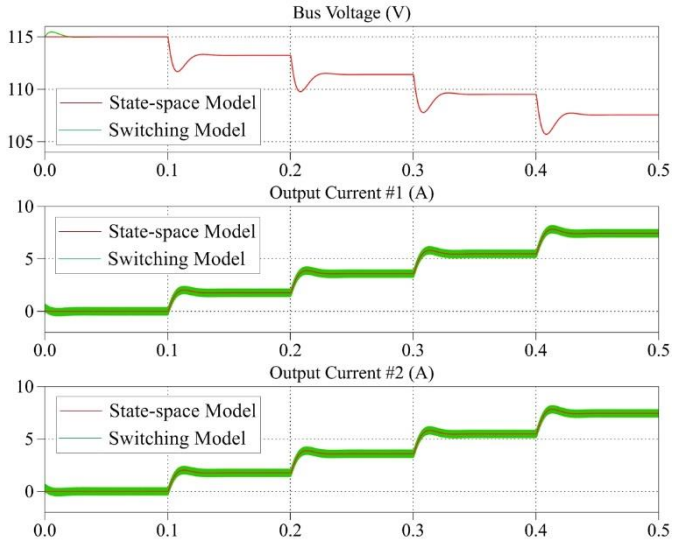

Figure 3-4 Simulation results of impedance-type controlled case [58].

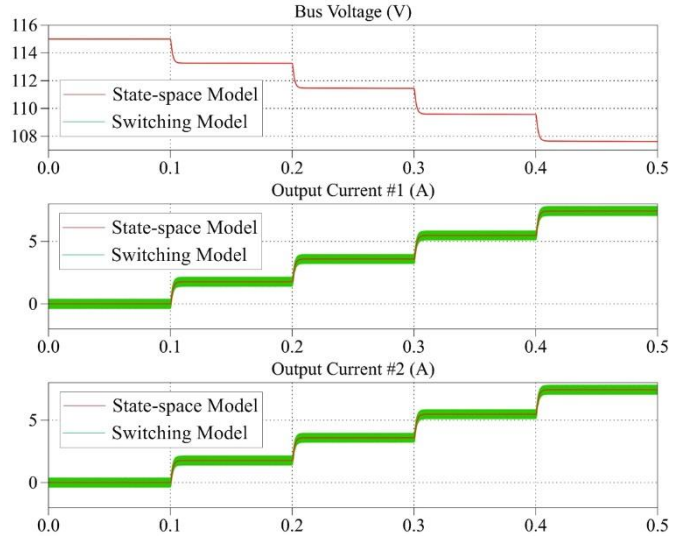

Figure 3-5 Simulation results of admittance-type controlled case [58].

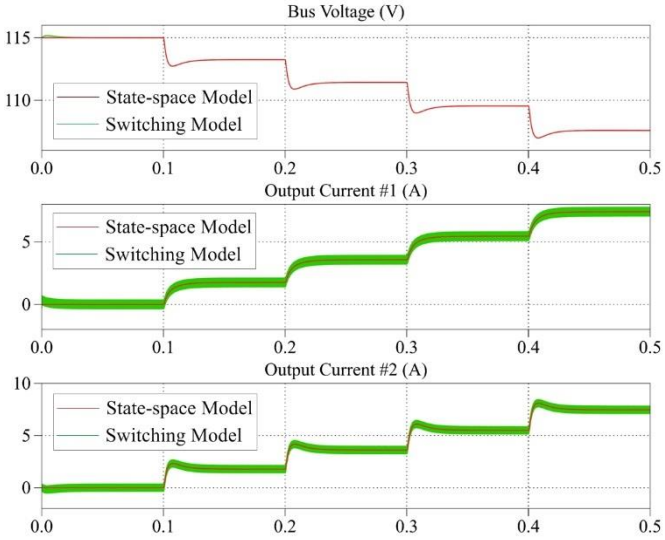

Figure 3-6 Simulation results of mixed case: converter #1 is controlled by impedance-type controller, converter#2 is controlled by admittance-type controller [58].

In addition to that, in Figure 3-6 [58], simulation results of the mixed combination of impedance-type controllers and admittance-type controllers is presented.

All of the simulation results above show that the derived scalable state-space model is sufficiently accurate to describe the dynamic behavior of a DC microgrid with any combination of different types of droop controllers

3.2. ADMITTANCE BASED ANALYSIS

3.2.1. DERIVING OUTPUT ADMITTANCE FROM STATE-SPACE MODEL

According to the Thévenin's theorem, the output admittance of a source converter can be calculated by:

$$Y_{eq}(s) = \frac{I(s)}{V_{oc} - u(s)} = \frac{I_o(s) - I_c(s)}{V_{oc} - u(s)} = sC + \frac{\Delta I_o(s)}{-\Delta u(s)} \tag{3.16}$$

where $I(s)$, $I_o(s)$, $I_c(s)$ and $u(s)$ are the output current to the distribution lines, output current before filter (i.e. inductor current of Buck converter), capacitor current and the terminal voltage; V_{oc} is the open-circuit voltage, which equals to the global no-load voltage reference.

By using the proposed state-space model, the last term can be derived by:

$$\boldsymbol{G}=\begin{bmatrix} G_{i_{o1}ref}(s) & G_{i_{o1}Load}(s) \\ G_{i_{ref\,1}ref}(s) & G_{i_{ref\,1}Load}(s) \\ G_{d_1ref}(s) & G_{d_1Load}(s) \\ G_{i_{o2}ref}(s) & G_{i_{o2}Load}(s) \\ G_{i_{ref\,2}ref}(s) & G_{i_{ref\,2}Load}(s) \\ G_{d_2ref}(s) & G_{d_2Load}(s) \\ G_{uref}(s) & G_{uLoad}(s) \end{bmatrix}=\boldsymbol{C}(s\boldsymbol{I}-\boldsymbol{A})^{-1}\boldsymbol{B} \tag{3.17}$$

$$\frac{\Delta I_o(s)}{\Delta u(s)}=\frac{G_{i_{o1}ref}(s)\Delta V_{ref}(s)+G_{i_{o1}Load}(s)\Delta I_{Load}(s)+G_{i_{o2}ref}(s)\Delta V_{ref}(s)+G_{i_{o2}Load}(s)\Delta I_{Load}(s)}{G_{uref}(s)\Delta V_{ref}(s)+G_{uLoad}(s)\Delta I_{Load}(s)} \tag{3.18}$$

In (3.18), the open-circuit voltage reference V_{ref} is a constant while talking only about droop control, therefore the equation can be simplified as:

$$\frac{\Delta I_o(s)}{\Delta u(s)}=\frac{G_{i_{o1}Load}(s)+G_{i_{o2}Load}(s)}{G_{uLoad}(s)} \tag{3.19}$$

To validate this conclusion, the source-side output admittance is measured using the impedance analyzing function of PLECS. In Figure 3-7 [58], the measured output admittance and derived admittance from state-space model are compared.

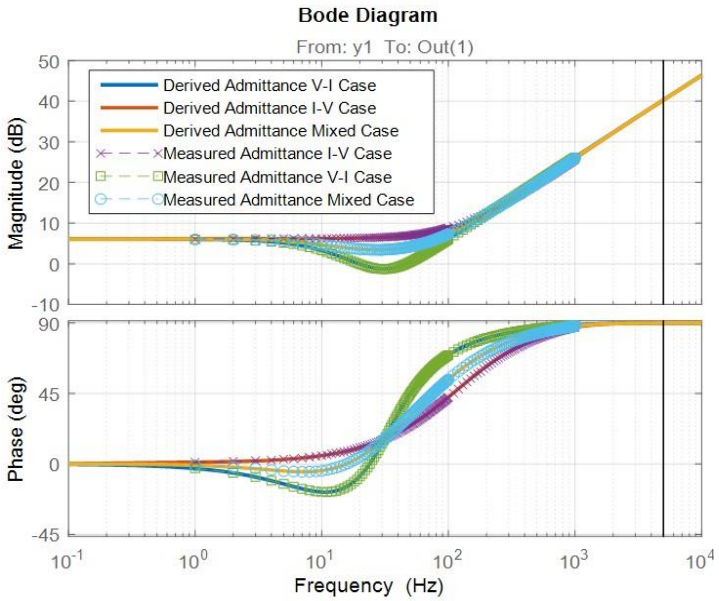

Figure 3-7 Output admittance measured by PLECS and derived from state-space model [58].

3.2.2. GENERALIZED ANALYTICAL MODEL AND EQUIVALENT CIRCUIT

To analyze the behavior of dual-loop controllers, the inner current loop is commonly simplified as a first order delay with control bandwidth ω_{clc}. By applying this assumption, the control behavior and output admittance of an impedance-type controller can be described by:

$$I_o^{V-I}(s) = \frac{G_v(s)G_{clc}(s)}{1+R_vG_v(s)G_{clc}(s)}\left[V_{ref}(s)-u(s)\right] \tag{3.20}$$

$$Y_o^{V-I}(s) = \frac{I_o^{V-I}(s)}{V_{ref}(s)-u(s)} + sC = Y_{conv}{}^{V-I}(s) + sC \tag{3.21}$$

where $G_v(s)$ is the transfer function of voltage controller, $G_{clc}(s)$ is the close-loop transfer function of the whole current loop. The superscripts are to differentiate the droop modes.

Similarly, the control behavior and output admittance of an admittance-type controller can be described by:

$$I_o^{I-V}(s) = \frac{G_{clc}(s)}{R_v}\left[V_{ref}(s)-u(s)\right] \tag{3.22}$$

$$Y_o^{I-V}(s) = \frac{I_o^{I-V}(s)}{V_{ref}(s)-u(s)} + sC = Y_{conv}{}^{I-V}(s) + sC \tag{3.23}$$

For analytical purpose, the component derived by control behavior can be defined as intrinsic admittance of the converter. Substitute parameters into (3.21) and (3.23), equivalent circuit of the converter can be derived to be as shown in Figure 3-8 [58], where the value of these components can be found in (3.24).

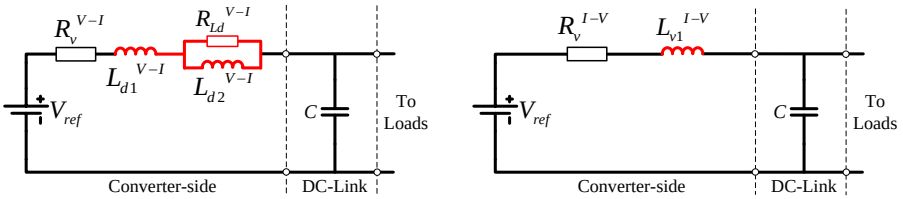

Figure 3-8 Derived equivalent circuit for droop controllers: (a) impedance-type controller; (b) admittance-type controller [58].

$$\begin{cases} R_v^{V-I} = R_{vi} \\ L_{d1}^{V-I} = \dfrac{1}{K_{pvi}\omega_{clc}} \\ L_{d2}^{V-I} = \dfrac{\omega_{clc} - K_{ivi}/K_{pvi}}{K_{ivi}\omega_{clc}} \\ R_{Ld}^{V-I} = \dfrac{\omega_{clc} - K_{ivi}/K_{pvi}}{K_{pvi}\omega_{clc}} \end{cases} \qquad \begin{cases} R_v^{I-V} = R_{vi} \\ L_{v1}^{I-V} = \dfrac{R_{vi}}{\omega_{clc}} \end{cases} \tag{3.24}$$

3.3. IMPACT OF USING DIFFERENT REALIZATION ON STABILITY MARGIN OF THE SYSTEM

3.3.1. ADMITTANCE FEATURE OF DIFFERENT REALIZATION

It can be derived from (3.22) and (3.24), the intrinsic admittance and its impedance counterpart can be derived as:

$$\begin{cases} Y_{conv}^{V-I}(s) = \dfrac{G_v(s)G_{clc}(s)}{1 + R_v G_v(s) G_{clc}(s)} \\ Z_{conv}^{V-I}(s) = \dfrac{1}{Y_{conv}^{V-I}(s)} = R_v + \dfrac{1}{G_v(s)G_{clc}(s)} \end{cases} \tag{3.25}$$

$$\begin{cases} Y_{conv}^{I-V}(s) = \dfrac{1}{R_v}\dfrac{\omega_{clc}}{s + \omega_{clc}} \\ Z_{conv}^{I-V}(s) = \dfrac{1}{Y_{conv}^{I-V}(s)} = R_v + s\dfrac{R_v}{\omega_{clc}} \end{cases} \tag{3.26}$$

These equation reveals the different feature of the intrinsic admittance introduced by controller behavior. For impedance-type control, the major term will not be related to the droop design or virtual resistor, whereas both terms are involved in admittance-type control.

3.3.2. IMPACT OF DIFFERENT REALIZATION ON STABILITY MARGIN

According to the immittance-based stability analysis and its stability criterion, the stability margin of the system is strongly related to the maximum magnitude of the source-side output impedance, which is also the minimum magnitude of the source-side output admittance.

In Figure 3-9 [58] and 3-10 [58], the output admittance of virtual resistor design from 0.2Ω to 4Ω for both realization methods are illustrated. By comparing them, it can be

seen that impedance-type controller will have worse stability margin than admittance-type controller along with the reduction of virtual resistor.

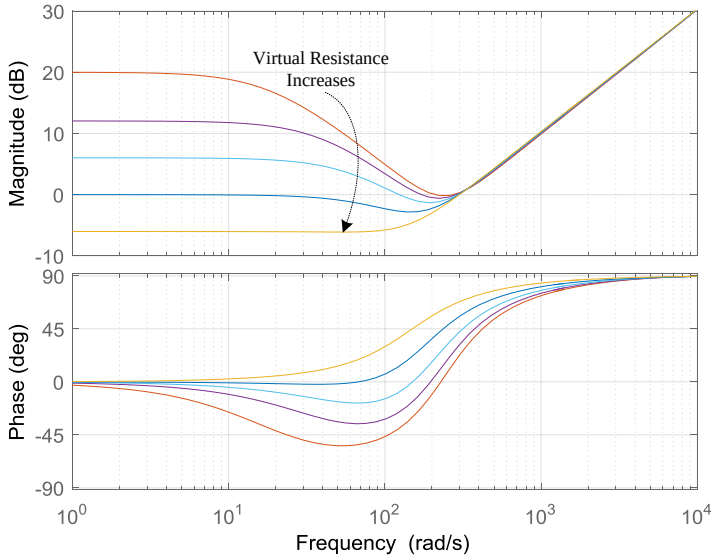

Figure 3-9 Frequency response of source-side output admittance with impedance-type droop-controlled converters under different virtual resistance (0.2Ω-4Ω) [58].

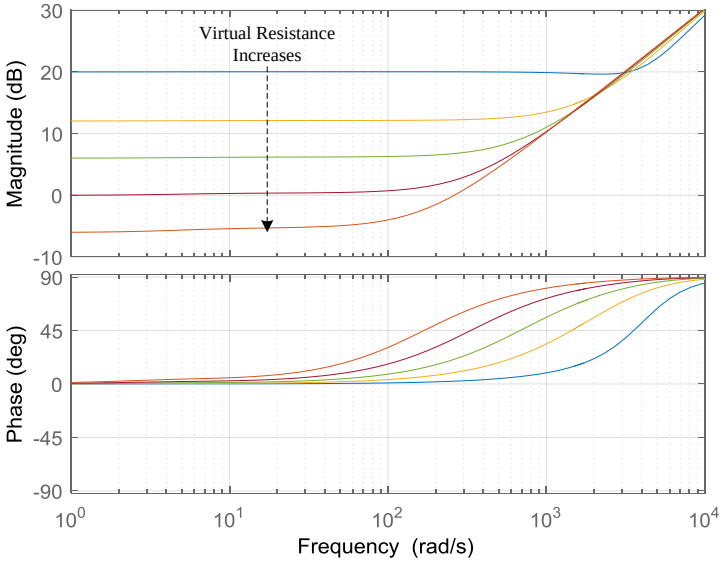

Figure 3-10 Frequency response of source-side output admittance with admittance-type droop-controlled converters under different virtual resistance (0.2Ω-4Ω) [58].

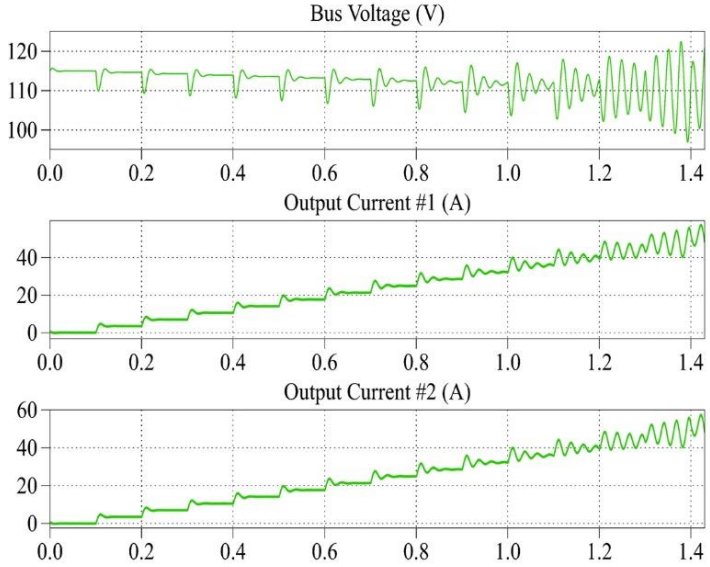

Figure 3-11 Simulation results of impedance-type droop-controlled case (R_{vi}=0.1Ω) feeding high-power CPL [58].

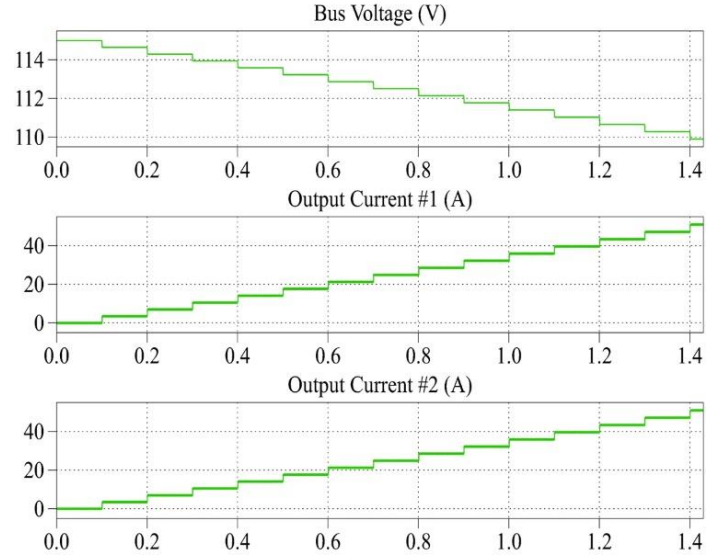

Figure 3-12 Simulation results of admittance-type droop-controlled case (R_{vi}=0.1Ω) feeding high-power CPL [58].

In Figure 3-11 [58] and Figure 3-12 [58], simulation results of study-case DC microgrid feeding constant power load are shown. In this simulation, each load step is a 400W load increase. It can be easily found that, the admittance-type droop control will show better capability feeding constant power load and stability margin.

CHAPTER 4. SYSTEM STABILITY ENHANCEMENT METHOD DEVELOPED FOR IMPEDANCE-TYPE CONTROLLERS

In this chapter, a negative series virtual inductor (NSVI) method is developed to enhance the stability of DC shipboard microgrid using impedance-type controllers (including both droop control and conventional voltage control) feeding CPL.

4.1. MECHANISM OF PROPOSED METHOD

As analyzed in the previouse chapter, the stability margin of a DC microgrid is strongly related to the maximum magnitude of source converter's output impedance. The lower peak magnitude of source-side output impedance is, the larger stability margin of the system will have. Therefore, to mitigate the CPL instability issue of DC microgrids, a possible solution is to reduce the peak magnitude of source converter's output impedance. In this way, performance of power consumers will not be affected. In Figure 4-1 and Figure 4-2 [59], the frequency response of the output impedance in the source-side for both conventional dual-loop voltage control (marked as VCM) and impedance-type droop control (marked as DCM) are presented, respectively.

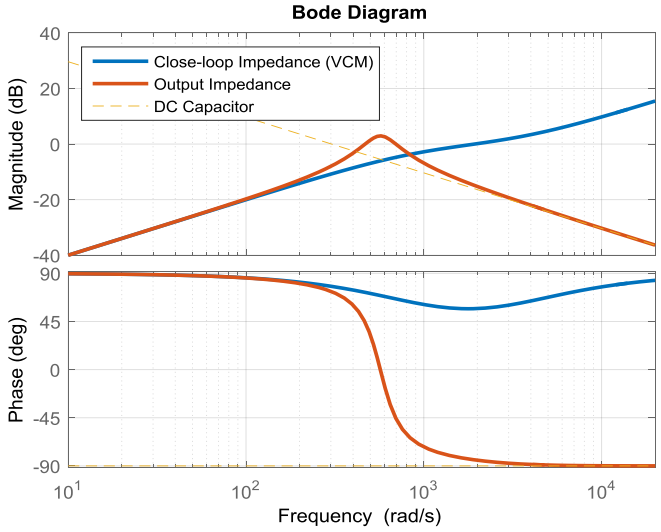

Figure 4-1 Frequency response of source-side output impedance for conventional dual-loop voltage control (i.e. impedance-type controller with R_{vi}=0) [59].

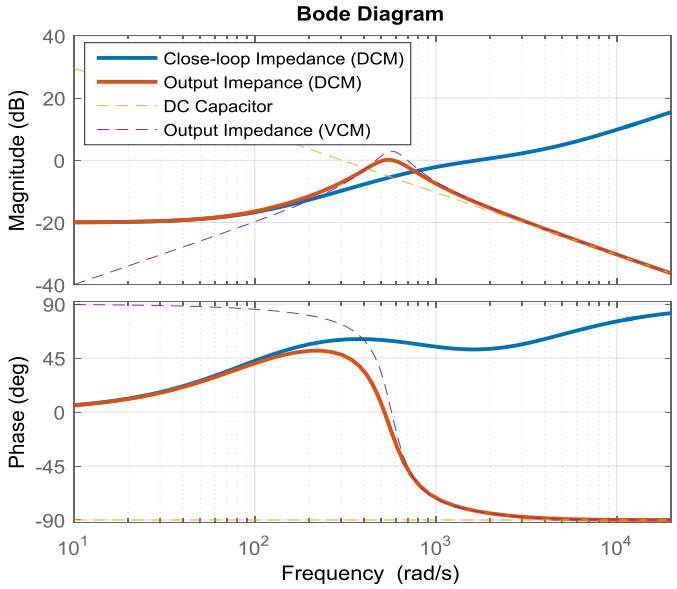

Figure 4-2 Frequency response of source-side output impedance for impedance-type droop control (with R_{vi}=0.1Ω) [59].

To reduce the peak magnitude of output impedance, three possible solution can be obtained by comparing the results shown above:

(1) By increasing the series virtual resistance;

(2) By increasing the capacitance of DC capacitor;

(3) By decreasing the inductance of the equivalent circuit;

In this chapter, the proposed methods are focusing on decreasing the inductance of the equivalent circuit, thus improving stability margin of the system.

As mentioned in Section 3.3.1, the major feature of impedance-type realization is that the virtual component it introduced to the output impedance will always be irrelavent to the intrinsic impedance introduced by dual-loop control. For this reason, adding a negative sries virtual inductor (NSVI) to the impedance-type controller is a possible choice. In Figure 4-3, the control diagram is shown, where the virtual impedance term in this control diagram is given by:

$$Z_v(s) = R_v - sL_v \tag{4.1}$$

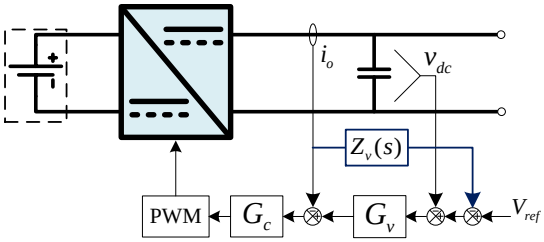

Figure 4-3 Control diagram of proposed method [59].

4.2. DESIGN RULES OF PROPOSED METHOD

It can be derived from the equivalent circuit shown in Figure 3-8, the introduction of NSVI will cancel the effect of virtual component L_{d1}, however, there will also be limitation for the value selection of NSVI.

In Figure 4-4 [59], output impedance of dual-loop voltage controller using proposed NSVI with different settings of L_v are illustrated. In Figure 4-5 [59], the locations of poles and zeros for the minor loop gain $T_m(s)$ in different settings L_v of are shown.

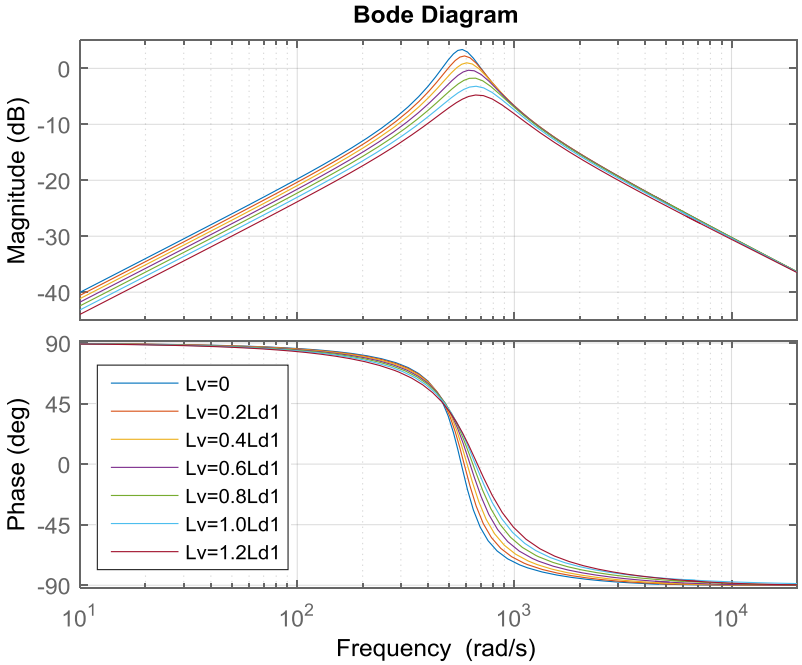

Figure 4-4 Output impedance after adding proposed NSVI (voltage control as example) [59].

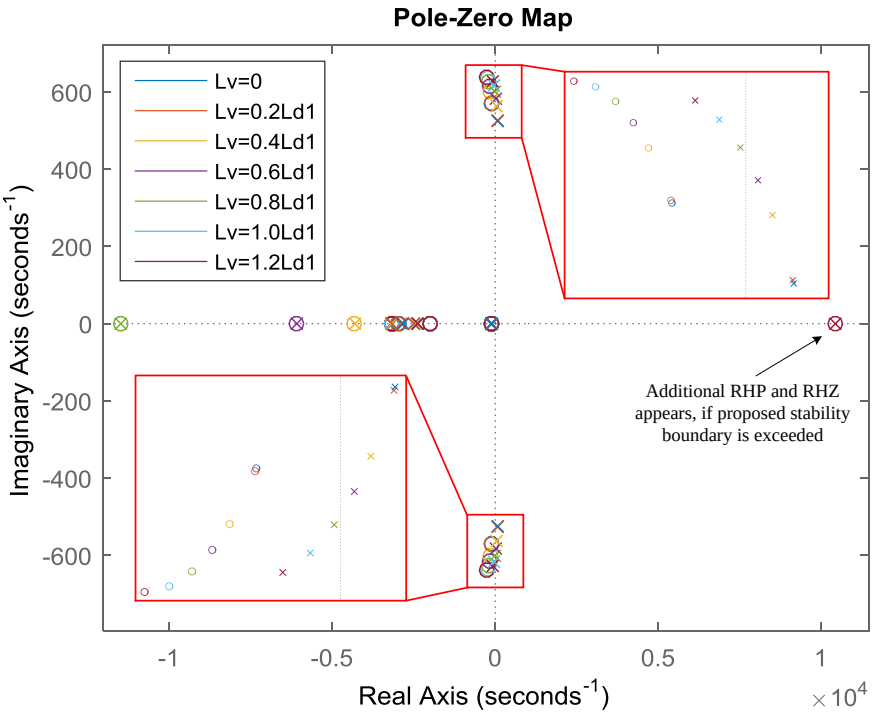

Figure 4-5 Map of poles and zeros of $T_m(s)$ in different setting of NSVI (P_{CPL}=6.5MW) [59].

From the analytical results shown in these figures, although the peak magnitude will continuously decrease with larger negative virtual inductor design, a set of pole and zero of $T_m(s)$ will move to the right half plain if the NSVI is set to be larger than L_{d1} in (3.24), which offends the stability boundary.

For this reason, the value of NSVI shall satisfy the following rules:

$$0 \le L_v \le L_{d1} \tag{4.2}$$

4.3. SIMULATION VERIFICATION OF PROPOSED METHOD

To validate the proposed method, simulations are carried out using PLECS with a study case DC shipboard microgrid composed by two source converters and a controllable CPL performing propulsion loads. The parameters used in the simulations are given in Table 4-1. Simulations are carried out for both conventional dual-loop voltage control and impedance-type droop control in detailed switching level.

In Figure 4-6, the simulation results of using proposed NSVI method in conventional dual-loop voltage control is shown, whereas the simulation results of using proposed method in impedance-type droop controllers are shown in Figure 4-7 [59].

Description of the Parameter	***Symbol***	***Value***
Voltage Reference	V_{ref}	1500 V
Source Voltage	E_1, E_2	3000 V, 3000 V,
Inductance of Buck Converters	L_1, L_2	8 mH, 8 mH
Stary Resistance of inductors,	r_1, r_2	0.1 Ω, 0.1 Ω
Switching Frequency	f_{sw}	2 kHz
Total Capacitance in DC Bus	C	3.3 mF
Proportion Term of Voltage Controller	K_{pv1}, K_{pv2}	1, 1
Integral Term of Voltage Controller	K_{iv1}, K_{iv2}	1000, 1000
Proportion Term of Current Controller	K_{pc1}, K_{pc2}	0.009, 0.009
Integral Term of Current Controller	K_{ic1}, K_{ic2}	0.1, 0.1
Virtual Resistances for Droop Control	R_{v1}, R_{v2}	0.05 Ω, 0.05 Ω,
CPL Control Bandwidth	ω_{CPL}	2000 rad/s
Load Profile	P_{Load}	500 kW/step (10 steps/s)
Inductance of Negative Series Virtual Inductor	L_{v1}, L_{v2}	-0.243mH, -0.243mH, ($\approx -0.8L_{d1}$)

Table 4-1 Parameters of the study-case shipboard microgrid [59].

The simulation results proved that, by using proposed NSVI method, the stability of the system can be still maintained with more CPL. When operating in conventional voltage control, maximum capability of CPL is increased from 3.5 MW to 6.5 MW. The system's maximum capability of feeding CPL is also increased from 3.5MW to 5.5 MW, when operating in the impedance-type droop control.

It is noteworthy that theoretically (as shown in Figure 4-2 [59]) impedance-type droop controller should have a lower peak magnitude of output impedance, but the capability of feeding CPL (i.e. its stability margin) is worse than the case of using conventional voltage controller. It is because of the fact that its voltage drop behavior will lead to increased negative incremental impedance. As a result, the system stability margin when feeding CPL may decrease, when compared with more conventional voltage control.

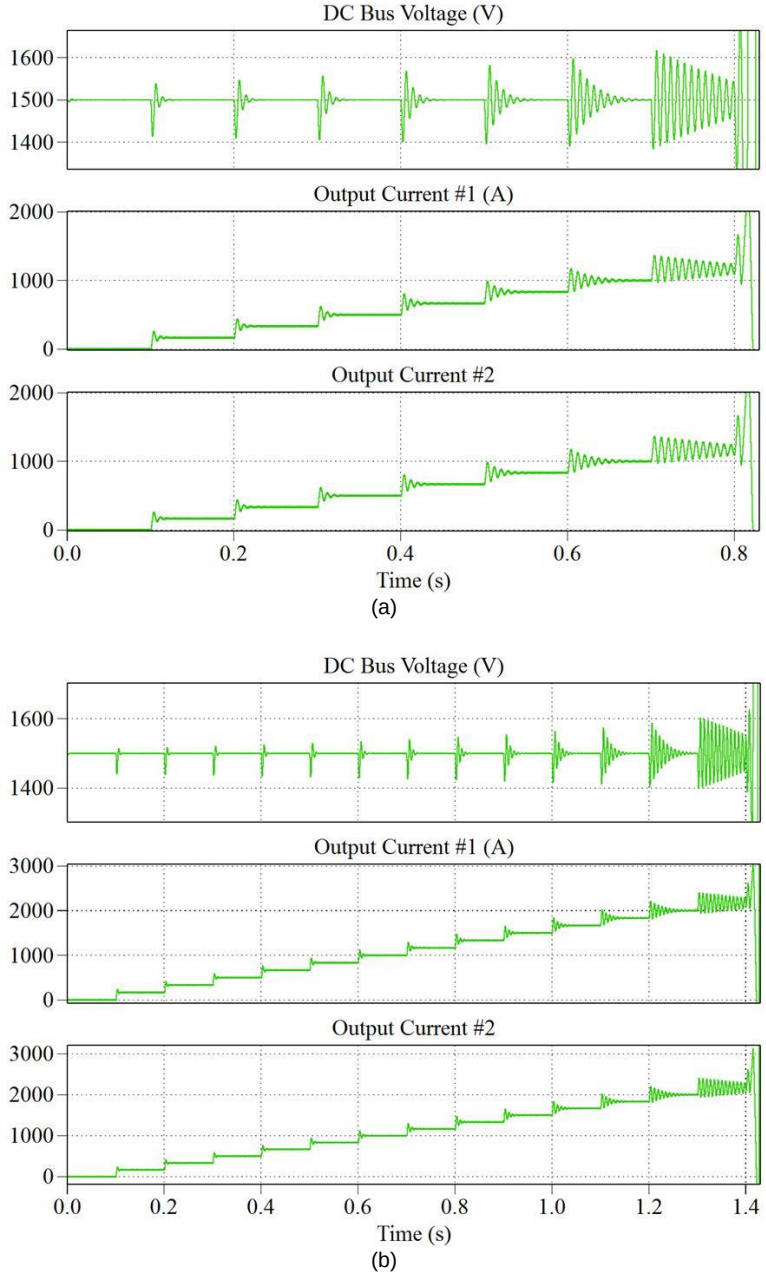

Figure 4-6 Simulation results of dual-loop voltage controlled converters feeding CPL with/without proposed NSVI method: (a)without NSVI method; (b) with NSVI method [59].

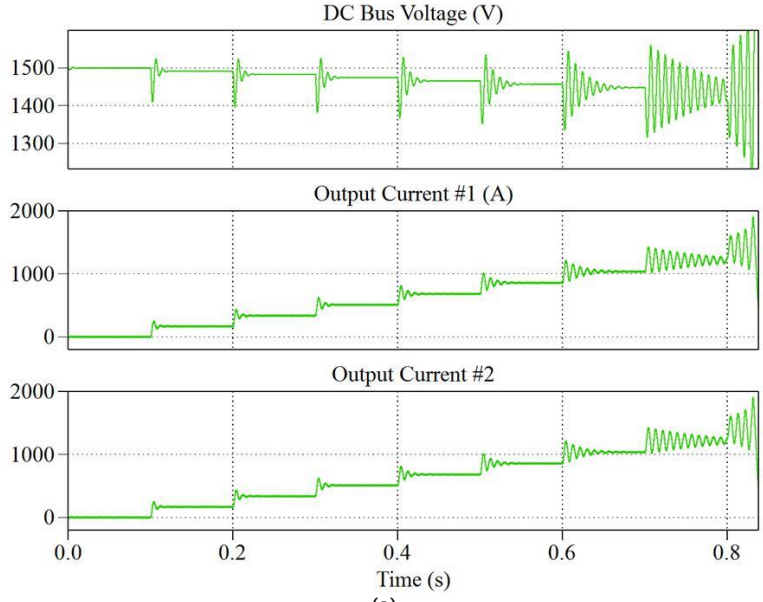

(a)

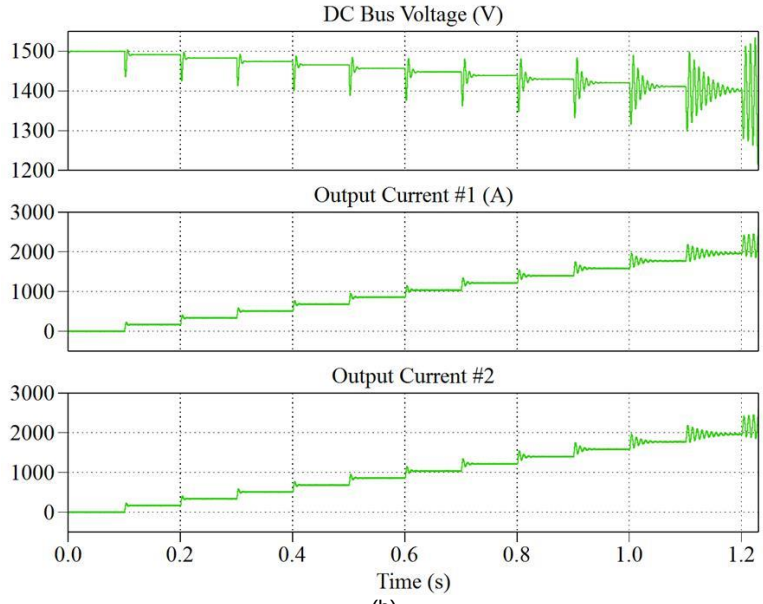

(b)

Figure 4-7 Simulation results of impedance-type droop controlled converters feeding CPL with/without proposed NSVI method: (a)without NSVI method; (b)with NSVI method [59].

CHAPTER 5. SYSTEM PERFORMANCE IMPROVEMENT WITH ADMITTANCE-TYPE DROOP CONTROLLERS

In this chapter, RC-mode admittance-type droop control is introduced. The methos is initially proposed for system enhancement, however, during the investigation, the author found that its potential improvement on system-level inertial behavior and transient response are even more considerable.

5.1. MECHANISM OF PROPOSED METHOD

As analyzed in the previous chapters, to modify the output impedance characterisitic and, therefore, enhancing the system stability margin, there will be three kinds of solutions:

(1) By increasing the series virtual resistance;

(2) By increasing the equivalent capacitance in output terminal;

(3) By decreasing the equivalent inductance of the equivalent circuit;

In this chapter, the proposed methods are focusing on increasing the equivalent capacitance of the DC bus, thus improving not only stability margin but also inertial behavior and transient response of the system.

5.1.1. RELATIONSHIP BETWEEN SYSTEM INERTIA AND DROOP CONTROL

Generally, the inertia of a power system behaves to prevent sudden change in critical variable spontaneously be releasing its stored energy, and thereby allowing the power sources to rebuild equilibrium timely [60]. In AC power system, the inertial behavior can be presented by swing equation of synchronous machine:

$$P_{set} - P_o - D_p(\omega - \omega_n) = J\omega\frac{d\omega}{dt} = P_{vi} \tag{5.1}$$

where P_{set}, P_o, P_{vi}, ω, ω_n, D_p, J are the active power reference, the output power, released power of inertial behavior, the real-time angular frequency, the rated angular frequency, the damping coefficient, and the moment of inertia, respectively.

When setting *J=0*, the equation (5.1) can be rewritten as:

$$\omega = \omega_{no} - mP_o \quad \text{where} \quad \omega_{no} = \omega_n + P_{set}/D_p; \quad m = 1/D_p; \tag{5.2}$$

This equation is also known as the widely used ω-*P* droop method in the field of AC microgrids [12]. In another word, the ω-*P* droop principle is mimicking the behavior of a synchronous generator without inertia.

Similarly, in DC MGs, the inertial behavior can be presented by:

$$P_{set} - P_o - D_p(u - u_n) = C_v u \frac{du}{dt} = P_{vi} \tag{5.3}$$

where u, u_n, C_v are the DC bus voltage, the rated DC bus voltage and the inertia coefficient (physically as a capacitance).

When setting $C_v=0$, the equation (5.3) can be rewritten as:

$$u = u_{no} - mP_o \quad \text{where} \quad u_{no} = u_n + P_{set}/D_p; \quad m = 1/D_p; \tag{5.4}$$

where i_v represents the desired current injection, u_{no} is the original bus voltage of DC droop control, m presents the droop coefficient of the power source.

Conclusively, the droop control (no matter AC or DC) emulates the damping effect of natural power source, except for the inertial behavior. As a result, the system inertia of microgrids are usually very limited.

5.1.2. VIRTUAL INERTIA INJECTION THROUGH DROOP CONTROL

It can be derived from (5.3), to perform virtual inertia, the additional current will be:

$$i_{vi} = -\frac{kP_{vi}}{u} = -kC_v \frac{du}{dt} = C_v' \frac{d(u_{no} - u)}{dt} \tag{5.5}$$

where the injected power of virtual inertia control is k times of the system's original inertial behavior, the negative sign is to present that power is injecting to the system, $C_v'=kC_v$ is the virtual inertia coefficient introduced to the system.

This equation can be reformulated as:

$$u(s) = u_{no} - \frac{1}{sC_v'} i_{vi}(s) \tag{5.6}$$

$$i_{vi}(s) = sC_v'\left(u_{no} - u(s)\right) \tag{5.7}$$

The new equations show that by adding capacitive virtual component to the droop control framework, virtual inertia injection can be performed simultaneously with the power sharing, which forms RC-mode droop control function:

$$u(s) = u_{no} - \left(\frac{1}{sC_v'} \| R_d\right) i_{vi}(s) = u_{no} - Z_d(s) i_o(s) \tag{5.8}$$

$$i_o(s) = \left(\frac{1}{R_d} + sC_v'\right)\left(u_{no} - u(s)\right) = Y_d(s)\left(u_{no} - u(s)\right) \tag{5.9}$$

5.1.3. IMPACT OF REALIZATION

As analyzed in Chapter 3, the major feature of impedance-type droop controller is that the virtual component introduced will be irrelevant to the converter's intrinsic impedance, whereas virtual components introduced by admittance-type droop controller will be relevant with both droop coefficient design and control bandwidth of current loop.

Using the same analytical model used in Section 3.2.2, the equivalent circuit of proposed RC-mode droop control using different realizations can be derived as shown in Figure 5-1 [60] and Figure 5-2 [60].

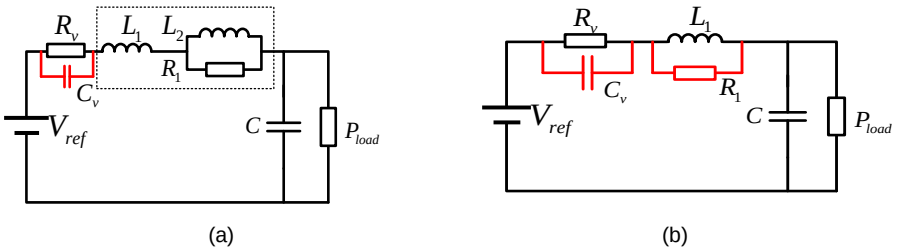

Figure 5-1 Derived equivalent circuit for RC-mode droop controllers: (a) impedance-type controller; (b)admittance-type controller [60].

where the additional components are given by:

$$R_1 = \omega_c C_v \tag{5.10}$$

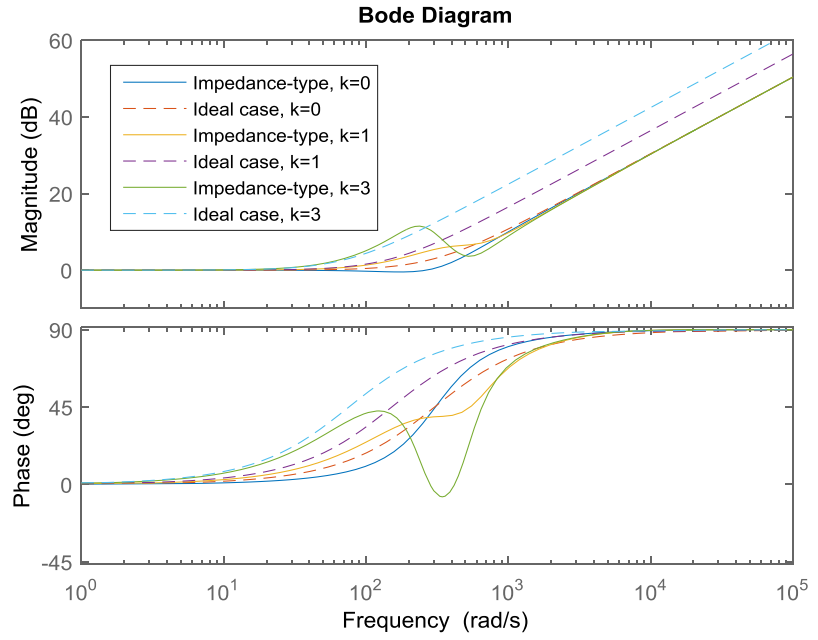

(a)

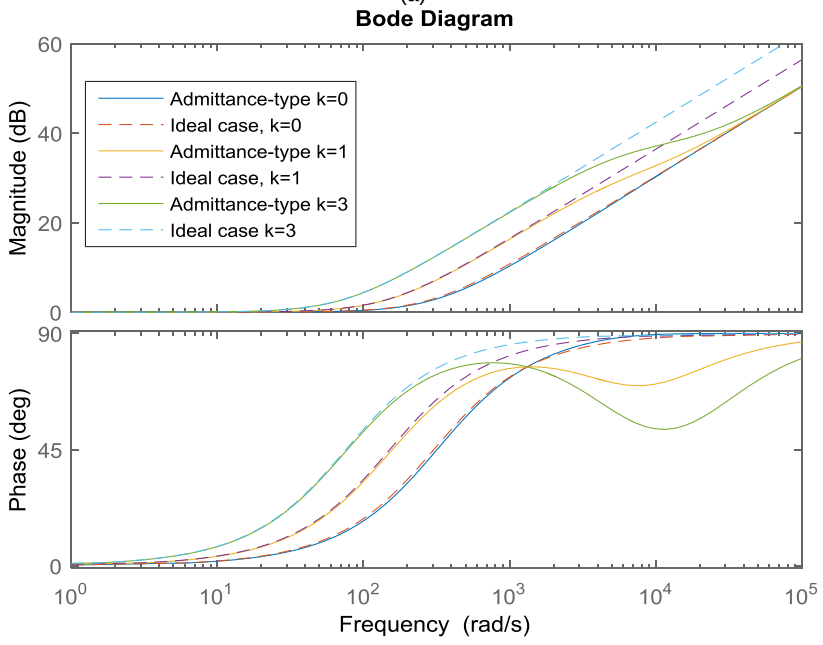

(b)

Figure 5-2 Derived source-side admittance of RC-mode droop control with different realizations: (a) impedance-type controller; (b)admittance-type controller [60].

In Figure 5-2(a) [60], the frequency response of derived output admittance with more conventional impedance-type controller is shown, whereas the results of admittance-type controller is shown in Figure 5-2(b) [60]. For comparison, different virtual inertia setting (i.e. $k=0,1,3$) are performed, and the ideal output admittance, in which the physical capacitance connected to the DC bus is increased directly is also included.

It can be easily found that admittance-type controller shows better characteristic and can maintain desired equivalent capacitance in a much larger frequency range.

5.2. SIMULATION AND EXPERIMENTAL RESULTS

Simulations carried out using PLECS and experiments using experimental setup are carried out to validate the proposed method.

5.2.1. SIMULATION RESULTS

In the simulation, two converters are connected in parallel feeding a resistive load. The system parameters are listed in Table 5-1.

Description of the Parameter	*Symbol*	*Value*
Voltage Reference	V_{ref}	115 V
Source Voltage	E_1, E_2	230 V, 230 V,
Inductance of Buck Converters	L_1, L_2	8 mH, 8 mH
Stary Resistance of inductors,	r_1, r_2	0.1 Ω, 0.1 Ω
Switching Frequency	f_{sw}	10 kHz
Total Capacitance in DC Bus	C	3.3 mF
Proportion Term of Current Controller	K_{pc1}, K_{pc2}	0.02, 0.02
Integral Term of Current Controller	K_{ic1}, K_{ic2}	0.1, 0.1
Virtual Resistances for Droop Control	R_{v1}, R_{v2}	1.5 Ω, 1.5 Ω,
Resistance of Load	R_{Load}	28.75 Ω
Virtual Capacitance for Inertia Injection	C_v	3.3 mF

Table 5-1 Parameters of the simulated study case [60].

The simulation results show that with proposed method, the dynamic response of DC bus voltage will have reduced overshoot and smoother transient when load changing occurs in the system.

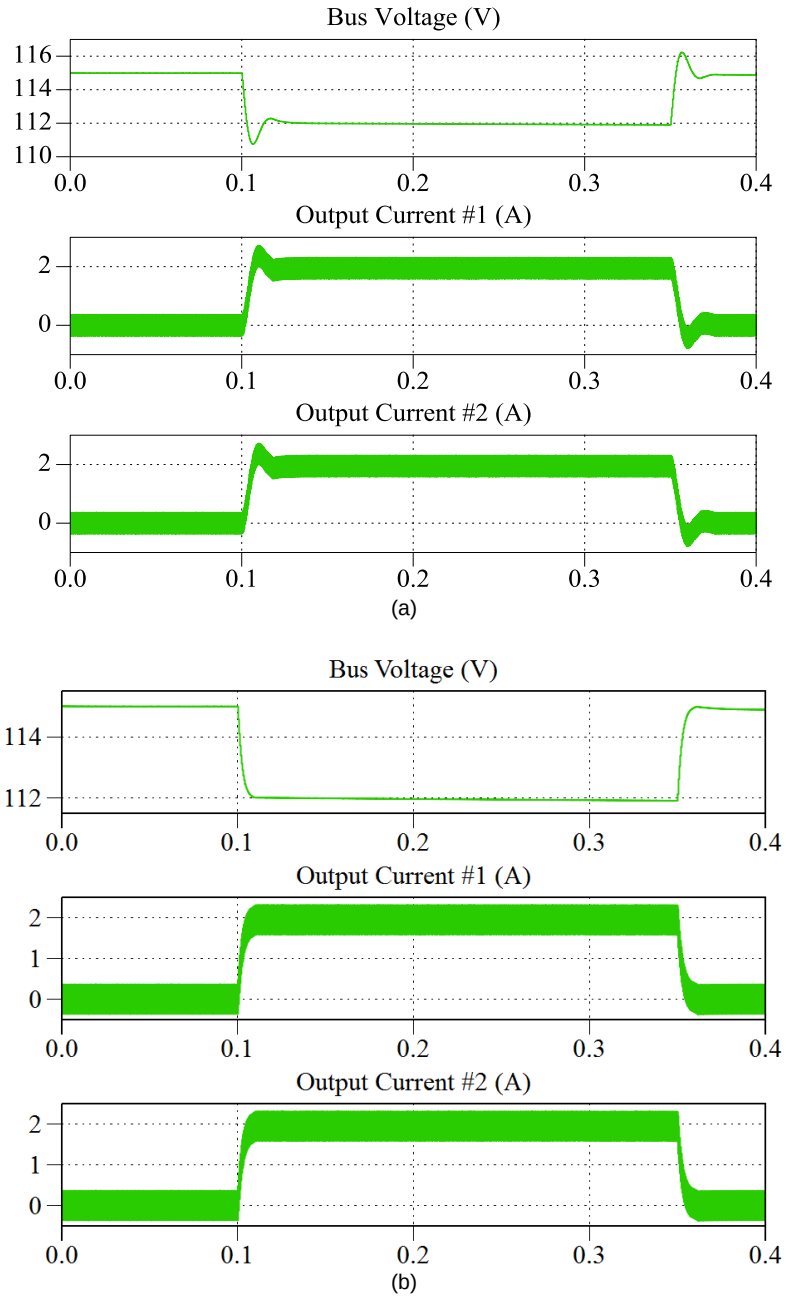

Figure 5-3 Simulation results of load changing with and without proposed RC-mode droop control (a) without proposed method; (b) with proposed method [60].

5.2.2. EXPERIMENTAL RESULTS

The experiments are carried out with the DC microgrid experimental set-up as shown in Figure 5-4. The set-up is composed by four DC/DC converters, controlled individually using dSpace RT1006, detailed parameters of the set-up are given in Table 5-2 [60].

Description of the Parameter	*Symbol*	*Value*
Voltage Reference	V_{ref}	120 V
Source Voltage	E_1, E_2	240 V
Inductance of Buck Converters	L_1, L_2	8 mH
Stary Resistance of inductors,	r_1, r_2	0.1 Ω
Switching Frequency	f_{sw}	10 kHz
Total Capacitance in DC Bus	C	3.3 mF
Proportion Term of Current Controller	K_{pci}	0.02
Integral Term of Current Controller	K_{ici}	0.1
Virtual Resistances for Droop Control	R_{vi}	4 Ω
Resistance of Load	R_{Load}	17 Ω
Virtual Capacitance for Inertia Injection	C_{vi}	2 mF

Table 5-2 Parameters of the experimental setup [60].

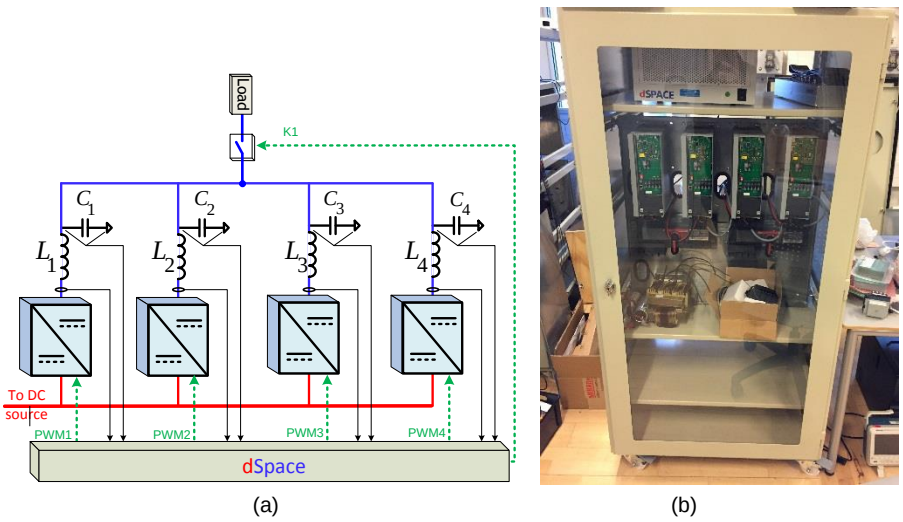

Figure 5-4 The experimental setup: (a) schematic of set-up; (b)photo of set-up.

In Figure 5-5 and Figure 5-6 [60], the experimental results for normal admittance-type droop control without using proposed method is presented. The bus voltage and output currents of the four paralleled are shown, respectively.

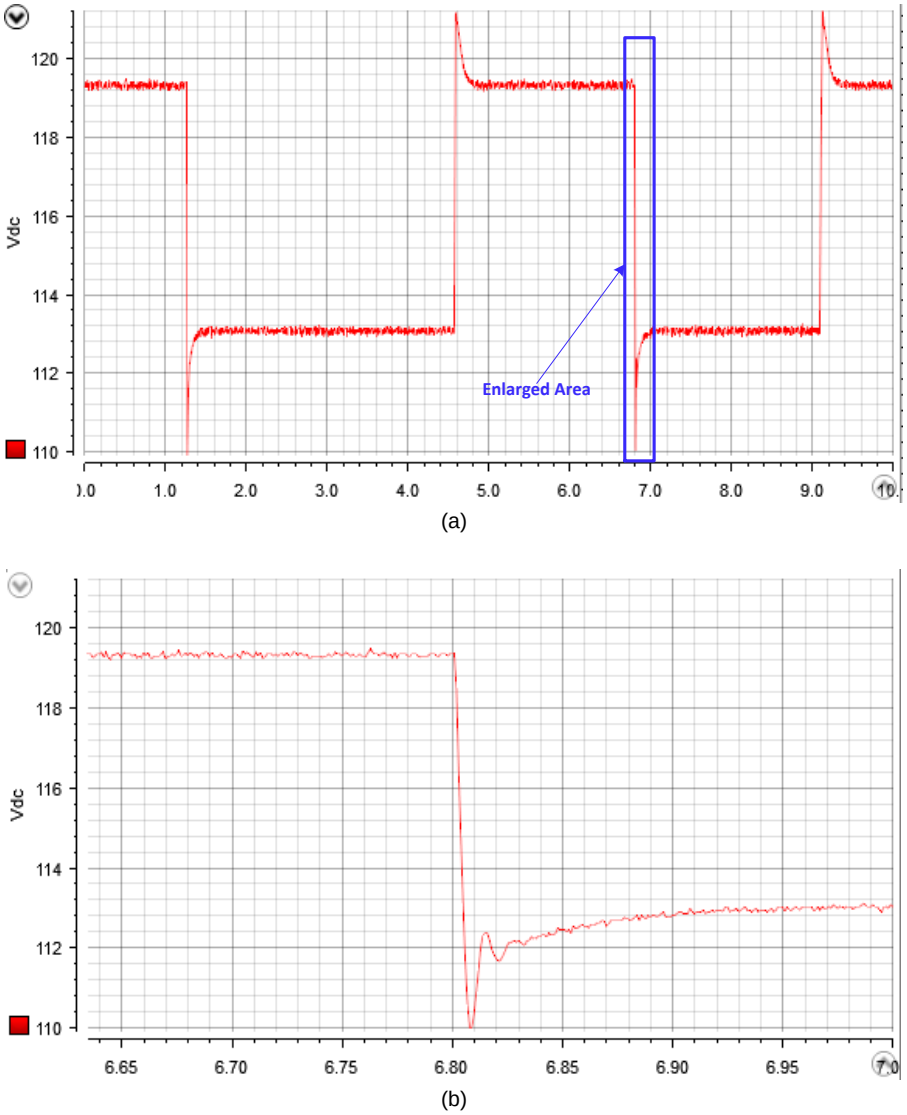

Figure 5-5 Experimental results of load changing with normal admittance-type droop control: (a)bus voltage; (b) enlarged area [60].

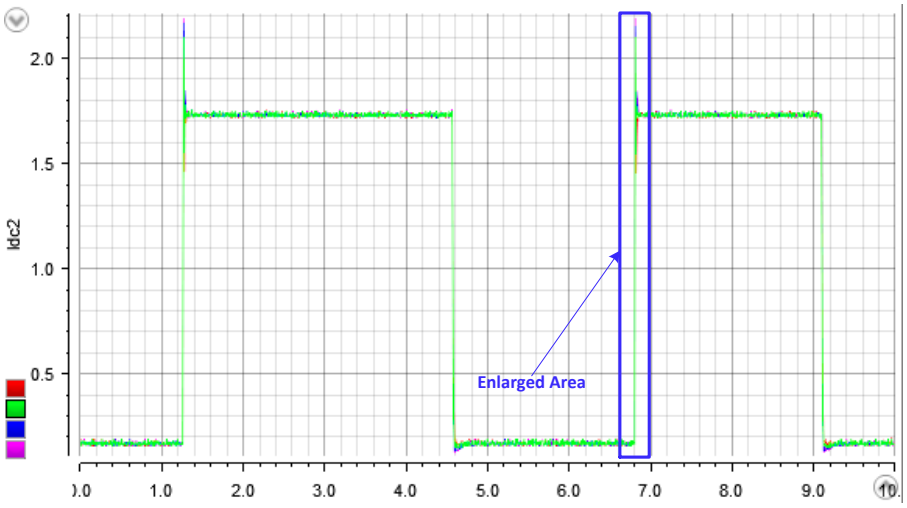

(a)

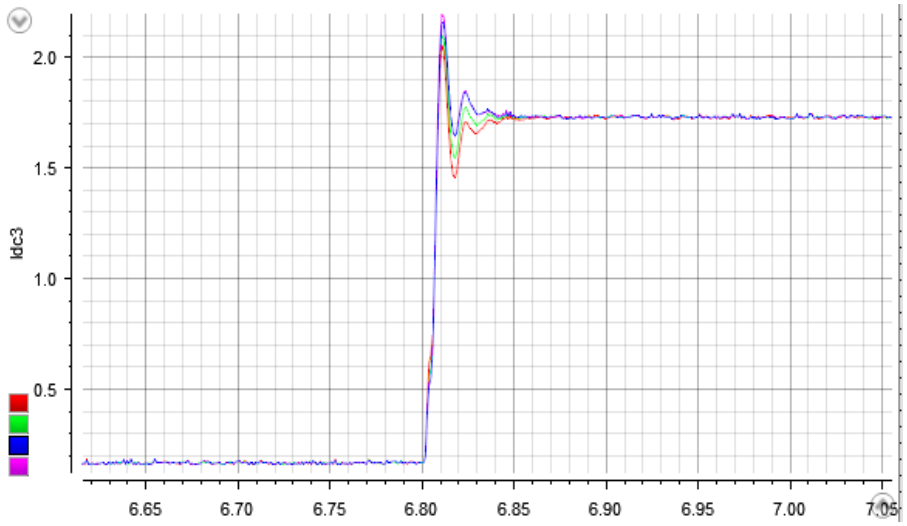

(b)

Figure 5-6 Experimental results of load changing with normal admittance-type droop control: (a)output currents of converters; (b) enlarged area [60].

In Figure 5-7 and Figure 5-8 [60], the experimental results for proposed RC-mode admittance-type droop control is presented. The bus voltage and output currents of the four paralleled are shown, respectively.

By comparing the simulation results shown in these figures, by adding proposed virtual inertia injection function to droop method, the inertial behavior of the DC

microgrid is enhanced. It is presented by smoother transient response, increased time constant of the system, and significantly reduced overshoots when load changes. At the same time, the proper power sharing effect of conventional droop method is not affected by the virtual injection function.

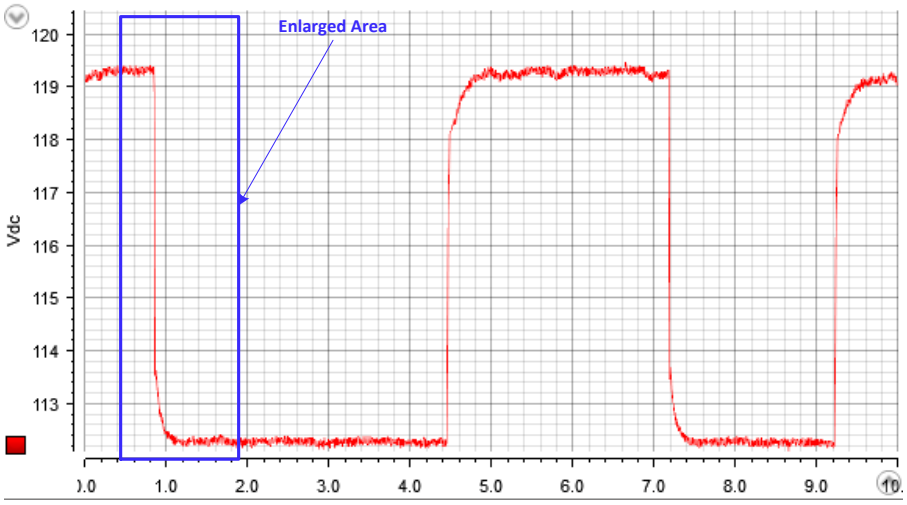

(a)

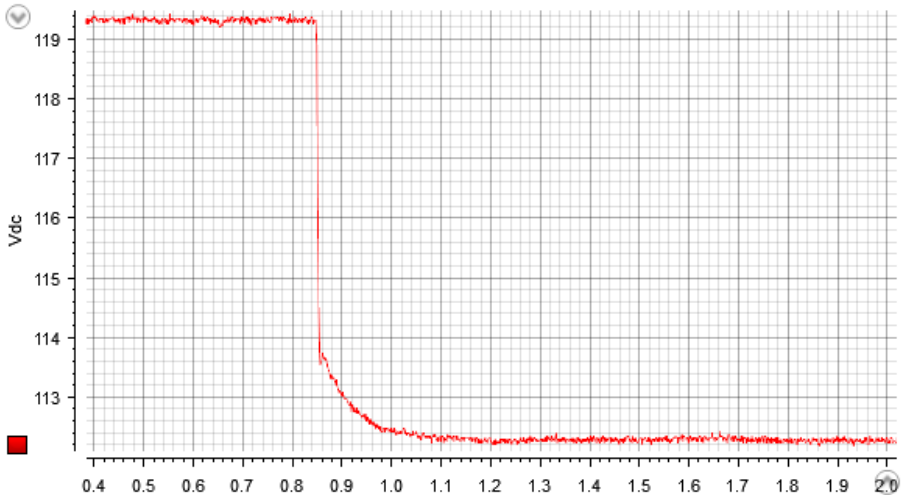

(b)

Figure 5-7 Experimental results of load changing with proposed RC-mode droop control: (a) bus voltage; (b) enlarged area [60].

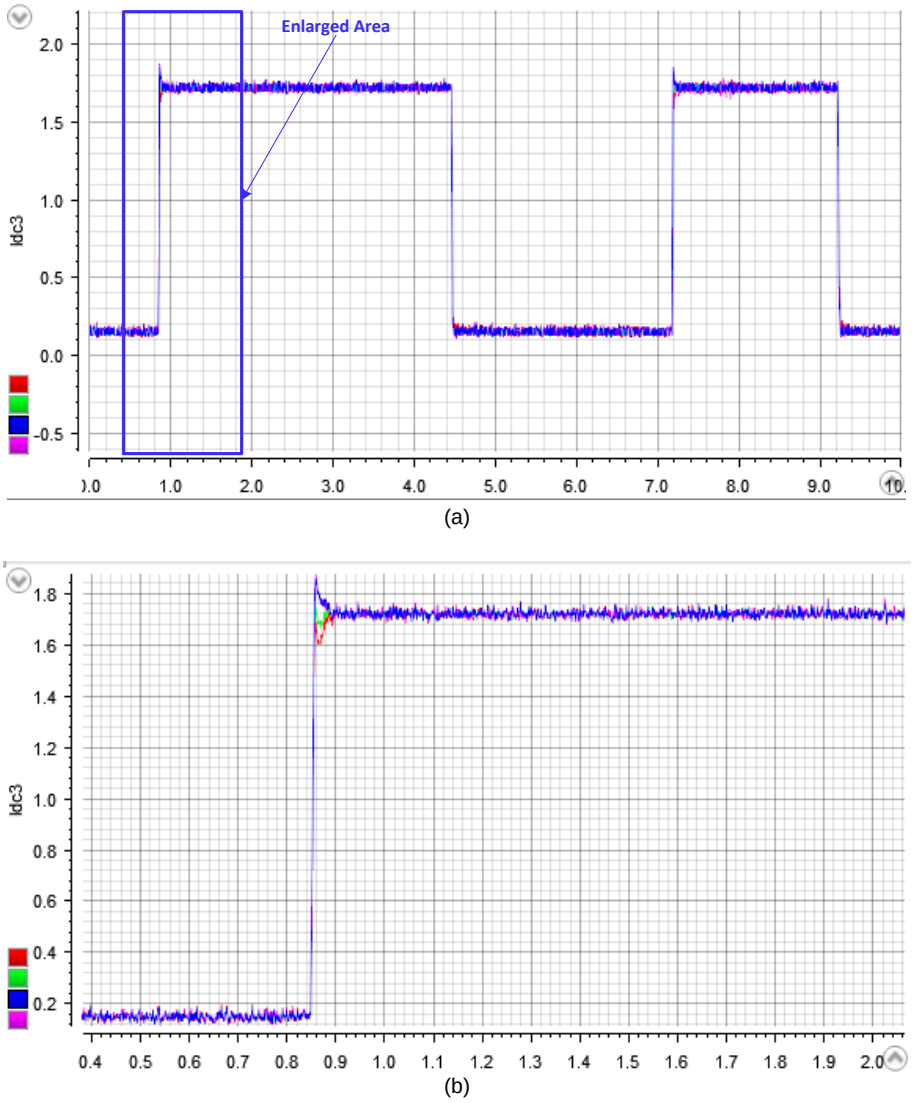

Figure 5-8 Experimental results of load changing with proposed RC-mode droop control (a)output currents of converters; (b) enlarged area [60].

CHAPTER 6. CONCLUSIONS AND FUTURE WORK

6.1. CONCLUDING REMARKS

In this thesis, coordinated control and stability issue of DC shipboard microgrids are discussed.

Regarding the coordinated control, the following contributions are made:

- Characteristic-based power sharing techniques are proposed to coordinate different kinds of power sources in a DC shipboard microgrid. Compared with more conventional proportional power sharing techniques, the new proposal is possible to grants a better fuel-efficiency in harsh load profiles, thus saving cost and reducing emission of the ship.
- A new hierarchical control architecture is proposed for DC shipboard microgrids. The new proposal re-arragned conventional control layers to meet the need of shipboard application. At the same time, the major functionalities of the conventional hierarhical control architecture used in terrestrial microgrids are maintained.

Regarding the stability issue, the following contributions are made:

- The two major categories of control approaches used in DC microgrids, which are impedance-type control and admittance-type control, are modeled, analyzed and compared. The impact of using different approaches on output charactersitic and stability margin of the system are proposed.
- Generalized analytical models and equivalent circuits of different control approaches are proposed.
- Inspired by the analytical results, a negative series virtual inductor (NSVI) method is proposed for stability enhancement of impedance-type controllers, including both dual-loop voltage controllers and droop controllers. With a proper design of NSVI, the capability of feeding high-power CPL can be increased significantly.
- An admittance-type RC-mode droop control method is also proposed. In the proposed method, virtual capacitor is included in parallel with conventional virtual resistor. The introduction of virtual capacitor modifies the output impedance characteristic, and, more importantly the inertial behavior of the system. As a result, with porposed method, the bus voltage will have smoother transient response.

6.2. POTENTIAL FUTURE WORK OF THIS THESIS

There are many works can be further proceeded in future based on this thesis. The future works include but are not limited to followings:

- For the coordinated control of DC shipboard microgrids, the control solution for operation under abnormal and emergency conditions need to be designed and validated. The control shall be cooperative with the protective functions, of the system, especially for DC short-circuit fault. For example, converters can be used to inject certain power flow to the system to locate the fault.
- Currently, when operating in DP process, the state-of-the-art shipboard microgrids are usually operated with open buses, in which all tie lines are opened. It is because the dramatic load changing may sometimes trigger the protective funtion of genset, and open-bus operation can prevent single-point fault to spread into system failure. This problem can be at least partially solved by introducing energy stroage and/or inertia injection. However, case study, detailed analysis, and trade-off will be needed. In addition to that, coordination between multiple shipboard microgrids is another potential direction of this work.
- Another potential direction of this work is the impedance design of power electronic converters. The power sharing, in both transient and steady states, can be regarded to be driven by the equivalent impedance of converters. Therefore, with proper design of converter's impedance characteristic, more desired power sharing and dynamic response can be achieved.
- In this thesis, a number of control solutions are developed for DC systems. Some of them are potential to work also in the AC systems. Further analysis and attempt will be needed in the future work.

LITERATURE LIST

[1]. E. Skjong, R. Volden, E. Rødskar, M. Molinas, T. A. Johansen and J. Cunningham, "Past, Present, and Future Challenges of the Marine Vessel's Electrical Power System," in *IEEE Transactions on Transportation Electrification*, vol. 2, no. 4, pp. 522-537, Dec. 2016.

[2]. E. Skjong, E. Rødskar, M. Molinas, T. Johansen, J. Cunningham, "The marine vessel's electrical power system: From its birth to present day", *Proc. IEEE*, vol. 103, no. 12, pp. 2410-2424, Dec. 2015.

[3]. J. F. Hansen and F. Wendt, "History and State of the Art in Commercial Electric Ship Propulsion, Integrated Power Systems, and Future Trends," in *Proceedings of the IEEE*, vol. 103, no. 12, pp. 2229-2242, Dec. 2015.

[4]. International Maritime Organization: Prevention of Air Pollution from Ships, Aug. 2015.

[5]. Wärtsilä: Viking Lady, available at: https://www.wartsila.com/resources/customer-references/view/viking-lady

[6]. Corvus Energy: CASE STUDY: Eidesvik Offshore, Viking Lady OSV, available at: http://corvusenergy.com/wp-content/uploads/2015/09/Corvus-Energy-CASE-STUDY_Viking-Lady_May-2015.pdf

[7]. DNV GL, "IN FOCUS: The future is Hybrid - A guide for the use of batteries"

[8]. DNV GL, "Rules for classification: ships" available at: http://rules.dnvgl.com/docs/pdf/DNVGL/RU-SHIP/2015-10/DNVGL-RU-SHIP-Pt6Ch2.pdf

[9]. R. Lasseter, "Microgrids", *Proc. IEEE Power Eng. Soc. Winter Meeting*, vol. 1, pp. 305-308, 2002.

[10]. R. H. Lasseter and P. Paigi, "Microgrid: a conceptual solution," *2004 IEEE 35th Annual Power Electronics Specialists Conference (IEEE Cat. No.04CH37551)*, Aachen, Germany, 2004, pp. 4285-4290 Vol.6.

[11]. N. Hatziargyriou, H. Asano, R. Iravani and C. Marnay, "Microgrids," in *IEEE Power and Energy Magazine*, vol. 5, no. 4, pp. 78-94, July-Aug. 2007.

[12]. J. M. Guerrero, J. C. Vasquez, J. Matas, L. G. de Vicuna and M. Castilla, "Hierarchical Control of Droop-Controlled AC and DC Microgrids—A General Approach Toward Standardization," in *IEEE Transactions on Industrial Electronics*, vol. 58, no. 1, pp. 158-172, Jan. 2011.

[13]. J. A. P. Lopes, C. L. Moreira and A. G. Madureira, "Defining control strategies for MicroGrids islanded operation," in *IEEE Transactions on Power Systems*, vol. 21, no. 2, pp. 916-924, May 2006.

[14]. D. E. Olivares *et al*., "Trends in Microgrid Control," in *IEEE Transactions on Smart Grid*, vol. 5, no. 4, pp. 1905-1919, July 2014.

[15]. R. E. Hebner et al., "Technical cross-fertilization between terrestrial microgrids and ship power systems", *J. Modern Power Syst. Clean Energy*, vol. 4, no. 2, pp. 161-179, 2015.

[16]. R. E. Hebner *et al*., "Dynamic Load and Storage Integration," in *Proceedings of the IEEE*, vol. 103, no. 12, pp. 2344-2354, Dec. 2015.

[17]. F. D. Kanellos, G. J. Tsekouras, and J. Prousalidis, “Onboard DC grid employing smart grid technology: challenges, state of the art and future prospects,” *IET Electr. Syst. Transp.*, vol. 5, no. 1, pp. 1–11, 2015.

[18]. Z. Jin, M. Savaghebi, J. C. Vasquez, Lexuan Meng and J. M. Guerrero, "Maritime DC microgrids - a combination of microgrid technologies and maritime onboard power system for future ships," *2016 IEEE 8th International Power Electronics and Motion Control Conference (IPEMC-ECCE Asia)*, Hefei, 2016, pp. 179-184.

[19]. Z. Jin, G. Sulligoi, R. Cuzner, L. Meng, J. C. Vasquez and J. M. Guerrero, "Next-Generation Shipboard DC Power System: Introduction Smart Grid and dc Microgrid Technologies into Maritime Electrical Netowrks," in *IEEE Electrification Magazine*, vol. 4, no. 2, pp. 45-57, June 2016.

[20]. Kyunghwa Kim, Kido Park, Jongwoo Ahn, Gilltae Roh and Kangwoo Chun, "A study on applicability of Battery Energy Storage System (BESS) for electric propulsion ships," *2016 IEEE Transportation Electrification Conference and Expo, Asia-Pacific (ITEC Asia-Pacific)*, Busan, 2016, pp. 203-207.

[21]. K. Kim, K. Park, J. Lee, K. Chun and S. Lee, "Analysis of Battery/Generator Hybrid Container Ship for CO_2Reduction," in *IEEE Access*, vol. 6, pp. 14537-14543, 2018.

[22]. A. M. Bassam, A. B. Phillips, S. R. Turnock and P. A. Wilson, "Sizing optimization of a fuel cell/battery hybrid system for a domestic ferry using a whole ship system simulator," *2016 International Conference on Electrical Systems for Aircraft, Railway, Ship Propulsion and Road Vehicles & International Transportation Electrification Conference (ESARS-ITEC)*, Toulouse, 2016, pp. 1-6.

[23]. M. Godjevac *et al*., "Electrical energy storage for dynamic positiong operations: Investigation of three application case," *2017 IEEE Electric Ship Technologies Symposium (ESTS)*, Arlington, VA, 2017, pp. 182-186.

[24]. A. Monti, S. D'Arco, L. Gao and R. A. Dougal, "Energy storage management as key issue in control of power systems in future all electric ships," *2008 International Symposium on Power Electronics, Electrical Drives, Automation and Motion*, Ischia, 2008, pp. 580-585.

[25]. A. T. Elsayed and O. A. Mohammed, "A comparative study on the optimal combination of hybrid energy storage system for ship power systems," *2015 IEEE Electric Ship Technologies Symposium (ESTS)*, Alexandria, VA, 2015, pp. 140-144.

[26]. J. Zhang, Q. Li, W. Cong and L. Zhang, "Restraining integrated electric propulsion system power fluctuation using hybrid energy storage system," *2015 IEEE International Conference on Mechatronics and Automation (ICMA)*, Beijing, 2015, pp. 336-340.

[27]. J. Hou, J. Sun and H. F. Hofmann, "Mitigating Power Fluctuations in Electric Ship Propulsion with Hybrid Energy Storage System: Design and Analysis," in *IEEE Journal of Oceanic Engineering*, vol. 43, no. 1, pp. 93-107, Jan. 2018.

[28]. D. Gonsoulin, T. Vu, F. Diaz, H. Vahedi, D. Perkins and C. Edrington, "Centralized MPC for multiple energy storages in ship power systems," *IECON 2017 - 43rd Annual Conference of the IEEE Industrial Electronics Society*, Beijing, 2017, pp. 6777-6782.

[29]. M. M. S. Khan and M. O. Faruque, "Management of hybrid energy storage systems for MVDC power system of all electric ship," *2016 North American Power Symposium (NAPS)*, Denver, CO, 2016, pp. 1-6.

[30]. J. Sanchez, D. Wetz, Q. Dong and J. Heinzel, "Integration and study of hardware in the loop diesel generator with a hybrid energy storage module for naval applications," *2017 IEEE Electric Ship Technologies Symposium (ESTS)*, Arlington, VA, 2017, pp. 580-585.

[31]. J. McGroarty, J. Schmeller, R. Hockney and M. Polimeno, "Flywheel energy storage system for electric start and an all-electric ship," *IEEE Electric Ship Technologies Symposium, 2005.*, Philadelphia, PA, 2005, pp. 400-406.

[32]. S. Kulkarni and S. Santoso, "Impact of pulse loads on electric ship power system: With and without flywheel energy storage systems," *2009 IEEE Electric Ship Technologies Symposium*, Baltimore, MD, 2009, pp. 568-573.

[33]. J. Hou, J. Sun and H. Hofmann, "Battery/flywheel Hybrid Energy Storage to mitigate load fluctuations in electric ship propulsion systems," *2017 American Control Conference (ACC)*, Seattle, WA, 2017, pp. 1296-1301.

[34]. G. Sulligoi, A. Tessarolo, V. Benucci, A. Millerani Trapani, M. Baret and F. Luise, "Shipboard Power Generation: Design and Development of a Medium-Voltage dc Generation System," *IEEE Ind. Appl. Mag.*, vol. 19, no. 4, pp. 47-55, July-Aug. 2013.

[35]. B. Zahedi and L. E. Norum, "Voltage regulation and power sharing control in ship LVDC power distribution systems," *Power Electronics and Applications (EPE), European Conference on*, Lille, 2013, pp. 1-8.

[36]. B. Zahedi and L. E. Norum, "Modeling and Simulation of All-Electric Ships with Low-Voltage DC Hybrid Power Systems," in *IEEE Transactions on Power Electronics*, vol. 28, no. 10, pp. 4525-4537, Oct. 2013.

[37]. G. M. Foglia, A. Di Gerlando, M. F. Iacchetti, and R. Perini, "Comprehensive steady-state analytical model of a three-phase diode rectifier connected to a constant DC voltage source," *IET Power Electron.*, vol. 6, no. January, pp. 1927–1938, 2013.

[38]. P. C. Krause, O. Wasynczuk, and S. D. Sudhoff, Analysis of Electric Machinery and Drive Systems, 2nd ed. Piscataway, NJ: IEEE Press, 2002.

[39]. Sudhoff, S., Pekarek, S., Glover, S., Zak, S. et al., "Stability Analysis of a DC Power Electronics Based Distribution System," SAE Technical Paper 2002-01-3184, 2002, doi:10.4271/2002-01-3184.

[40]. K. Satpathi, N. Thukral, A. Ukil and M. A. Zagrodnik, "Flux estimation based dc bus voltage control in marine dc power system," *IECON 2016 - 42nd Annual Conference of the IEEE Industrial Electronics Society*, Florence, 2016, pp. 1815-1820.

[41]. R. Redl, B. P. Erisman, and Z. Zansky, “Optimizing the load transient response of the Buck Converter,” in Proc. 13th Annu. APEC’98, vol. 1, 1998, pp. 170–176

[42]. A. B. Jusoh, "The instability effect of constant power loads," *PECon 2004. Proceedings. National Power and Energy Conference, 2004.*, Kuala Lumpur, Malaysia, 2004, pp. 175-179.

[43]. A. Khaligh, "Realization of Parasitics in Stability of DC–DC Converters Loaded by Constant Power Loads in Advanced Multiconverter Automotive Systems," in *IEEE Transactions on Industrial Electronics*, vol. 55, no. 6, pp. 2295-2305, June 2008.

[44]. Yiming Tu, Zeng Liu, Jinjun Liu, Teng Liu and Zipeng Liu, "An additional stabilizer for mitigating the instability in DC/DC cascaded system with constant power loads," *2017 IEEE 3rd International Future Energy Electronics Conference and ECCE Asia (IFEEC 2017 - ECCE Asia)*, Kaohsiung, 2017, pp. 1982-1986.

[45]. X. Lu, K. Sun, J. M. Guerrero, J. C. Vasquez, L. Huang and J. Wang, "Stability Enhancement Based on Virtual Impedance for DC Microgrids With Constant Power Loads," in *IEEE Transactions on Smart Grid*, vol. 6, no. 6, pp. 2770-2783, Nov. 2015.

[46]. A. Emadi, A. Khaligh, C. H. Rivetta and G. A. Williamson, "Constant power loads and negative impedance instability in automotive systems: definition, modeling, stability, and control of power electronic converters and motor drives," in *IEEE Transactions on Vehicular Technology*, vol. 55, no. 4, pp. 1112-1125, July 2006.

[47]. Y. Zhao, W. Qiao and D. Ha, "A Sliding-Mode Duty-Ratio Controller for DC/DC Buck Converters With Constant Power Loads," in *IEEE Transactions on Industry Applications*, vol. 50, no. 2, pp. 1448-1458, March-April 2014.

[48]. Y. Li, K. R. Vannorsdel, A. J. Zirger, M. Norris and D. Maksimovic, "Current Mode Control for Boost Converters With Constant Power Loads," in *IEEE Transactions on Circuits and Systems I: Regular Papers*, vol. 59, no. 1, pp. 198-206, Jan. 2012.

[49]. D. Marx, P. Magne, B. Nahid-Mobarakeh, S. Pierfederici and B. Davat, "Large Signal Stability Analysis Tools in DC Power Systems With Constant Power Loads and Variable Power Loads—A Review," in *IEEE Transactions on Power Electronics*, vol. 27, no. 4, pp. 1773-1787, April 2012.

[50]. G. Sulligoi, D. Bosich, G. Giadrossi, L. Zhu, M. Cupelli and A. Monti, "Multiconverter Medium Voltage DC Power Systems on Ships: Constant-Power Loads Instability Solution Using Linearization via State Feedback Control," in *IEEE Transactions on Smart Grid*, vol. 5, no. 5, pp. 2543-2552, Sept. 2014.

[51]. M. Cupelli, M. Mirz and A. Monti, "Application of backstepping to MVDC ship power systems with constant power loads," *2015 International Conference on Electrical Systems for Aircraft, Railway, Ship Propulsion and Road Vehicles (ESARS)*, Aachen, 2015, pp. 1-6.

[52]. L. Zhu, J. Liu, M. Cupelli and A. Monti, "Decentralized Linear Quadratic Gaussian control of multi-generator MVDC shipboard power system with Constant Power Loads," *2013 IEEE Electric Ship Technologies Symposium (ESTS)*, Arlington, VA, 2013, pp. 308-313.

[53]. G. Sulligoi, A. Vicenzutti, V. Arcidiacono and Y. Khersonsky, "Voltage Stability in Large Marine-Integrated Electrical and Electronic Power Systems," in *IEEE Transactions on Industry Applications*, vol. 52, no. 4, pp. 3584-3594, July-Aug. 2016.

[54]. D. Bosich, A. Vicenzutti and G. Sulligoi, "Robust voltage control in large multi-converter MVDC power systems on ships using thyristor interface converters," *2017 IEEE Electric Ship Technologies Symposium (ESTS)*, Arlington, VA, 2017, pp. 267-273.

[55]. S. Cooper and H. Nehrir, "Ensuring stability in a multi-zone MVDC shipboard power system," *2017 IEEE Electric Ship Technologies Symposium (ESTS)*, Arlington, VA, 2017, pp. 380-387.

[56]. G. Sulligoi, D. Bosich, L. Zhu, M. Cupelli and A. Monti, "Linearizing control of shipboard multi-machine MVDC power systems feeding Constant Power Loads," 2012 IEEE Energy Conversion Congress and Exposition (ECCE), Raleigh, NC, 2012, pp. 691-697.

[57]. Z. Jin, L. Meng, J. M. Guerrero and R. Han, "Hierarchical Control Design for a Shipboard Power System With DC Distribution and Energy Storage Aboard Future More-Electric Ships," in IEEE Transactions on Industrial Informatics, vol. 14, no. 2, pp. 703-714, Feb. 2018.

[58]. Z. Jin, L. Meng and J. M. Guerrero, "Comparative admittance-based analysis for different droop control approaches in DC microgrids," *2017 IEEE Second International Conference on DC Microgrids (ICDCM)*, Nuremburg, 2017, pp. 515-522.

[59]. Z. Jin, L. Meng and J. M. Guerrero, "Constant power load instability mitigation in DC shipboard power systems using negative series virtual inductor method," *IECON 2017 - 43rd Annual Conference of the IEEE Industrial Electronics Society*, Beijing, 2017, pp. 6789-6794.

[60]. Z. Jin, L. Meng, R. Han, J. M. Guerrero and J. C. Vasquez, "Admittance-type RC-mode droop control to introduce virtual inertia in DC microgrids," *2017 IEEE Energy Conversion Congress and Exposition (ECCE)*, Cincinnati, OH, 2017, pp. 4107-4112.

APPENDIX PAPERS

PAPER A. Reference [57]

Hierarchical Control Design for Shipboard Power System with DC Distribution and Energy Storage aboard Future More-Electric Ships

Zheming Jin, Lexuan Meng, Josep M. Guerrero, and Renke Han

The paper has been published in

IEEE Transactions on Industrial Informatics, vol. 14, no. 2, pp. 703-714, Feb. 2018.

Hierarchical Control Design for a Shipboard Power System With DC Distribution and Energy Storage Aboard Future More-Electric Ships

Zheming Jin, *Student Member, IEEE*, Lexuan Meng, *Member, IEEE*, Josep M. Guerrero, *Fellow, IEEE*, and Renke Han, *Student Member, IEEE*

***Abstract*—DC distribution is now becoming the major trend of future mobile power systems, such as more-electric aircrafts and ships. As dc distribution has different nature to the conventional ac system, a new design of well-structured control and management methods will be mandatory. In this paper, a shipboard power system with dc distribution and energy storage system (ESS) is picked as the study case. To meet the requirement of control and management of such a large-scale mobile power system, a hierarchical control design is proposed in this paper. In order to fully exploit the benefit of the ESS, as well as to overcome the limitation in controllability, a novel inverse-droop control method is proposed, in which the power sharing is according to the source characteristic, instead of their power rating. A frequency-division method is also proposed as an extension to the inverse-droop method for enabling a hybrid ESS and its autonomous operation. On the basis of the proposed methods, the control methods for management and voltage restoration levels are also proposed to establish a comprehensive control solution. Real-time simulations are carried out to validate the performance of the proposed control design under different operating conditions. When compared to more conventional droop-based approaches, the new proposal shows enhancement in efficiency.**

***Index Terms*—DC distribution, energy storage, hierarchical control, islanded microgrid, more-electric ship (MES), shipboard power system (SPS).**

I. Introduction

DRIVEN by the increased onboard electrical power demand and the progressively stricter environmental requirements, marine industry is dedicating to develop new solutions for the future vessels [1]–[4]. In 1990s, power electronic converters (PECs) have made breakthrough in the field of marine vessels for enabling electrification of the propulsion systems through variable-voltage-variable-frequency drive technology [2]–[4]. The advantages obtained from PECs, including efficiency improvement, space saving, and maneuverability enhancement, have resulted in the current tendency to further electrify the vessel, namely more-electric ship (MES). In addition to the use of electric propulsion, the most important change is the new integrated power system design, in which the power generated aboard a vessel is now available for all the onboard systems instead of being exclusive for either propulsion or ship service loads [5]–[8].

In recent studies, several emerging technologies are being considered and installed aboard prototyping vessels to enhance the system performance, including dc distribution [9]–[11], energy storage systems (ESSs) [12], [13], low-emission power sources, e.g., fuel cell (FC) [14] and gas turbine genset [15], [16], and onboard renewable energy sources (e.g., photovoltaic (PV) array) [17]. Among them, dc distribution and the ESS can contribute to both the efficiency and reliability of the shipboard power system (SPS), thus becoming the trend of future MES [1], [2], [12]. Moreover, it is noteworthy that ESSs inherently operate in dc; therefore, the dc-distribution-based SPS (DC-SPS) is more efficient to integrate ESSs, as well as to support electric propulsion systems. Meanwhile, with the presence of ESSs, generators with slow dynamic (e.g., FC and gas turbine) or intermittence (i.e., renewables) and specific operating scenarios (e.g., zero-emission operation in port) can be easily enabled. In this case, future DC-SPSs are expected to be the flexible platform, which allows using various power sources as well as effectively supporting onboard loads with different characteristics, such as dynamic and pulsed-power loads [18]. However, the system-level control and management will remain a challenging issue, especially considering the fast-changing load conditions and mission setting of the vessel.

The PEC is the enabling technology of the DC-SPS, through which components with either ac or dc nature in different voltage levels can be connected to the dc distribution network. Several innovative PEC designs have been proposed in [19]–[21], aiming at the high-voltage high-power requirement of marine applications. However, the fast-switching nature of PECs makes their reliability and robustness much poorer than conventional transformers, which is a major obstacle to their application in marine vessels. For this reason, six-pulse and 12-pulse diode rectifiers are also used as a present-stage solution for interfacing gensets to the dc distribution network [1], [22]. Meanwhile, controllable PECs are indispensable as the

Manuscript received June 16, 2017; revised September 12, 2017; accepted October 19, 2017. Date of publication November 10, 2017; date of current version February 1, 2018. Paper no. TII-17-1282. *(Corresponding author: Zheming Jin.)*

The authors are with the Department of Energy Technology, Aalborg University, 9100 Aalborg, Denmark (e-mail: zhe@et.aau.dk; lme@et.aau.dk; joz@et.aau.dk; rha@et.aau.dk).

Color versions of one or more of the figures in this paper are available online at http://ieeexplore.ieee.org.

Digital Object Identifier 10.1109/TII.2017.2772343

1551-3203 © 2017 IEEE. Personal use is permitted, but republication/redistribution requires IEEE permission.
See http://www.ieee.org/publications_standards/publications/rights/index.html for more information.

"dc transformers" to interface ESSs and FCs. In this context, the present-stage DC-SPS is an interesting mix of uncontrollable and controllable PECs, thus introducing unique challenges and additional troubles on control design.

Technically speaking, the future DC-SPS features in isolated operation and diversified power sources; thus, it is reasonable to identify them as islanding microgrids (MGs). It is noteworthy that the major challenges are essentially the same in both applications, which is to maintain self-sustainable operation of the islanding power system. During the past decade, there have been active research activities undergoing in the field of terrestrial MGs, resulting in advanced research outcomes reported in [23]–[28]. Currently, the multilayer hierarchical control architecture is widely used and becoming a standardized solution for terrestrial MGs, in which different control and management objectives are solved independently as different control layers [23]. However, the hierarchical control architecture is rarely reported in the field of DC-SPSs.

In this paper, a three-layer hierarchical control design is proposed for the DC-SPS with considerations of the particularities in shipboard applications and diesel-dominant generation. For the power-sharing level control, a novel inverse-droop control method is proposed to coordinate the output power of gensets and ESSs with respect of their different characteristics. In addition to that, a frequency-division method is also proposed as an extension of an inverse-droop method to enable a hybrid energy storage system (HESS) and its characteristic-based autonomous operation. For the higher level control, the control method to achieve power management and nominal bus voltage restoration functions are presented to provide a comprehensive control architecture for the DC-SPS.

The rest of this paper is organized as follows. In Section II, the state of the art of the DC-SPS is introduced. Section III gives a detailed introduction of the proposed methods and hierarchical control design. In Section IV, hardware-in-loop simulations are carried out with the study case of the DC-SPS. A comparison is made between droop-controlled and inverse-droop-controlled cases. Section V concludes this paper.

II. DC-SPS and Its Major Components

Recommended by *IEEE Standard 1709-2010* [1], a typical case DC-SPS includes gensets, FCs, and ESSs as power sources, electric propulsion systems, and ship-service loads as power consumer. Moreover, onboard renewables are recently taken into consideration as optional power sources. For all vessels to be classified by classification societies like DNV GL and ABS, the most important rule in early-stage design of the SPS is to always have enough power to keep the vessel in position, even if some major parts have failed. For this reason, an SPS should have at least two independent subsystems, and therefore, a zonal electric distribution system (ZEDS), as illustrated in Fig. 1, is preferred for its fault tolerance and reconfiguration capability [10], [11]. Such a system can be sectionalized into several MGs with a simplified single-line structure, as shown in Fig. 2. It is also noteworthy that each of these zonal MGs is expected to be self-sustainable and controlled independently, especially in

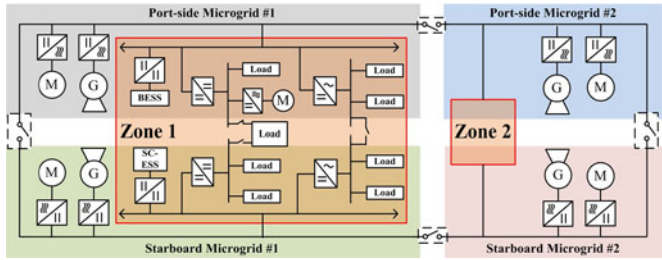

Fig. 1. Illustration of a typical ZEDS-based architecture and its sectionalizing.

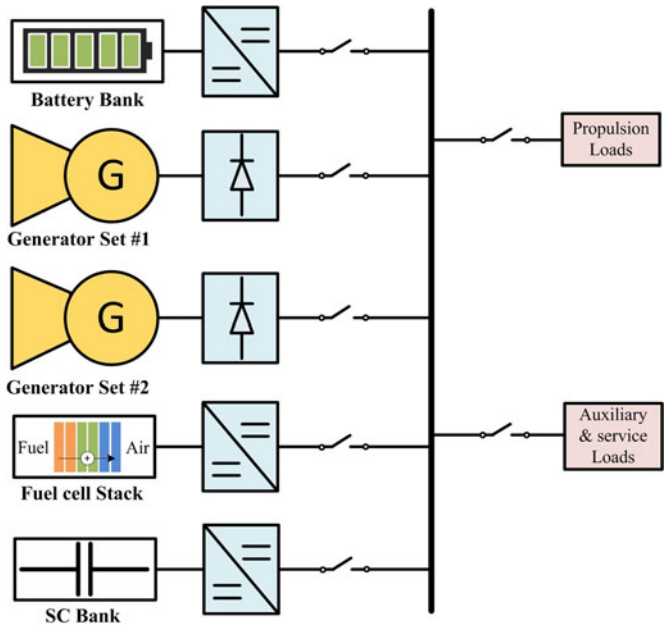

Fig. 2. Simplified single-line diagram of a sectionalized MG in the DC-SPS.

the case of naval vessels. Meanwhile, "$N+X$" redundant design is common in marine vessels, in which extra gensets with the same type are installed for backup and alternation.

The nominal voltage of a DC-SPS is case-by-case designed, varying from 690 to 6600 V [1], [29]. Correspondingly, the total power demand of the system can be hundreds of kilowatts to tens of megawatts depending on the different types/classes and the different usage of the vessel. Normally, the propulsion systems will consume most of the onboard power with some load fluctuations due to the inherent uncertainty of the water surface [2]. In addition, the unique dynamic positioning (DP) operation of drilling and supporting vessels will introduce fast and dramatic load changing to the system.

In the following part of this section, the major components and the state-of-the-art control solution are introduced.

A. Gensets: The Major Power Sources

In marine applications, gensets composed by prime movers (either diesel engine or gas turbine) and well-proven alternators are the most important power sources. So far, a diesel engine with a synchronous generator (SG) is the mainstream choice for both AC and DC SPSs. Meanwhile, a high-speed gas turbine

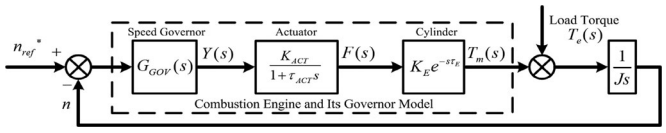

Fig. 3. Block diagram of the reduce-order mechanical model for genset.

coupled with a permanent magnet generator (PMG) is drawing attention for its better efficiency and reduced volume. In the case of DC-SPS application, an active or passive rectifier is also mandatory to utilize the power of gensets. Due to industrial concerns of cost and robustness, passive rectifiers are currently more frequently used in present-stage DC-SPSs. It is noteworthy that passive rectifiers cannot achieve decoupled control of output power, which means the mechanical dynamics will affect the transient of the DC-SPS. Therefore, it is necessary to model the mechanical part while analyzing DC-SPSs. In this paper, mature generator models provided by SimPowerSystem are employed, while the mechanical part is approximately modeled by a conventional PID controller, an actuator, and engine delay as shown in Fig.3 [29], [30], formulated as

$$T_m(s) = \frac{K_{\text{act}}}{1+\tau_{\text{act}}s} \times K_{de}e^{-\tau_{de}s} \times Y(s) \tag{1}$$

$$\tau_{\text{act}} \approx 0.9/2\pi n \quad \tau_{de} \approx 1/2nN \tag{2}$$

where T_m is the mechanical torque, K_{act} is the actuator gain, K_{de} is the engine torque gain, J is the moment of inertia, n is the rotating speed of the coaxial structure, and N is the number of cylinders.

In the case of using a diode rectifier, a comprehensive steady-state analysis of its output characteristic when connected to a voltage-controlled bus has been made in [30]. In the practical operation, the diode-rectified SG will typically work in the commutation mode, in which an approximated linear relationship between output power and bus voltage is reported and analyzed in [31] and [32]; the average value function is given as

$$V_{\text{dc}} = \frac{3\sqrt{3}}{\pi}V_m - \frac{3}{\pi}\omega_e L_{\text{ac}} I_{\text{dc}} \tag{3}$$

where V_m is the peak value of phase voltage, ω_e is the electrical angular speed, L_{ac} is the ac-side inductance (i.e., synchronous inductance of the SG), and I_{dc} is the average value of output current.

B. Excitation Control Scheme: State-of-the-Art Solution

Excitation-based control is a cost-effective state-of-the-art solution for bus voltage regulation in DC-SPSs [22], [33]. In Fig. 4, the control scheme is illustrated. It can be regarded as a variant of the automatic voltage regulator from ac applications in the DC-SPS. The control principle is to adjust the output voltage of the SG by controlling the excitation current [33]. A detailed control principle can be formulated as follows:

$$\begin{cases} V_{\text{qs}} = R_{\text{qs}}I_{\text{qs}} + \omega_e L_{\text{ds}} I_{\text{ds}} + \omega_e L_m I_f \\ V_{\text{ds}} = R_{\text{ds}}I_{\text{ds}} - \omega_e L_{\text{qs}} I_{\text{qs}} \end{cases}$$

$$V_m = \sqrt{{V_{\text{ds}}}^2 + {V_{\text{qs}}}^2}\Big|_{I_{\text{ds}}=I_{\text{qs}}=0} = \omega_e L_m I_f = \omega_e \psi_f \tag{4}$$

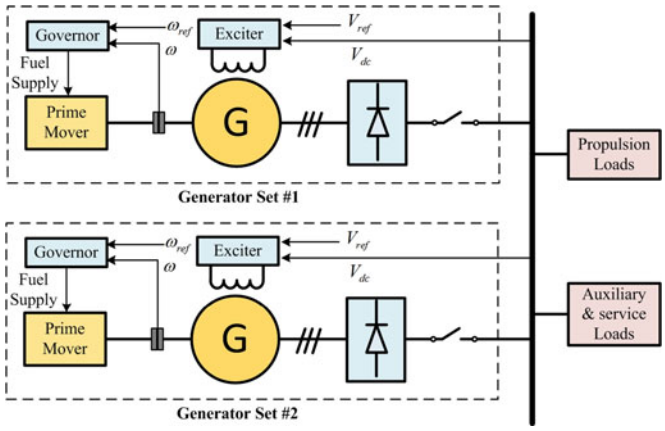

Fig. 4. Illustration of the excitation control scheme.

$$V_{\text{dc}} = \frac{3\sqrt{3}}{\pi}\omega_e\psi_f + \frac{3\sqrt{3}}{\pi}\omega_e\delta\psi - \frac{3}{\pi}\omega_e L_s I_{\text{dc}} \tag{5}$$

$$\delta\psi = K_p^{\text{ex}}\left(V_{\text{ref}}^* - V_{\text{dc}}\right) + K_i^{\text{ex}}\int\left(V_{\text{ref}}^* - V_{\text{dc}}\right)dt \tag{6}$$

where ψ_f is the excitation flux established by an exciter; L_m is the magnetizing inductance of the SG; I_{ds}, I_{qs}, L_{ds}, and L_{qs} are the stator current and inductance components expressed in the dq reference frame, respectively; and I_f is the excitation current.

Although the excitation control scheme is easy to implement in the real-world engineering, its drawbacks are also noteworthy. First, the control bandwidth of excitation control is limited, which is a considerable problem due to the highly dynamic load conditions of marine vessels. Second, the control scheme will not provide damping effect to the measurement errors among paralleled gensets. Therefore, the measurement error of the bus voltage can lead to inappropriate power sharing among gensets, which can result in overloading and idling. Last but not least, it is also noteworthy that the excitation control solution is inherently impossible to work with the PMG.

C. Onboard ESS

During the recent decades, the energy storage and associated technologies have received a substantial increase in attention. In marine applications, the battery takes an overwhelming majority of the existing shipboard ESSs, growing steadily because of its ever-improving performance. Meanwhile, supercapacitor (SC)-based ESSs are also gaining population in short-term power-intensive or repetitive applications. In addition, flywheels are also considered for their power density and inherent resistance to humid operating environment, even though their installation and operation need to be done in pairs, thus compensating the mechanical effect on the vessel's balancing.

One of the major challenges for shipboard ESSs is that the marine applications have high requirements on both peak power and capacity, which is usually neither technically easy nor economically efficient to be fulfilled simultaneously by any single type of storage. Therefore, the HESS is a potential solution to this problem; however, it will leave a challenging task to the power and energy management of the system.

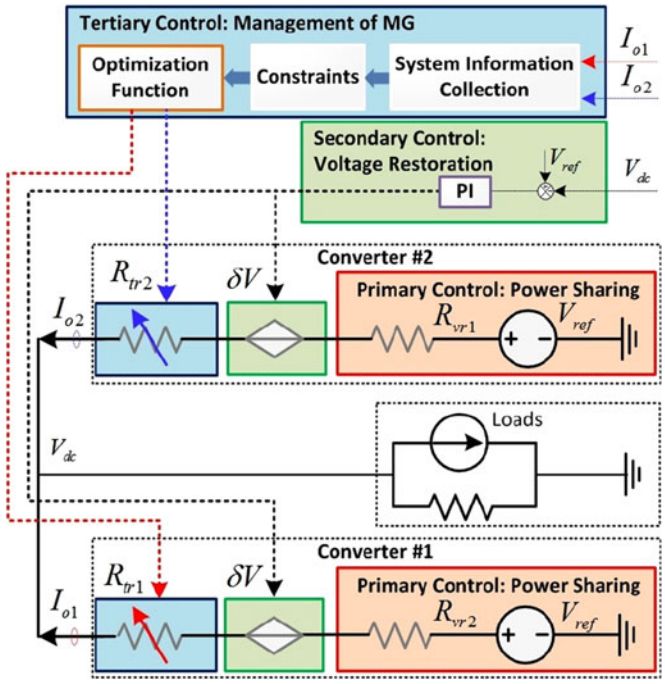

Fig. 5. Illustration of hierarchical control architecture in terrestrial DC MGs.

D. Alternative Power Sources: FC and PV Array

Recently, alternative power sources have been considered to be installed aboard a ship to reduce the cost and emission. FCs have been installed aboard several prototype vessels to provide cleaner power source. There are also conceptual designs using the PV array to fully or partially power the onboard equipment. The noteworthy problem is that the dynamic power response of an FC is far slower than other kinds of electrical power sources, whereas the PV array is an intermittent source with inherent uncertainty. For this reason, it is necessary to install FCs and the PV array coupled with the ESS, and therefore, meet the requirement of power availability.

III. Proposed Hierarchical Control Design for the DC-SPS

Droop-based hierarchical control architecture is currently the state-of-the-art control solution in the field of terrestrial dc MGs and other similar systems [23]–[28]. In Fig. 5, the physical model of typical droop-based hierarchical control architecture is illustrated. The three control layers are defined as follows [23]:

1) primary control: the control layer focusing on proper power sharing among generation units;
2) secondary control: the control layer that focusing on power quality issue (mainly bus voltage in DC MG) of the system;
3) tertiary control: the control layer that focusing on power/energy management and optimization of the system.

Although hierarchical control is an advanced comprehensive solution, it may not be suitable to implement in the DC-SPS directly. The major problem is that the conventional voltage droop method is not recommended in diesel-dominant systems because the fuel efficiency of genset is not constant. On the contrary, the optimal fuel efficiency will only appear at a certain operating point around 80–90% of the rated power and degrades considerably under both light- and heavy-load conditions [2]. Moreover, the load fluctuations will also increase the fuel consumption and introduce mechanical issues.

In addition to that, the limited controllability will be another major challenge. It is noteworthy that the control bandwidth of excitation control is very limited; nevertheless, the situation can be even worse if PMGs coupled with a diode rectifier are used (as recommended in [1]).

In order to resolve the aforementioned problems, especially to overcome the limited controllability, the concept of the inverse-droop control method is proposed in this paper. Based on the new proposal, a hierarchical control design is presented. The detailed method and implementation are shown in the following parts of this section.

A. Proposed Methods: Cooperative Inverse-Droop Control

The conventional droop control method is typically used as the primary control level of hierarchical control architecture. Its control effect is to add a virtual resistance (VR), thus achieving properly power-sharing effect among all the power sources in the droop control mode (DCM). The principle is formulated as

$$V_{\rm dc} = V^*_{\rm ref} - R_{\rm vri} I_{\rm oi} \tag{7}$$

or linearized as follows, which is also widely used:

$$V_{\rm dc} = V^*_{\rm ref} - m_i P_{\rm oi} \quad m_i = R_{\rm vri}/V_{\rm nom} \quad \text{when} \quad V_{\rm dc} \approx V_{\rm nom} \tag{8}$$

where $R_{\rm vri}$ is the VR of the ith converter, $I_{\rm oi}$ is the output current of the ith converter, $P_{\rm oi}$ is the output power of the ith converter, $V^*_{\rm ref}$ is the voltage reference, $V_{\rm nom}$ is the nominal voltage, and m_i is named as the droop coefficient or the power droop coefficient.

When compared with more conventional voltage control mode (VCM) and current control mode (CCM), the DCM shows swing characteristic. In practical works, DCM sources are usually achieved by a conventional VCM controller with voltage reference determined by (7). The equation clearly shows the mechanism of the DCM; however, it can also be deformed into the following form:

$$I_{\rm oi} = \tfrac{1}{R_{\rm vri}} \left(V^*_{\rm ref} - V_{\rm dc}\right) \text{ or } P_{\rm oi} = \tfrac{1}{m_i} \left(V^*_{\rm ref} - V_{\rm dc}\right). \tag{9}$$

Equation (9) reveals the hidden side of DCM sources instead of conventional understanding (i.e., controlled voltage source). It shows that DCM sources can be identified as controlled current/power sources with respond to the voltage deviation. If the voltage deviation is determined, the output of the DCM source will be accordingly determined and *vice versa*. It also indicates the possibility to coordinate the output power of DCM sources by controlling the voltage deviation (i.e., intentional control of the bus voltage), which is defined as the inverse-droop control method. For a determined amount of output power, the voltage

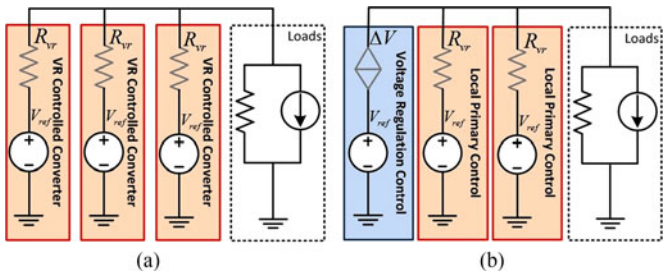

Fig. 6. Equivalent circuit of droop and inverse-droop methods. (a) Droop method. (b) Proposed inverse-droop method.

reference can be calculated by

$$V_{\mathrm{dc}}^{*}=\frac{1}{2}\left(V_{\mathrm{ref}}^{*}+\sqrt{V_{\mathrm{ref}}^{*2}-4R_{\mathrm{eq}}P_{\mathrm{ref}}}\right)\quad R_{\mathrm{eq}}=1/\sum_{i=1}^{n}\left(\frac{1}{R_{\mathrm{vri}}}\right) \tag{10}$$

$$V_{\mathrm{dc}}^{*}=V_{\mathrm{ref}}^{*}-m_{\mathrm{eq}}P_{\mathrm{ref}}\quad m_{\mathrm{eq}}=1/\sum_{i=1}^{n}\left(\frac{1}{m_i}\right) \tag{11}$$

where R_{eq} is the equivalent droop resistance of the system, m_{eq} is the equivalent power droop coefficient of the system, P_{ref} is the total amount output power, V_{dc}^{*} is the calculated reference.

In Fig. 6, the equivalent circuits of more conventional droop method and inverse-droop method are illustrated. In an inverse-droop-based system, the proportional power-sharing effect among DCM sources is maintained. Meanwhile, the entire system will still be well damped for the measurement error if there is only one source operating in the VCM to clamp the bus voltage.

However, the differences are noteworthy. In the inverse-droop-based system, the voltage is regulated directly instead of floating; therefore, DCM sources are behaving more in the CCM side. Meanwhile, the VCM source is providing controllability to the whole system, while the DCM sources are providing power and damping effect. Conclusively, from the perspective of functionality, power sources are symmetrical in the droop method, whereas they are asymmetrical but cooperative in the proposed inverse-droop method.

In the case of using diode-rectified gensets, their inherent droop characteristic presented in (3) can also be generalized in the same form as (7), therefore following the same principle in both sides. By assuming that excitation current is constant (i.e., regarding the SG as the PMG), the relationship in (11) is deformed as follows to describe the behavior in different operation points of the alternator:

$$V_{\mathrm{dc}}=(\omega_{ei}/\omega_{\mathrm{base}})\left[V_{\mathrm{base}}-m_{\mathrm{base}i}P_{\mathrm{oi}}\right],\ \text{where}\quad m_{\mathrm{base}i}=m_i\big|_{\omega_e=\omega_{base}} \tag{12}$$

where ω_{ei} is the rotational speed of the ith genset, ω_{base} is the base speed for calculation, P_{oi} is the output power of the ith genset, V_{base}^{*} is the open-circuit voltage in base speed.

From the viewpoint of the DC-SPS, the benefits of the proposed inverse-droop control method are very considerable. First, the load fluctuations will be naturally absorbed by the VCM source, so that the DCM sources can work under the constant load condition; moreover, the operation point is fully adjustable. In this case, the VCM source will automatically provide supporting functions to the system, including spinning reserve, peak-shaving, and load conditioning. It is important to notice that these supporting functions are exactly the same as the expected functions of using ESSs in SPSs as listed in [2]. In another word, the new proposal provides an effective method to integrate ESSs in the DC-SPS and to exploit the benefit. Second, when compared with conventional methods, the regulation of bus voltage can benefit from the higher control bandwidth and faster dynamic response with the help of a controllable PEC. Third, in the new proposal, the controllable PECs (as VCM sources) can be used to coordinate operation of DCM sources (e.g., diode-rectified gensets), thus exploiting the complementary advantages. It also makes it possible to use PMGs with a simple diode rectifier as a power source, which can reduce the cost and volume of the generating units.

B. Proposed Methods: Frequency-Division Control Method as an Extension to Inverse-Droop Control

As mentioned in Section II, the HESS is a potential solution to meet the high requirement on both power and energy densities instead of the centralized ESS in shipboard applications. However, it will also introduce a challenge to the control and management because the complexity will increase dramatically. In addition to that, the introduction of the HESS in the proposed inverse-droop control method requires additional control design; otherwise, it will introduce a paralleled VCM source without enough damping resistance. For these reasons, additional control methods are worthy and necessary to be introduced into the proposed inverse-droop control method to make it compatible with the HESS and benefits from HESS's advantage.

Since the initial intention of using the HESS is to take the complementary advantage in power and energy densities, the power sharing among different ESSs should be compliant with their diverse nature of dynamic response rather than capacity or power rating. SCs can provide good performance in high-power or repetitive applications. Batteries, on the other hand, are much better in long-term power support with limited dynamics. From the perspective of frequency domain, the asymmetrical power-sharing effect of the inverse-droop method can be regarded as dividing the load power into baseline power ($f = 0$) and power fluctuations ($f > 0$), and only baseline power is shared among DCM sources. One step further, the power fluctuations can be subdivided into low-frequency part and high-frequency part In Fig. 7, the principle of proposed frequency-division method is illustrated. These two parts can be taken by batteries and SCs, respectively, thus making them cooperative in the dynamic power sharing.

In order to subdivide the power fluctuations cooperatively, the simplest method is to insert paired low-pass and high-pass filters into the inner-loop controllers, thus differentiating the dynamic response of different ESSs. With effective frequency- division design, the system can spontaneously employ the complementary advantage from the HESS without interventions from the management level. Moreover, the stability issue can also be overcome because the measurement error (especially the static

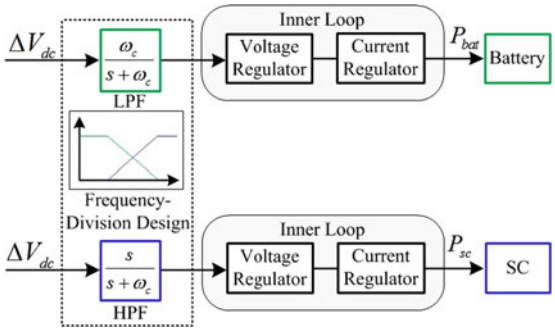

Fig. 7. Frequency-division design for inverse-droop control with the HESS.

component) will be filtered by a high-pass filter, thus avoiding unwanted incremental currents. In addition to that, it is noteworthy that with the proposed frequency-division control method together with the inverse-droop method, the characteristic-based power sharing can be achieved among different sources.

C. Proposed Methods: Higher Levels of Hierarchical Control Design

In addition to the control and coordination of multiple power sources, the medium-/long-term management of fuel efficiency is equally important in the practical operation of the DC-SPS due to the "pay-per-used" nature of diesel generation. Meanwhile, the zonal-level subsystems should be able to merge as entirety; thus, secondary control of the bus voltage is needed. In this case, higher level control methods are introduced on the basis of the proposed power-sharing-level control methods in the earlier discussion.

1) Management-Level Control: For SPSs, the management-level control of power generation typically includes two control activities, i.e., the management of the number of running gensets and the optimization of the fuel efficiency of the running gensets. With the presence of ESSs in the DC-SPS, it is possible to perform ON/OFF control of gensets according to the state of charge of battery-based ESSs. For this reason, the discussion of management-level control in this paper focuses more on the methods of realizing desired fuel efficiency. The fuel efficiency of a genset is related to many different variables, including the load torque, engine speed, air temperature, coolant temperature, atmospheric pressure, etc. As an empirical conclusion, in a standard test environment, the optimal fuel efficiency will appear when the output is 80–90% of the rated torque/load, and it will vary according to the engine speed. An approximated fuel efficiency calculation function is established and detailed in the Appendix.

In terrestrial MGs, the power management-level control is usually related to adjusting the VR of source converters and, therefore, managing their output power. However, the droop coefficient of the diode rectifier is determined by (3), and it cannot be intentionally adjusted. Thus, the conventional VR-based method for system management needs to be changed. With the proposed inverse-droop control method, the outputs of gensets are determined by the voltage deviation, as shown in (9). It indicates that the power management can also be achieved by introducing additional adjustable voltage deviation to different sources to achieve desired outputs. To realize that, a simple PI controller can be used, as shown in (13). In practical work, the voltage deviation can be generated by an excitation regulator, as shown in (14):

$$\begin{cases} P_{\mathrm{oi}} = \left(V_{\mathrm{ref}}^{*} - V_{\mathrm{dc}} + \delta V_i\right)/m_i \\ \delta V_i = K_p^{ML}\left(P_{\mathrm{oi}}^{*} - P_{\mathrm{oi}}\right) + K_i^{ML}\int\left(P_{\mathrm{oi}}^{*} - P_{\mathrm{oi}}\right)dt \end{cases} \tag{13}$$

$$\delta V_i = K_p^{ML}\left(P_{\mathrm{oi}}^{*} - P_{\mathrm{oi}}\right) + K_i^{ML}\int\left(P_{\mathrm{oi}}^{*} - P_{\mathrm{oi}}\right)dt = \frac{3\sqrt{3}}{\pi}\omega_e\delta\psi_i. \tag{14}$$

2) Voltage-Restoration-Level Control: In terrestrial MGs, voltage restoration control is working as secondary control to compensate the voltage drop introduced by the droop method. However, this control level is hardly reported in the field of DC-SPSs. It is mainly because that shipboard equipment is required to be able to work within a wide range of dc-bus voltage. Yet, this control level will be necessary to achieve system-level interconnection [34].

To proceed the voltage restoration function, a global offset will be needed to the original open-circuit voltage setting; thus, the desired power-sharing function can be maintained. To generate the global offset, an additional PI controller can be used and added into the proposed control scheme as an independent level to its lower control levels. It is also noteworthy that the PI controller needs to be relatively slow to avoid conflicting with other control levels. Ultimately, the comprehensive control diagram of the proposed hierarchical control design is shown in Fig. 8.

IV. Real-Time Simulation Results

In order to validate the methods presented in this paper, real-time simulations in detailed switching level are carried out with the Opal-RT real-time simulator. A notional DC-SPS with the same configuration as shown in Fig. 2 is used as the study case. The parameters of each component and corresponding control loops are shown in Table I. To compare the performance of the proposed method with a more conventional droop-based control method, simulations of the same study case are also carried out using the droop method, which is shown in Fig. 9 with detailed parameters in Table I.

Two operating scenarios are set to verify the proposed methods. In the first scenario, the load condition is set to emulate the acceleration process, in which the propulsion load increased from zero to its full power. In the second scenario, the load condition is set to emulate the DP process of vessel, in which the propulsion power performs a fast periodical change, therefore verifying the performance of the proposed control methods. Simulations are carried out with the conventional droop method (for comparison) and the proposed hierarchical control design with centralized ESS (using battery) and HESS (using the frequency-division method), respectively, as a comparative study. The simulation results of the two scenarios with these control methods are shown in the following parts.

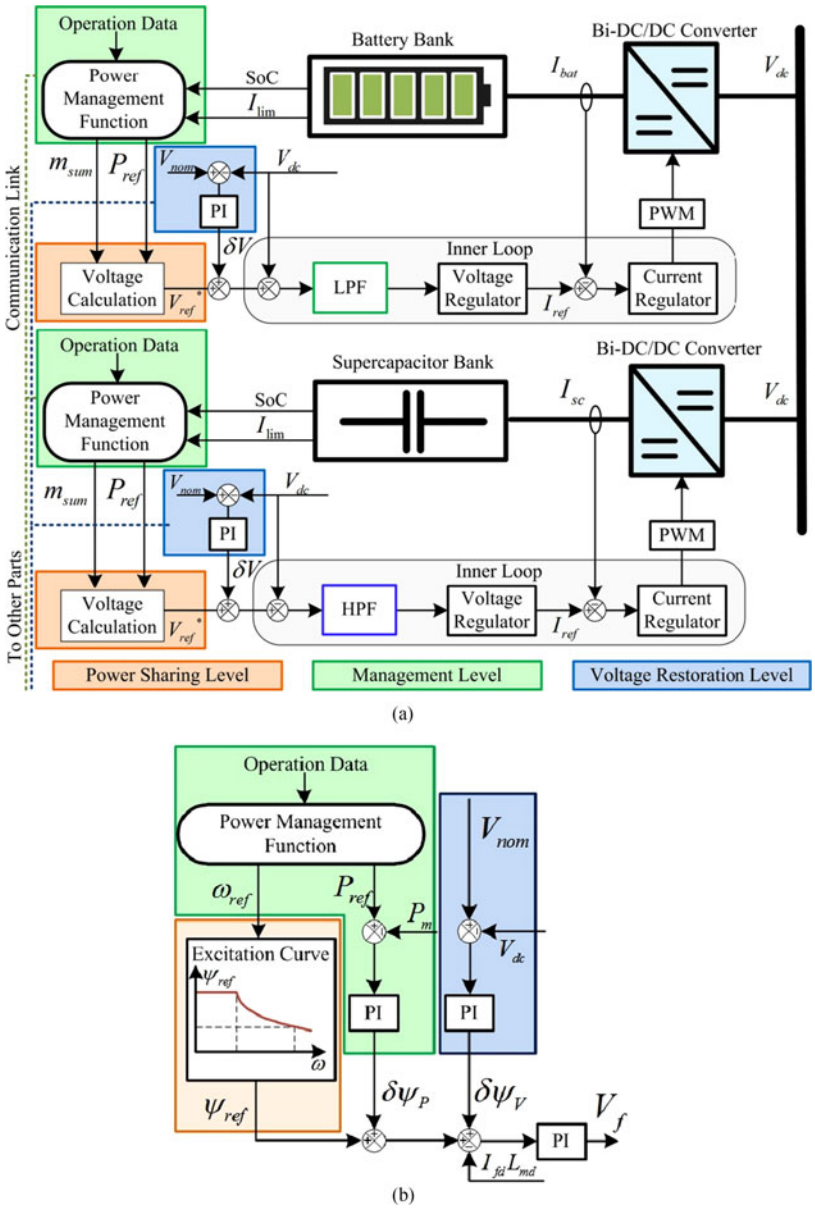

Fig. 8. Implementation of the proposed hierarchical control design in different controllers. (a) In ESS controllers. (b) In excitation regulator.

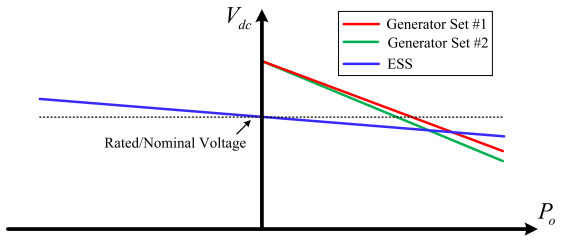

Fig. 9. Illustration of the droop control method used for comparison.

A. Scenario 1: Full-Load Acceleration Process

In this simulation scenario, a notional full-load operation is emulated, including initializing of the system followed by an acceleration process. In Fig. 10, the simulation results of droop-controlled operation are shown. In Figs. 12 and 14, the results using the proposed method with the centralized ESS and HESS are detailed. The simulation scenario can be divided into the following stages.

1) *Stage 1* $(0$–$t_1)$*:* In this stage, the grid-forming process is emulated. The bus voltage is initialized by the ESS in this stage. Meanwhile, the genset #1 accelerates from idle speed to its rated speed to supply power in the next stage.
2) *Stage 2* $(t_1$–$t_2)$*:* At t_1, genset #1 is connected to supply power and the propulsion load starts increasing to maximum. The voltage reference decreases as response of power-sharing level. In the droop-based approach, the droop coefficient is set to make the output of a single genset equal to 85% of its rated power (280 kW) at a full-load condition. In the proposed method, the power reference is also set to be 280 kW.

TABLE I
POWER STAGE AND CONTROL PARAMETERS

Category	Parameter	Value	Unit
DC Bus	Nominal voltage (range)	1500 (±10%)	V
Gensets	Nominal rotational speed	1800	r/min
	Rated power	330	kW
	Synchronous inductance	0.969	mH
	Rated line voltage (@1800 r/min)	1215	Vrms
Battery	Rated capacity	265.2	kWh
	Maximum power (dis-/charge)	390/390	kW
	Switching frequency	1	kHz
SC	Rated capacitance	2200	F
	Rated voltage	288	V
	Maximum capacity	91	MJ
	Switching frequency	10	kHz
FC	Rated power	100	kW
Loads	Rated propulsion power	625	kW
	Auxiliary power	85	kW
Inner-loop Controllers	Battery voltage controller (P/I)	1/125	–
	Battery current controller (P/I)	0.0015/0.20	–
	SC voltage controller (P/I)	10/1000	–
	SC current controller (P/I)	0.0045/0.20	–
	Cutoff frequency of paired filters	5	Hz
Power-Sharing Level	Base voltage	1640	V
	Base rotational speed	1800	rpm
	Base droop coefficient	0.5	V/kW
Management Level	Notional optimal operation point 1	300/1800	kW/r/min
	Notional optimal operation point 2	260/1700	kW/r/min
	Voltage deviation controller (P/I)	0.5/5	–
Voltage Restoration Level	Voltage restoration controller (P/I)	0.1/10	–
ESS Droop Control	Initial voltage reference	1500	V
	Droop coefficient	0.3	V/kW

3) *Stage 3* (t_2–t_3)*:* At the start of this stage, the management level is activated, gradually updating the power reference.
4) *Stage 4* (t_3–t_4)*:* The state of charge of the battery falls below the threshold and triggers ON/OFF management. At t_3, genset #2 accelerates from idle speed and connected into the system. The management level optimizes the operation point after reaching the steady state, including both output power and rotational speed.
5) *Stage 5* (t_4–$20s$)*:* At t_4, the proposed voltage-restoration-level control is activated; the dc-bus voltage is gradually restored to its rated value (i.e., 1500 V).

B. Scenario 2: DP Process

In this simulation scenario, the propulsion load is set to be changing between 25% and 100% periodically, instead of being constant, to emulate the highly dynamic load behavior in a DP process. The simulation results are shown in Figs. 11, 13, and 15. This scenario can be divided into the following stages.

1) *Stage 1* (0–t_1)*:* The same grid forming as scenario 1 is performed in this stage to initialize the system.
2) *Stage 2* (t_1–t_2)*:* In this stage, the loads are supplied by genset #1 and ESSs; the peak-shaving function is performed.

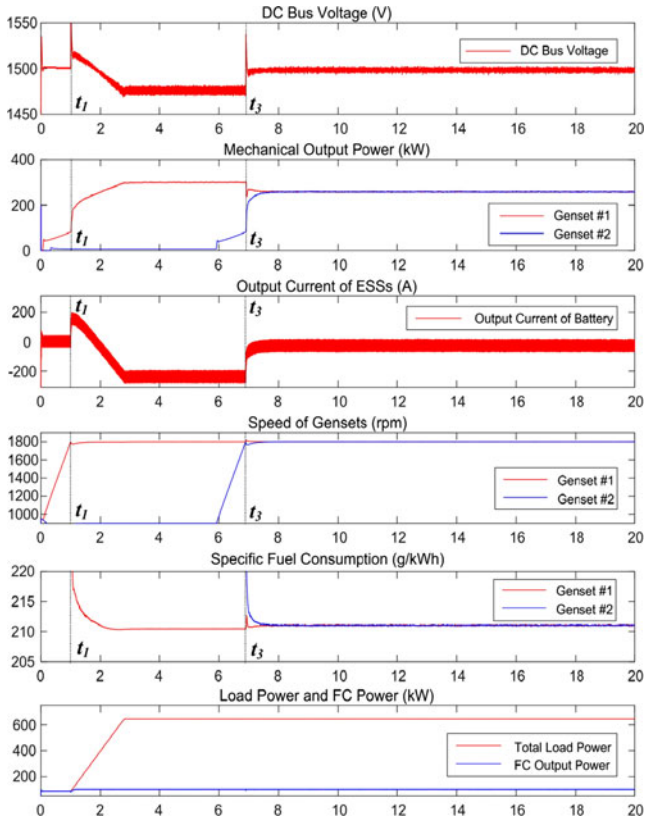

Fig. 10. Simulation results of scenario 1 using the conventional droop control method.

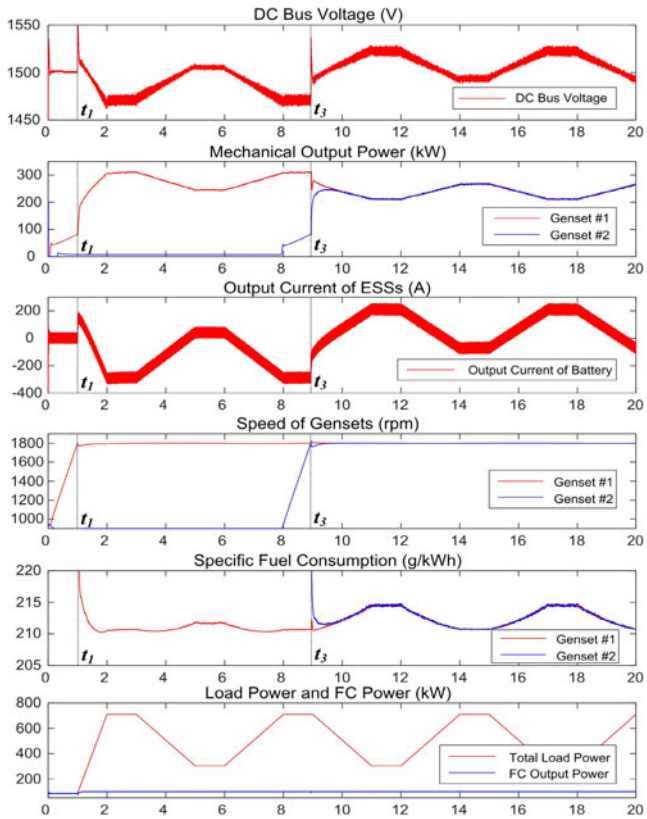

Fig. 11. Simulation results of scenario 2 using the conventional droop control method.

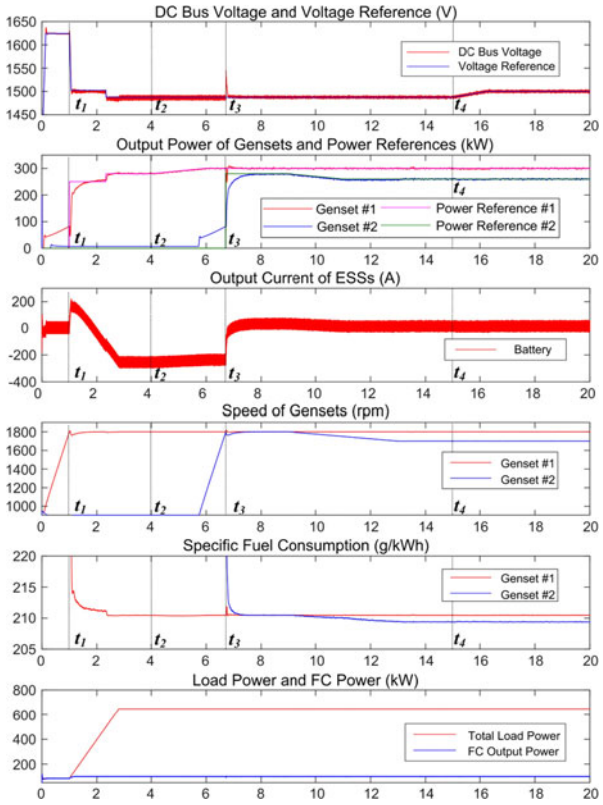

Fig. 12. Simulation results of scenario 1 using the proposed hierarchical control design with the centralized ESS.

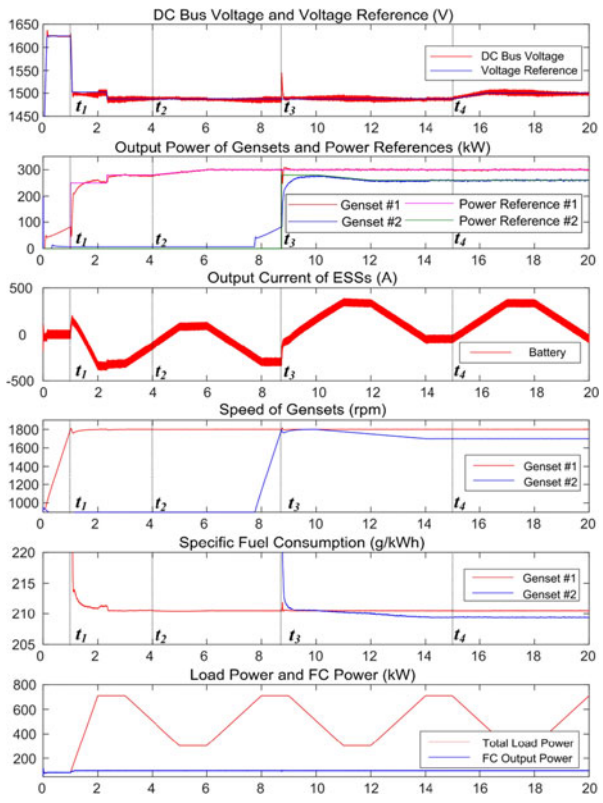

Fig. 13. Simulation results of scenario 2 using the proposed hierarchical control design with the centralized ESS.

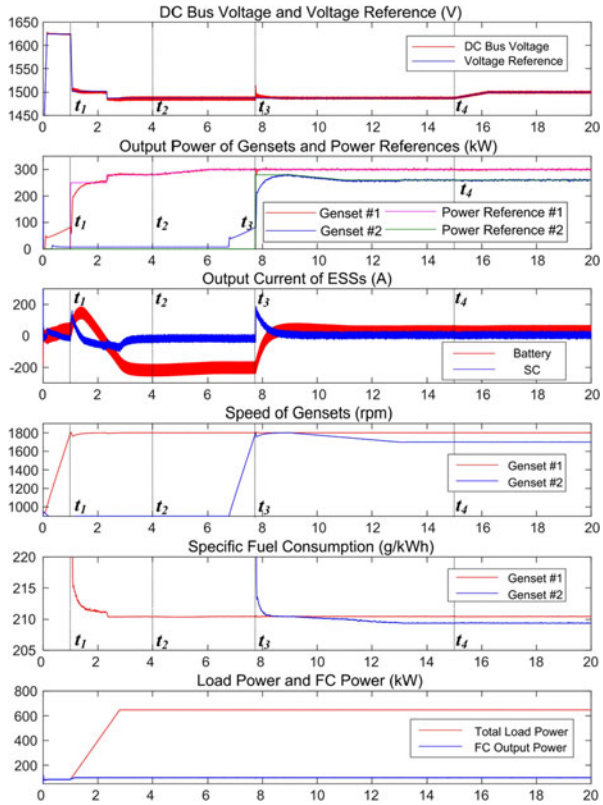

Fig. 14. Simulation results of scenario 1 using the proposed hierarchical control design with the HESS and the frequency-division method.

3) *Stage 3–*(t_2t_3)*:* During this stage, the management level starts to optimize the operation of genset #1 to its optimum.
4) *Stage 4* $(t_3$–$t_4)$*:* At t_3, the ON/OFF management is executed. Genset #2 is connected into the system after acceleration. Afterwards, the management level adjusted its operation point.
5) *Stage 5* $(t_4$–$20s)$*:* At t_4, the proposed voltage-restoration-level control is activated, and dc-bus voltage starts to be restored to its rated value (i.e., 1500 V).

C. Discussion and Comparison on Simulation Results

From the simulation results, several noteworthy conclusions can be derived. First, from Figs. 10 and 11, it is shown that the well-designed droop method can provide an acceptable fuel efficiency in its rated load condition; however, under dynamic load conditions, the fuel efficiency will degrade. Second, from Figs. 12 and 13, it is shown that the desirable power-sharing effect among onboard power sources can be achieved by the inverse-droop method, regardless of load conditions. It is worthy to notice that these two control methods are realized with exactly the same hardware configuration. In addition, the proposed management-level and voltage-restoration-level functions can be achieved independently. Third, from Figs. 14 and 15, with the proposed frequency-division method, the battery and SC-based ESSs can work cooperatively within the proposed hierarchical

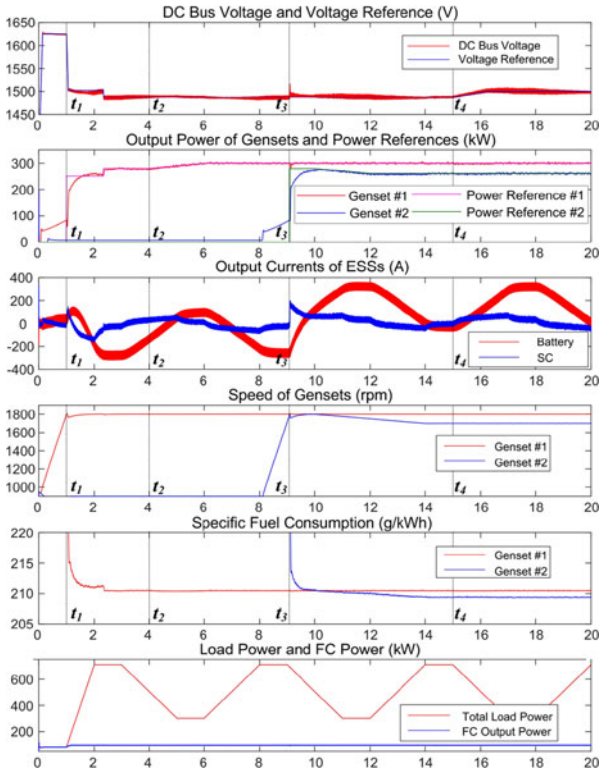

Fig. 15. Simulation results of scenario 2 using the proposed hierarchical control design with the HESS and the frequency-division method.

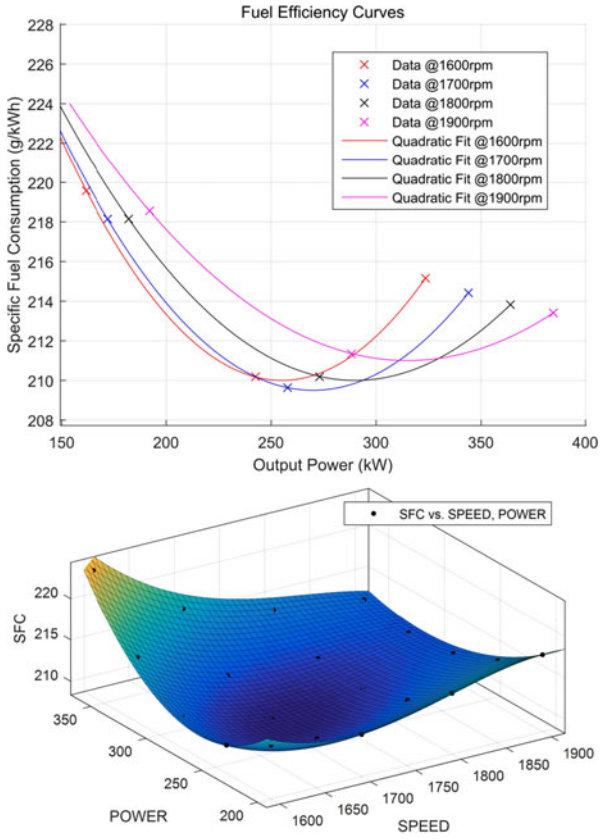

Fig. 16. Fuel efficiency evaluation model.

control design. The dynamic power sharing is desirable, i.e., the battery is providing long-term power supply with relatively slow dynamic while the SC is providing short-term power with a fast response.

Although the acceptable control effects are achieved with both the centralized ESS and frequency-division-controlled HESS solutions, there are still noteworthy differences. When compared with the battery solution, the voltage regulation using the HESS has a faster response and lower overshoot; the impact of connecting genset #2 is also limited. It shows that bus voltage regulation can benefit from the wider control bandwidth and faster response of the SC controller. Moreover, since the power-sharing effect of the proposed inverse-droop method is also coordinated through voltage regulation in common dc bus, the dynamic power-sharing effect will also benefit from such an improvement.

V. Conclusion

In this paper, a hierarchical control design for the DC-SPS is presented; the main contributions can be summarized as follows.

1) An inverse-droop control approach is proposed as the power-sharing strategy for the shipboard system and potentially other diesel-dominated applications. With the proposed method, the power sharing between different power sources is according to their different power, energy, and/or efficiency characteristics instead of rated power or capacity.
2) A frequency-division method is proposed as an extension of the inverse-droop method, which is aiming at enabling the HESS to exploit its advancements over single storage, as well as solving the internal power management issue of the HESS automatically.
3) Redesigned and reorganized control solutions for higher level control objectives beyond power-sharing control are also proposed, thus opening more degrees of freedom for different scenarios in the real-world operation.

To validate the proposed methods, real-time simulations are carried out with a study case of the DC-SPS. A comparison between the proposed control solution and a more conventional droop method is presented. The results show that the proposed method has advancement in real-time fuel efficiency and bus voltage regulation over the conventional method.

Appendix

Fuel Efficiency Evaluation Model

The fuel efficiency of a marine engine is related to a number of different operating conditions, in which the most important factor is the load torque and engine speed. In this paper, a fuel efficiency evaluation model is established using the operational data of a four-stroke engine with ISO standard rating of 360 kW (330 kW for electrical generation). In this paper, a quadratic fit method used in [35] is employed to evaluate the fuel efficiency in real-time simulation, as shown in Fig. 16.

References

[1] *IEEE Recommended Practice for 1 kV to 35 kV Medium-Voltage DC Power Systems on Ships*, IEEE Standard 1709-2010, Nov. 2010.

[2] J. F. Hansen and F. Wendt, "History and state of the art in commercial electric ship propulsion, integrated power systems, and future trends," *Proc. IEEE*, vol. 103, no. 12, pp. 2229–2242, Dec. 2015.

[3] E. Skjong, E. Rodskar, M. Molinas, T. A. Johansen, and J. Cunningham, "The marine vessel's electrical power system: From its birth to present day," *Proc. IEEE*, vol. 103, no. 12, pp. 2410–2424, Dec. 2015.

[4] E. Skjong, R. Volden, E. Rodskar, M. Molinas, T. Johansen, and J. Cunningham, "Past, present and future challenges of the marine vessel's electrical power system," *IEEE Trans. Transp. Electrif.*, vol. 2, no. 4, pp. 522–537, Dec. 2016.

[5] B. Zahedi and L. E. Norum, "Modeling and simulation of all-electric ships with low-voltage DC hybrid power systems," *IEEE Trans. Power Electron.*, vol. 28, no. 10, pp. 4525–4537, Oct. 2013.

[6] T. J. McCoy, "Integrated power systems—An outline of requirements and functionalities for ships," *Proc. IEEE*, vol. 103, no. 12, pp. 2276–2284, Dec. 2015.

[7] N. Doerry, "Next generation integrated power systems (NGIPS) for the future fleet," presented at the IEEE Electr. Ship Technol. Symp., 2009. [Online]. Available: http://www.doerry.org/norbert/papers/090305usna-ngips-final-presentation.pdf

[8] N. Doerry and K. McCoy, "Next generation integrated power system: NGIPS technology development roadmap," 2007.

[9] G. Sulligoi, A. Tessarolo, V. Benucci, M. Baret, A. Rebora, and A. Taffone, "Modeling, simulation, and experimental validation of a generation system for medium-voltage DC integrated power systems," *IEEE Trans. Ind. Appl.*, vol. 46, no. 4, pp. 1304–1310, Jul./Aug. 2010.

[10] Z. Jin, G. Sulligoi, R. Cuzner, L. Meng, J. C. Vasquez, and J. M. Guerrero, "Next-generation shipboard DC power system: Introduction smart grid and dc microgrid technologies into maritime electrical netowrks," *IEEE Electrific. Mag.*, vol. 4, no. 2, pp. 45–57, Jun. 2016.

[11] R. M. Cuzner and D. A. Esmaili, "Fault tolerant shipboard MVDC architectures," in *Proc. Int. Conf. Elect. Syst. Aircraft, Railway, Ship Propulsion Road Veh.*, 2015, pp. 1–6.

[12] A. Monti, S. D'Arco, L. Gao, and R. A. Dougal, "Energy storage management as key issue in control of power systems in future all electric ships," in *Proc. Int. Symp. Power Electron. Elect. Drives, Autom. Motion*, 2008, pp. 580–585.

[13] S. Y. Kim, S. Choe, S. Ko, and S. K. Sul, "A Naval Integrated power system with a battery energy storage system: Fuel efficiency, reliability, and quality of power," *IEEE Electrific. Mag.*, vol. 3, no. 2, pp. 22–33, Jun. 2015.

[14] G. Sattler, "Fuel cells going on-board," *J. Power Sources*, vol. 86, no. 1, pp. 61–67, Mar. 2000.

[15] A. Hasanzadeh, C. S. Edrington, N. Stroupe, and T. Bevis, "Real-time emulation of a high-speed microturbine permanent-magnet synchronous generator using multiplatform hardware-in-the-loop realization," *IEEE Trans. Ind. Electron.*, vol. 61, no. 6, pp. 3109–3118, Jun. 2014.

[16] S. Z. Vijlee, A. Ouroua, L. N. Domaschk, and J. H. Beno, "Directly-coupled gas turbine permanent magnet generator sets for prime power generation on board electric ships," in *Proc. IEEE Electr. Ship Technol. Symp.*, Arlington, VA, USA, 2007, pp. 340–347.

[17] X. J. Tang, T. Wang, C. Zhi, and Y. M. Huang, "The design of power management system for solar ship," in *Proc. 3rd Int. Conf. Transp. Inf. Safety*, 2015, pp. 548–553.

[18] R. E. Hebner *et al.*, "Dynamic load and storage integration," *Proc. IEEE*, vol. 103, no. 12, pp. 2344–2354, Dec. 2015.

[19] F. Wang, Z. Zhang, T. Ericsen, R. Raju, R. Burgos, and D. Boroyevich, "Advances in power conversion and drives for shipboard systems," *Proc. IEEE*, vol. 103, no. 12, pp. 2285–2311, Dec. 2015.

[20] R. Mo, R. Li, and H. Li, "Isolated modular multilevel (IMM) DC/DC converter with energy storage and active filter function for shipboard MVDC system applications," in *Proc. IEEE Electr. Ship Technol. Symp.*, Alexandria, VA, USA, 2015, pp. 113–117.

[21] R. M. Cuzner, V. Singh, M. Rashidi, and A. Nasiri, "Converter topological and solid state protective device trade-offs for future shipboard MVDC systems," in *Proc. IEEE Electr. Ship Technol. Symp.*, Alexandria, VA, USA, 2015, pp. 34–39.

[22] G. Sulligoi, A. Tessarolo, V. Benucci, A. Millerani Trapani, M. Baret, and F. Luise, "Shipboard power generation: Design and development of a medium-voltage dc generation system," *IEEE Ind. Appl. Mag.*, vol. 19, no. 4, pp. 47–55, Jul./Aug. 2013.

[23] J. M. Guerrero, J. C. Vasquez, J. Matas, L. G. De Vicuña, and M. Castilla, "Hierarchical control of droop-controlled AC and DC microgrids—A general approach toward standardization," *IEEE Trans. Ind. Electron.*, vol. 58, no. 1, pp. 158–172, Jan. 2011.

[24] J. M. Guerrero, M. Chandorkar, T. Lee, and P. C. Loh, "Advanced control architectures for intelligent microgrids—Part I: Decentralized and hierarchical control," *IEEE Trans. Ind. Electron.*, vol. 60, no. 4, pp. 1254–1262, Apr. 2013.

[25] J. M. Guerrero, P. C. Loh, T. L. Lee, and M. Chandorkar, "Advanced control architectures for intelligent microgrids—Part II: Power quality, energy storage, and AC/DC microgrids," *IEEE Trans. Ind. Electron.*, vol. 60, no. 4, pp. 1263–1270, Apr. 2013.

[26] X. Lu, J. M. Guerrero, K. Sun, J. C. Vasquez, R. Teodorescu, and L. Huang, "Hierarchical control of parallel AC-DC converter interfaces for hybrid microgrids," *IEEE Trans. Smart Grid*, vol. 5, no. 2, pp. 683–692, Mar. 2014.

[27] Y. Wang, S. Mao, and R. M. Nelms, "On hierarchical power scheduling for the macrogrid and cooperative microgrids," *IEEE Trans. Ind. Informat.*, vol. 11, no. 6, pp. 1574–1584, Dec. 2015.

[28] A. Vaccaro, V. Loia, G. Formato, P. Wall, and V. Terzija, "A self-organizing architecture for decentralized smart microgrids synchronization, control, and monitoring," *IEEE Trans. Ind. Informat.*, vol. 11, no. 1, pp. 289–298, Feb. 2015.

[29] Y. Khersonsky and G. Sulligoi, "Standards for ships and oil platforms: A review of the latest from the IEEE and IEC," *IEEE Ind. Appl. Mag.*, vol. 22, no. 1, pp. 20–27, Jan./Feb. 2016.

[30] G. M. Foglia, A. Di Gerlando, M. F. Iacchetti, and R. Perini, "Comprehensive steady-state analytical model of a three-phase diode rectifier connected to a constant DC voltage source," *IET Power Electron.*, vol. 6, no. 9, pp. 1927–1938, Nov. 2013.

[31] P. C. Krause, O. Wasynczuk, and S. D. Sudhoff, *Analysis of Electric Machinery and Drive Systems*, 2nd ed. Piscataway, NJ, USA: IEEE Press, 2002.

[32] S. Sudhoff *et al.*, "Stability analysis of a DC power electronics based distribution system," SAE Tech. Paper 2002-01-3184, 2002, doi:10.4271/2002-01-3184.

[33] B. Zahedi and L. E. Norum, "Voltage regulation and power sharing control in ship LVDC power distribution systems," in *Proc. Eur. Conf. Power Electron. Appl.*, Lille, France, 2013, pp. 1–8.

[34] L. Meng, T. Dragicevic, J. M. Guerrero, and J. C. Vasquez, "Optimization with system damping restoration for droop controlled DC/DC converters," in *Proc. IEEE Energy Convers. Congr. Expo.*, 2013, pp. 65–72.

[35] B. Zahedi, L. E. Norum, and K. B. Ludvigsen, "Optimized efficiency of all-electric ships by dc hybrid power systems," *J. Power Sources*, vol. 255, pp. 341–354, 2014. [Online]. Available: http://dx.doi.org/10.1016/j.jpowsour.2014.01.031

Zheming Jin (S'15) received the B.S. degree in electrical engineering and the M.S. degree in power electronics and ac drives from Beijing Jiaotong University, Beijing, China, in 2013 and 2015, respectively. He is currently working toward the Ph.D. degree in power electronic systems with the Department of Energy Technology, Aalborg University, Aalborg, Denmark.

His research interests include control of power electronic converters, stability of power electronic systems, energy storage, dc microgrids, and their applications in transportation electrification.

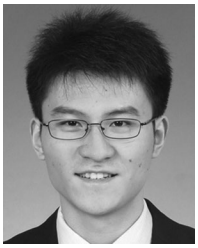

Lexuan Meng (S'13–M'15) received the B.S. degree in electrical engineering and the M.S. degree in electrical machine and apparatus from Nanjing University of Aeronautics and Astronautics, Nanjing, China, in 2009 and 2012, respectively, and the Ph.D. degree in power electronic systems from the Department of Energy Technology, Aalborg University, Aalborg, Denmark, in 2015.

He is currently a Postdoctoral Researcher with the Department of Energy Technology, Aalborg University, working on flywheel energy storage and onboard electric power systems. His research interests include microgrids, grid integration of energy storage systems, power quality, and distributed control.

Dr. Meng is a Guest Associate Editor of the special Issue entitled "Structured DC Microgrids" in the IEEE Journal of Emerging and Selected Topics in Power Electronics. He is a member of the IEEE Power Electronics Society, the IEEE Industry Applications Society, the IEEE Power and Energy Society, and the IEEE Industrial Electronics Society.

Josep M. Guerrero (S'01–M'04–SM'08–F'15) received the B.S. degree in telecommunications engineering, the M.S. degree in electronics engineering, and the Ph.D. degree in power electronics from the Technical University of Catalonia, Barcelona, Spain, in 1997, 2000, and 2003, respectively.

Since 2011, he has been a Full Professor with the Department of Energy Technology, Aalborg University, Aalborg, Denmark, where he is responsible for the Microgrid Research Program (www.microgrids.et.aau.dk). Since 2012, he has been a Guest Professor with the Chinese Academy of Science and Nanjing University of Aeronautics and Astronautics. Since 2014, he has been a Chair Professor with Shandong University. Since 2015, he has been a Distinguished Guest Professor with Hunan University. Since 2016, he has been a Visiting Professor Fellow with Aston University, U.K., and a Guest Professor with Nanjing University of Posts and Telecommunications. His research interests are oriented to different microgrid aspects, including power electronics, distributed energy-storage systems, hierarchical and cooperative control, energy management systems, smart metering, and the Internet of Things for ac/dc microgrid clusters and islanded minigrids. His recent research interests have especially included maritime microgrids for electrical ships, vessels, ferries, and seaports.

Prof. Guerrero is an Associate Editor for the IEEE Transactions on Power Electronics, the IEEE Transactions on Industrial Electronics, and the IEEE Industrial Electronics Magazine and an Editor for the IEEE Transactions on Smart Grid and the IEEE Transactions on Energy Conversion. He has been Guest Editor of the IEEE Transactions on Power Electronics Special Issues: Power Electronics for Wind Energy Conversion and Power Electronics for Microgrids; the IEEE Transactions on Industrial Electronics Special Sections: Uninterruptible Power Supplies systems, Renewable Energy Systems, Distributed Generation and Microgrids, and Industrial Applications and Implementation Issues of the Kalman Filter; the IEEE Transactions on Smart Grid Special Issues: Smart DC Distribution Systems and Power Quality in Smart Grids; and the IEEE Transactions on Energy Conversion Special Issue on Energy Conversion in Next-generation Electric Ships. He was the Chair of the Renewable Energy Systems Technical Committee of the IEEE Industrial Electronics Society. He was a recipient of the Best Paper Award of the IEEE Transactions on Energy Conversion for the period 2014–2015 and the Best Paper Prize of the IEEE Power and Energy Society in 2015. In addition, he was a recipient of the Best Paper Award of the Journal of Power Electronics in 2016. In 2014, 2015, and 2016, he was awarded by Thomson Reuters as Highly Cited Researcher, and in 2015, he became a Fellow of the IEEE for his contributions on "distributed power systems and microgrids."

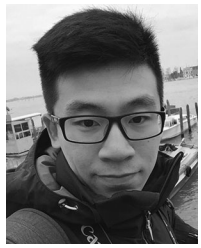

Renke Han (S'16) received the B.S. degree in automation and the M.S. degree in control theory and control engineering from Northeastern University, Shenyang, China, in 2013 and 2015, respectively. He is currently working toward the Ph.D. degree in power electronics system with the Department of Energy Technology, Aalborg University, Aalborg, Denmark.

From February to August 2017, he was a Visiting Scholar with the Laboratoire d'Automatique, Ecole Polytechnique Fédérale de Lausanne, Switzerland, under the supervision of Prof. G. Ferrari-Trecate. His research interests include the distributed control, event-triggered control, plug-and-play control to achieve stability operation, and reasonable power sharing for ac and dc microgrids.

PAPER B. Reference [58]

Comparative Admittance-based Analysis for Different Droop Control Approaches in DC Microgrids

Zheming Jin, Lexuan Meng, and Josep M. Guerrero

The paper has been published in

2017 IEEE Second International Conference on DC Microgrids (ICDCM), Nuremburg, 2017, pp. 515-522.

Comparative Admittance-based Analysis for Different Droop Control Approaches in DC Microgrids

Zheming Jin, Lexuan Meng, Josep M. Guerrero
Department of Energy Technology
Aalborg University
Aalborg, Denmark
zhe@et.aau.dk

***Abstract*—In DC microgrids, virtual resistance based droop control is broadly used as the fundamental coordination method. As the virtual resistance guarantees load sharing effect in steady states, the output admittance determines the dynamic response of converters in transient states, which is critical in stability analysis and system design. So far, two different approaches of droop control (i.e. *V-I* droop and *I-V* droop) are proposed. Although they can achieve the same steady-state power sharing effect and fully compliable with each other, the output characteristics are not the same due to significant difference in control architecture. In this paper, a comparative admittance-based analysis is carried out between these two approaches. State-space models and more general analytical models are established to derive the output admittance of droop-controlled converter in DC microgrids. Simulations and impedance measurement is carried out using PLECS to validate the analytical results.**

Keywords—DC microgrids; droop control; output impedance; stability; virtual resistance; constant power load

I. INTRODUCTION

With the increasing penetration of renewable energy and the rapid growth of modern electronic loads that inherently consume DC power, the concept of DC microgrids (MGs) is becoming attractive in both mobile and stationary applications, especially in off-grid and islanded cases [1-4]. By packing distributed energy sources and loads together with energy storages, DC MGs can operate as an independent and self-sustainable entity. When compared with its AC counterparts, DC MGs can provide better compliance and efficiency and eliminate several unwanted problems of AC distribution [2].

So far, droop control is broadly used in both AC and DC MGs to share the loads among paralleled power sources properly without introducing communication or additional losses [5], [6]. In DC MGs, virtual resistance based droop approaches are commonly implemented. With virtual resistance equal to the maximum voltage tolerance divided by the maximum output current of the converter, the loads can be shared among paralleled energy sources proportional to their power rating. In addition to that, the presence of virtual resistance effectively avoids circulating current caused by measurement errors, thus maintaining stable operation. So far, two different approaches have been proposed to achieve such a control function, which are the conventional *V-I* droop method presented in [7] and [8], and the emerging *I-V* droop method, as known as reverse-droop method, presented in [9], [10] and [11]. Fig. 1 illustrates the different control architectures of these two approaches. Although these two droop approaches are fully compatible with each other, considerable difference can be seen from transient responses, which means their stability margin are unequal.

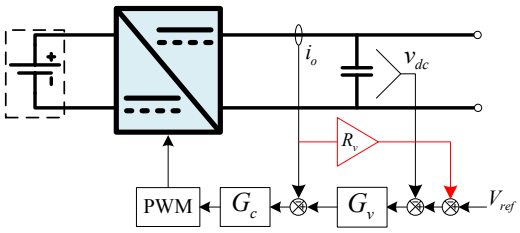

(a) Control diagram of *V-I* droop method

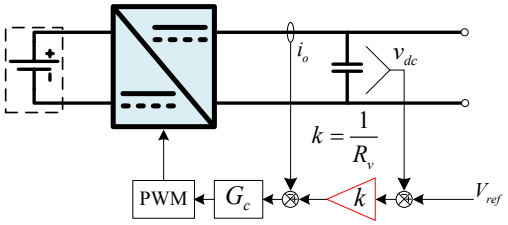

(b) Control diagram of *I-V* droop method

Fig. 1. Control architectures of different droop approaches.

The system-level stability is a critical and challenging issue in the field of DC MGs. As DC MGs are power electronic based distribution network, which means majority of the loads will be interfaced by tightly controlled converters with control bandwidth high enough to make the consumed power independent from the bus voltage variations, namely constant power loads (CPLs). When operating in DC systems, CPLs will perform a negative incremental impedance characteristic, which can lead to instability [12]. The study associated with this instability issue can be traced back to 1976, when the interaction between the input filter and power converter was firstly analyzed in [13], in which the Middlebrook stability criterion is proposed. As the criterion is very conservative for designing controllers, several relaxed stability criterions have been proposed in the later studies, as reviewed in [14] and [15]. For all these stability criterions, it is mandatory to derive the accurate output impedance/admittance of the source-side converters to conduct stability analysis. In [16], the output impedance characteristics of common types (Buck, Boost and

Buck-Boost) of DC/DC converters are analyzed in detail. However, the analysis is based on small-signal model that assumes the converter is working around a specific operation point, usually the system's nominal voltage. It is acceptable for voltage mode controlled system, but not for droop controlled cases that have load-dependent bus voltage within a considerable range (e.g. ±10%) of operational points. In [17] and [18], the authors modeled droop controlled source converters as Thévenin equivalents with open-circuit voltages equal to the voltage references and output resistance equal to the virtual resistance, and use such model to evaluate the stability of DC MGs. To the author's opinion, such a modeling method can be sufficiently accurate at the low-frequency range to make steady state analysis. However, due to the limited bandwidth of the voltage and/or current controllers, the output impedance shall vary with frequency, which is more critical to be evaluated in stability analysis.

In this paper, the output characteristics of both *V-I* and *I-V* droop-controlled converters are analyzed. For comparison, two detailed state-space based models are established for a notional DC MG feeding by two droop-controlled buck converters. By deriving the transfer functions from the established models, the output admittance of droop-controlled converters are obtained and compared. In addition, by fairly simplifying current loops as first-order delay with time constant derived by its control bandwidth, generalized analytical models are derived for other cases. From the generalized models, two modified Thévenin equivalents of both *V-I* and *I-V* droop-controlled converters are deduced. To verify the proposed modeling work and analytical results, especially the stability margin, simulations are carried out with both approaches using PLECS and its impedance measurement function.

II. Modeling of Droop-Controlled Converters

In this paper, a notional DC microgrid composed by two parallel connected droop controlled Buck converters as source converters feeding point-of-load converter (as CPL) is selected as the study case, as shown in Fig. 2. The notional microgrid is modeled based on the following assumptions:

1) The inputs of the source converters can be regarded as ideal voltage sources.
2) The distance between source converters and load converters are short, the line impedance is neglectable.

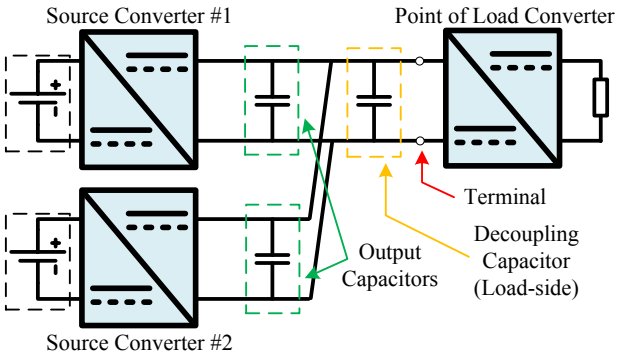

Fig. 2. Control architectures of different droop approaches.

A. State-space Model for V-I Droop Controlled Case

For the *i*-th Buck converters, the increment of the average output current can be described by the differential equations as:

$$\begin{cases} L_i \dfrac{di_{oi}}{dt} = E_i d_i - u - r_i i_{oi} \\ C \dfrac{du}{dt} = \sum i_{oi} - i_{Load} \end{cases} \quad (i \in \{1,2\}) \tag{1}$$

where the subscript i represents the i-th converter, E_i, and d_i are the input voltage and the duty cycle, respectively. L_i, r_i and i_{oi} stands for the inductance, the stray resistance, the average current of the inductor, respectively. C, u, and i_{Load} are the total capacitance connected to the common DC bus, the voltage of common DC bus, and the load current.

When adopting conventional *V-I* droop method, the duty cycle d_i follows the following equations:

$$d_i = K_{pci}\left(i_{refi} - i_{oi}\right) + K_{ici}\int_0^t \left(i_{refi} - i_{oi}\right)dt \tag{2}$$

$$i_{refi} = K_{pvi}\left(V_{ref} - u - R_{vi} i_{oi}\right) + K_{ivi}\int_0^t \left(V_{ref} - u - R_{vi} i_{oi}\right)dt \tag{3}$$

where K_{pci}, K_{pvi} represents the proportional term of current and voltage PI controller, respectively. Similarly, K_{ici} and K_{ivi} are the integral term of current and voltage PI controller. R_{vi} is the virtual resistance of the droop control. V_{ref} is the global no-load voltage reference of the droop control.

Rewrite (2) and (3) as differential equations:

$$\frac{dd_i}{dt} = K_{pci}\frac{di_{refi}}{dt} - K_{pci}\frac{di_{oi}}{dt} + K_{ici} i_{refi} - K_{ici} i_{oi} \tag{4}$$

$$\frac{di_{refi}}{dt} = K_{pvi}\frac{dV_{ref}}{dt} - K_{pvi}\frac{du}{dt} - K_{pvi}R_{vi}\frac{di_{oi}}{dt} + K_{ivi}\left(V_{ref} - u - R_{vi} i_{oi}\right) \tag{5}$$

As V_{ref} is a time-invariant parameter, substitute (1) into (5), the equation will be:

$$\begin{aligned} \frac{di_{refi}}{dt} = {} & K_{ivi}\left(V_{ref} - u - R_{vi} i_{oi}\right) - K_{pvi}\left(\sum \frac{i_{oi}}{C} - \frac{i_{Load}}{C}\right) \\ & - K_{pvi}R_{vi}\left(\frac{E_i}{L_i} d_i - \frac{u}{L_i} - \frac{r_i}{L_i} i_{oi}\right) \end{aligned} \tag{6}$$

Substitute (6) into (4), the equation can be rewritten as:

$$\begin{aligned} \frac{dd_i}{dt} = {} & K_{pci}K_{ivi}\left(V_{ref} - u - R_{vi} i_{oi}\right) - K_{pci}K_{pvi}\left(\sum \frac{i_{oi}}{C} - \frac{i_{Load}}{C}\right) \\ & - \left(K_{pci}K_{pvi}R_{vi} + K_{pci}\right)\left(\frac{E_i}{L_i} d_i - \frac{u}{L_i} - \frac{r_i}{L_i} i_{oi}\right) + K_{ici} i_{refi} - K_{ici} i_{oi} \end{aligned} \tag{7}$$

By combining (1), (6) and (7), a state-space model can be derived as following:

$$\dot{\boldsymbol{X}} = \boldsymbol{AX} + \boldsymbol{BU}, \quad \boldsymbol{Y} = \boldsymbol{CX}, \tag{8}$$

$$\boldsymbol{X} = \left[x_1, x_2, u\right]^T, \boldsymbol{U} = \left[V_{ref}, i_{Load}\right]^T, \boldsymbol{x_i} = \left[i_{oi}, i_{refi}, d_i\right]$$

$$\boldsymbol{A} = \begin{bmatrix} \boldsymbol{J_1} & \boldsymbol{M_1} & \boldsymbol{F_1} \\ \boldsymbol{M_2} & \boldsymbol{J_2} & \boldsymbol{F_2} \\ \boldsymbol{C_1} & \boldsymbol{C_1} & 0 \end{bmatrix}, \boldsymbol{B} = \begin{bmatrix} \boldsymbol{B_1} \\ \boldsymbol{B_2} \\ \boldsymbol{C_2} \end{bmatrix}, \boldsymbol{C} = \boldsymbol{I}_{7\times 7} \tag{9}$$

$$\boldsymbol{J_i} = \begin{bmatrix} -\frac{r_i}{L_i} & 0 & \frac{E_i}{L_i} \\ j_{i1} & 0 & \frac{K_{pvi}R_{vi}E_i}{L_i} \\ j_{i2} & K_{ici} & j_{i3} \end{bmatrix}, \boldsymbol{M_i} = \begin{bmatrix} 0 & 0 & 0 \\ -\frac{K_{pvi}}{C} & 0 & 0 \\ -\frac{K_{pvi}K_{pci}}{C} & 0 & 0 \end{bmatrix}, \tag{10}$$

$$\boldsymbol{F_i} = \begin{bmatrix} -\frac{1}{L_i} \\ f_{i1} \\ f_{i2} \end{bmatrix}, \boldsymbol{C_1} = \left[\frac{1}{C}, 0, 0\right], \boldsymbol{C_2} = \left[0, -\frac{1}{C}\right], \boldsymbol{B_i} = \begin{bmatrix} 0 & 0 \\ K_{ivi} & \frac{K_{pvi}}{C} \\ K_{pci}K_{ivi} & \frac{K_{pci}K_{pvi}}{C} \end{bmatrix}$$

$$\begin{cases} j_{i1} = \dfrac{K_{pvi}R_{vi}r_i}{L_i} - \dfrac{K_{pvi}}{C} - K_{ivi}R_{vi}, \\ j_{i2} = \dfrac{K_{pci}r_i\left(K_{pvi}R_{vi}+1\right)}{L_i} - \dfrac{K_{pci}K_{pvi}}{C} - K_{ici} - K_{pci}K_{ivi}R_{vi}, \\ j_{i3} = -\dfrac{K_{pci}E_i(K_{pvi}R_{vi}+1)}{L_i}, \end{cases} \tag{11}$$

$$\begin{cases} f_{i1} = \dfrac{K_{pvi}R_{vi}}{L_i} - K_{ivi}, \\ f_{i2} = \dfrac{K_{pci}\left(K_{pvi}R_{vi}+1\right)}{L_i} - K_{pci}K_{ivi}, \end{cases}$$

In the state-space model, the study case of this paper is modeled. To make the model scalable, the dynamic response of converters are described as a set of five component matrixes. Among them, the component matrix $\boldsymbol{M_i}$ is describing coupling effect among parallel connected converters, while the others are set to describe the internal control effect of *i*-th converter. When extended to a *n*-converter case, the matrixes $\boldsymbol{A}$, $\boldsymbol{B}$, and $\boldsymbol{C}$ shall be organized as following:

$$\boldsymbol{X} = \left[x_1, \cdots, x_n, u\right]^T, \boldsymbol{U} = \left[V_{ref}, i_{Load}\right]^T, \boldsymbol{x_i} = \left[i_{oi}, i_{refi}, d_i\right]$$

$$\boldsymbol{A} = \begin{bmatrix} \boldsymbol{J_1} & \boldsymbol{M_1} & \cdots & \boldsymbol{M_1} & \boldsymbol{F}_1 \\ \boldsymbol{M_2} & \boldsymbol{J_2} & \cdots & \boldsymbol{M_2} & \boldsymbol{F_2} \\ \vdots & \vdots & \ddots & \vdots & \vdots \\ \boldsymbol{M_n} & \boldsymbol{M_n} & \cdots & \boldsymbol{J_n} & \boldsymbol{F_n} \\ \boldsymbol{C_1} & \boldsymbol{C_1} & \cdots & \boldsymbol{C_1} & 0 \end{bmatrix}, \boldsymbol{B} = \begin{bmatrix} \boldsymbol{B_1} \\ \vdots \\ \boldsymbol{B_n} \\ \boldsymbol{C_2} \end{bmatrix}, \boldsymbol{C} = \boldsymbol{I}_{(3n+1)\times(3n+1)} \tag{12}$$

B. State-space Model for I-V Droop Controlled Case

When adopting *I-V* droop method, the output current of the *i*-th converters will follow the same equation as shown in (1). However, the current reference i_{refi} and the duty cycle d_i will be calculated by the following equations:

$$i_{refi} = k_i\left(V_{ref} - u\right) \tag{13}$$

$$d_i = K_{pci}\left(k_iV_{ref} - k_iu - i_{oi}\right) + K_{ici}\int_0^t\left(k_iV_{ref} - k_iu - i_{oi}\right)dt \tag{14}$$

$$\begin{cases} \dfrac{di_{refi}}{dt} = -k_i\dfrac{du}{dt} = k_i\dfrac{i_{Load}}{C} - k_i\sum\dfrac{i_{oi}}{C} \\ \dfrac{dd_i}{dt} = K_{ici}\left(k_iV_{ref} - k_iu - i_{oi}\right) + K_{pci}k_i\left(\dfrac{i_{Load}}{C} - \sum\dfrac{i_{oi}}{C}\right) \\ \qquad - K_{pci}\left(\dfrac{E_i}{L_i}d_i - \dfrac{u}{L_i} - \dfrac{r_i}{L_i}i_{oi}\right) \end{cases} \tag{15}$$

where k_i equals to the reciprocal of virtual resistance used in conventional *V-I* droop method, which represents conductance of the virtual resistor in physics.

By combining (1) and (15) a similar state-space model can be derived as following:

$$\dot{\boldsymbol{X}} = \boldsymbol{A'X} + \boldsymbol{B'U}, \quad \boldsymbol{Y} = \boldsymbol{CX}, \tag{16}$$

$$\boldsymbol{X} = \left[x_1, x_2, u\right]^T, \boldsymbol{U} = \left[V_{ref}, i_{Load}\right]^T, \boldsymbol{x_i} = \left[i_{oi}, i_{refi}, d_i\right]$$

$$\boldsymbol{A'} = \begin{bmatrix} \boldsymbol{J_1'} & \boldsymbol{M_1'} & \boldsymbol{F_1'} \\ \boldsymbol{M_2'} & \boldsymbol{J_2'} & \boldsymbol{F_2'} \\ \boldsymbol{C_1} & \boldsymbol{C_1} & 0 \end{bmatrix}, \boldsymbol{B'} = \begin{bmatrix} \boldsymbol{B_1'} \\ \boldsymbol{B_2'} \\ \boldsymbol{C_2} \end{bmatrix}, \boldsymbol{C} = \boldsymbol{I}_{7\times 7} \tag{17}$$

$$\boldsymbol{J_i'} = \begin{bmatrix} -\frac{r_i}{L_i} & 0 & \frac{E_i}{L_i} \\ -\frac{k_i}{C} & 0 & 0 \\ j_i' & 0 & -\frac{K_{pci}E_i}{L_i} \end{bmatrix}, \boldsymbol{M_i'} = \begin{bmatrix} 0 & 0 & 0 \\ -\frac{k_i}{C} & 0 & 0 \\ -\frac{k_iK_{pci}}{C} & 0 & 0 \end{bmatrix},$$

$$\boldsymbol{F_i'} = \begin{bmatrix} -\frac{1}{L_i} \\ 0 \\ \frac{K_{pci}}{L_i} - k_iK_{ici} \end{bmatrix}, \boldsymbol{C_1} = \left[\frac{1}{C}, 0, 0\right], \boldsymbol{C_2} = \left[0, -\frac{1}{C}\right], \boldsymbol{B_i'} = \begin{bmatrix} 0 & 0 \\ 0 & \frac{k_i}{C} \\ k_iK_{ici} & \frac{k_iK_{pci}}{C} \end{bmatrix} \tag{18}$$

$$j_i' = \frac{K_{pci}r_i}{L_i} - \frac{k_iK_{pci}}{C} - K_{ici}$$

The derived state-space model for *I-V* droop controlled case maintains the scalability of the previous model. By organizing the component matrixes as shown in (12), the state-space model can also be extended to a *n*-converter case. In addition to that, the component matrixes shown in (10) and (18) are interchangeable. Thus, the derived framework of state-

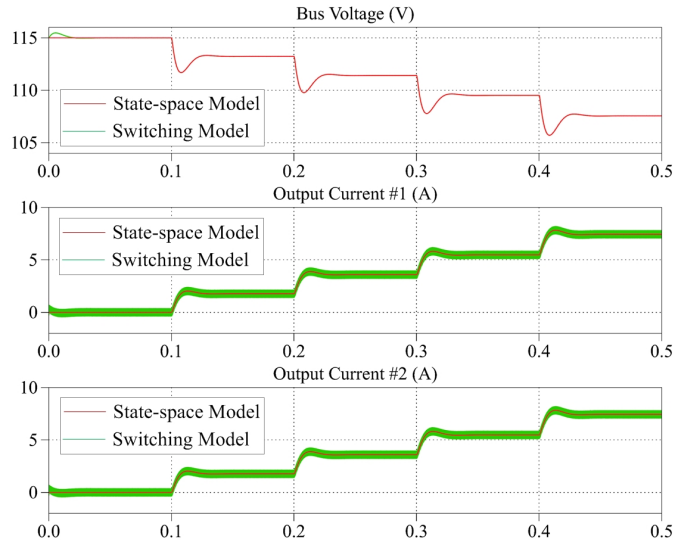

Fig. 3. Simulation results of *V-I* droop controlled case.

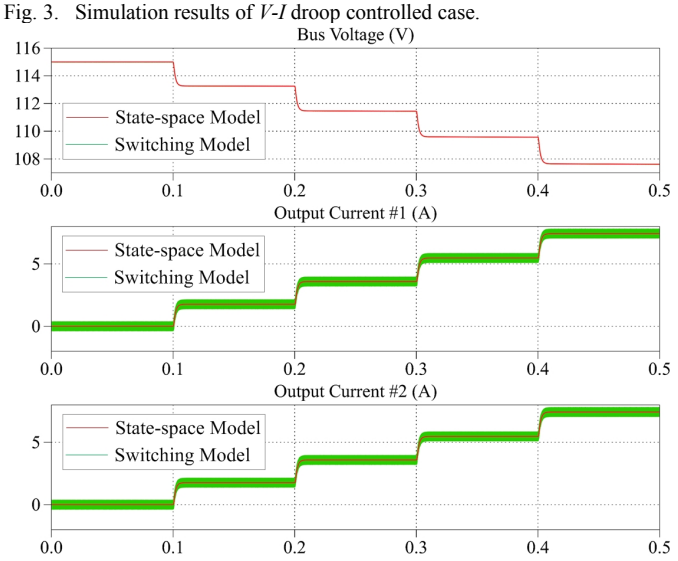

Fig. 4. Simulation results of *V-I* droop controlled case.

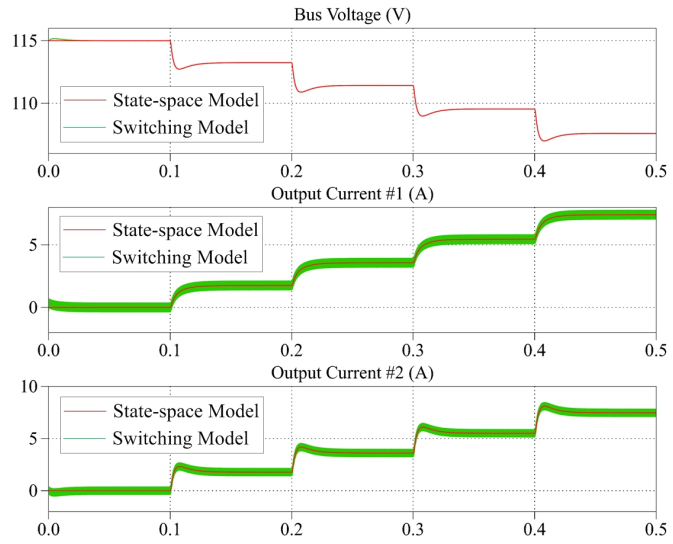

Fig. 5. Simulation results of mixed droop controlled case. Converter #1 is *V-I* droop controlled, converter #2 is *I-V* droop controlled.

space model can also describe the dynamic response of mixed droop-controlled cases of DC microgrids.

C. *Simulation Validation of the Derived Models*

To validate the derived state-space models, simulations of abovementioned study case are carried out using PLECS. The simulation results are as shown in Fig. 3, Fig. 4, and Fig. 5. For this simulation, the parameters of the simulated study case are listed in Table. I.

TABLE I. PARAMETERS OF SIMULATED STUDY CASE

Description of the Parameter	***Symbol***	***Value***
Global No-load Voltage Reference	V_{ref}	115 V
Source Voltage	E_1, E_2	230 V, 230 V
Inductance of Buck Converters	L_1, L_2	8 mH, 8 mH
Stary Resistance of inductors,	r_1, r_2	0.1 Ω, 0.1 Ω
Switching Frequency	f_{sw}	10 kHz
Virtual Resistances for Droop Control	R_{v1}, R_{v2}	1 Ω, 1 Ω
Total Capacitance in DC Bus	C	3.3 mF
Proportion Term of Voltage Controller	K_{pv1}, K_{pv2}	0.5, 0,5
Integral Term of Voltage Controller	K_{iv1}, K_{iv2}	100, 100
Proportion Term of Current Controller	K_{pc1}, K_{pc2}	0.2, 0.2
Integral Term of Current Controller	K_{ic1}, K_{ic2}	1, 1
Load Profile	P_{Load}	0.4 kW/step

As a conclusion, the derived state-space models have sufficient accuracy and can describe the dynamic of source converters properly.

III. OUTPUT ADMITTANCE ANALYSIS OF DROOP-CONTROLLED CONVERTERS

As shown in Fig. 5, even though the virtual resistances and the current controllers are exactly the same value, the dynamics of *V-I* and *I-V* droop controlled converters are different. In this section, the output admittance of *V-I* and *I-V* droop controlled converter is analyzed to address the mechanism.

A. *Deriving Output Admittance from State-space Models*

As droop control is to make the converter act as Thévenin equivalent branch, at least in its steady states, an effective way to describe their dynamic is the same way. According to the Thévenin's theorem, the output admittance of source converters can be calculated by:

$$Y_{eq} = \frac{I}{V_{oc} - u} \tag{19}$$

$$Y_{eq}(s) = \frac{\Delta I(s)}{\Delta\left(V_{ref}(s) - u(s)\right)} = \frac{\Delta I_o(s) - \Delta I_c(s)}{-\Delta u(s)} = \frac{\Delta I_o(s)}{-\Delta u(s)} + sC \tag{20}$$

where $I(s)$, $I_o(s)$, $I_c(s)$ and $u(s)$ are the terminal output current, inductor current, capacitor current and terminal voltage of the converter. V_{oc} is the open-circuit voltage, which equals to the global no-load voltage reference.

From (20) it can be derived that the output admittance of source converters is depending on converter's dynamic and the total capacitance of the common DC bus. As abovementioned, the converter's dynamic can be descripted by derived state-space models properly. Therefore, a small-signal model of the converter's output admittance can be derived by:

$$\boldsymbol{G}=\boldsymbol{C}(s\boldsymbol{I}-\boldsymbol{A})^{-1}\boldsymbol{B}=\begin{bmatrix} G_{i_{o1}ref}(s) & G_{i_{o1}Load}(s) \\ G_{i_{ref\,1}ref}(s) & G_{i_{ref\,1}Load}(s) \\ G_{d_1ref}(s) & G_{d_1Load}(s) \\ G_{i_{o2}ref}(s) & G_{i_{o2}Load}(s) \\ G_{i_{ref\,2}ref}(s) & G_{i_{ref\,2}Load}(s) \\ G_{d_2ref}(s) & G_{d_2Load}(s) \\ G_{uref}(s) & G_{uLoad}(s) \end{bmatrix} \tag{21}$$

$$\begin{aligned}\frac{\Delta I_o(s)}{\Delta u(s)}=&\frac{G_{i_{o1}ref}(s)\Delta V_{ref}(s)+G_{i_{o1}Load}(s)\Delta I_{Load}(s)}{G_{uref}(s)\Delta V_{ref}(s)+G_{uLoad}(s)\Delta I_{Load}(s)}\\&+\frac{G_{i_{o2}ref}(s)\Delta V_{ref}(s)+G_{i_{o2}Load}(s)\Delta I_{Load}(s)}{G_{uref}(s)\Delta V_{ref}(s)+G_{uLoad}(s)\Delta I_{Load}(s)}\end{aligned} \tag{22}$$

As the global voltage reference is constant while talking only about droop control, the equation can be simplified as:

$$\frac{\Delta I_o(s)}{\Delta u(s)}=\frac{G_{i_{o1}Load}(s)+G_{i_{o2}Load}(s)}{G_{uLoad}(s)} \tag{23}$$

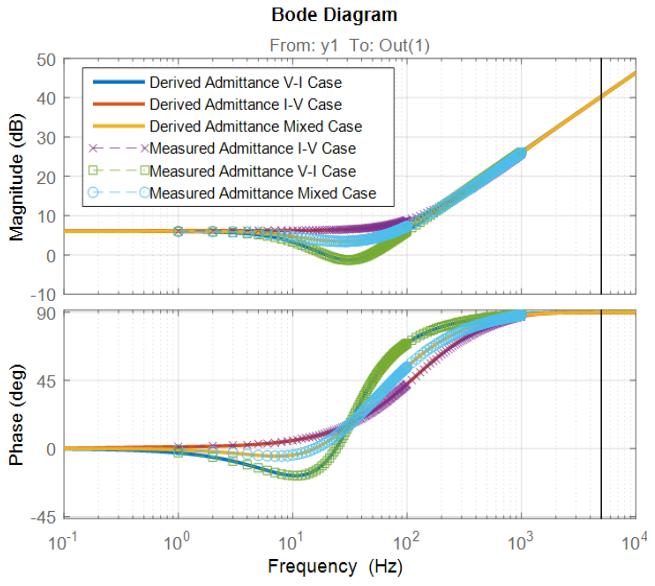

Fig. 6. Frequency response of state-space model derived and measured source-side output admittance.

For the study cases discussed in the above sections, their source-side output admittance is derived and illustrated in Fig. 6. At the same time, by using the impedance measurement function of PLECS, the output admittance of simulated study cases can be measured. The results of measured admittance are also shown as the dashed lines with marks in Fig. 6. It can be seen from the results that model-derived output admittance matched measured results very well.

B. Generalized Analytical Model of Output Admittance

From the results shown in Fig. 6, the source-side output admittance of *V-I* case and *I-V* case are considerably different, mainly happens in the frequency range of 10Hz to 100Hz. A maximum of 7.8 dB magnitude difference can be found. As the capacitance in DC bus is the same in these simulated cases, the converter's dynamic is the dominant factor of such a difference. To the author's opinion, the different controller configuration of *V-I* and *I-V* droop control is the main reason.

As illustrated in Fig. 1, the *V-I* droop controller is a dual-loop voltage controller with an additional feedback loop for the virtual resistance, while *I-V* droop controller is also a dual-loop controller with finite gain voltage controller. Therefore, their dynamic behavior can be descripted by:

$$I_o^{\,V-I}(s)=\frac{G_v(s)G_{clc}(s)}{1+R_vG_v(s)G_{clc}(s)}\left[V_{ref}(s)-u(s)\right] \tag{24}$$

$$I_o^{\,I-V}(s)=\frac{G_{clc}(s)}{R_v}\left[V_{ref}(s)-u(s)\right] \tag{25}$$

where $G_v(s)$ is the transfer function of voltage controller, $G_{clc}(s)$ is the close-loop transfer function of the whole current loop. The superscripts are to differentiate the droop modes.

By combining (24), (25) and (20), the converter's dynamic can be descripted by intrinsic admittance of converter:

$$Y_{conv}^{\,V-I}(s)=\frac{G_v(s)G_{clc}(s)}{1+R_vG_v(s)G_{clc}(s)} \tag{24}$$

$$Y_{conv}^{\,I-V}(s)=\frac{G_{clc}(s)}{R_v} \tag{25}$$

To analyze the behavior of dual-loop controllers, the inner current loop is commonly simplified as a first order delay. Therefore, the equations above can be presented by:

$$Y_{conv}^{\,V-I}(s)=\frac{G_v(s)G_{clc}(s)}{1+R_vG_v(s)G_{clc}(s)}=\frac{\dfrac{(K_{pvi}s+K_{ivi})}{s}\dfrac{\omega_{clc}}{s+\omega_{clc}}}{1+R_v\dfrac{(K_{pvi}s+K_{ivi})}{s}\dfrac{\omega_{clc}}{s+\omega_{clc}}} \tag{26}$$

$$Y_{conv}^{\,I-V}(s)=\frac{1}{R_v}\frac{\omega_{clc}}{s+\omega_{clc}} \tag{27}$$

where ω_{clc} stands for the bandwidth of current loop.

For Buck Converters, the control bandwidth of a well-designed current loop can be approximately calculated by:

$$\omega_{clc} \approx K_{pci} E_i / L_i \tag{28}$$

In Fig. 7, the converter's intrinsic admittance derived by state-space models and generalized analytical models are both illustrated by their frequency response. The results shows that the established generalized model is sufficient accurate to analyze the droop-controlled converter's intrinsic admittance.

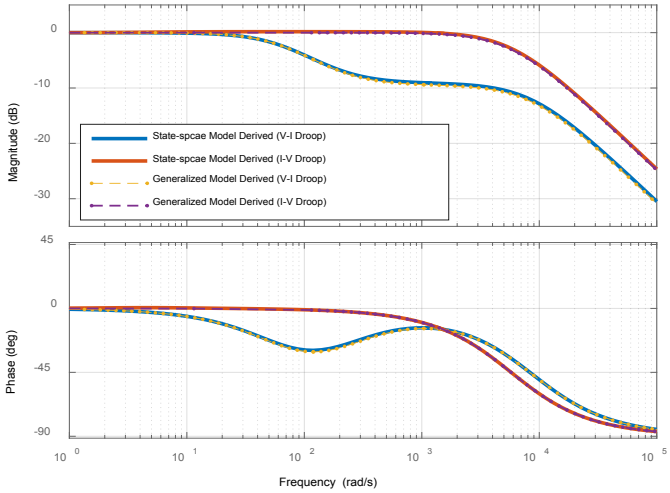

Fig. 7. Frequency response of converter's intrinsic admittance.

C. *Equivalent Circuit of Droop-controlled Converters*

In [17] and [18], the authors assume that the converter has pure resistive output impedance and established theoretical model based on such an assumption. However, as shown in Fig. 6 and Fig. 7, for both *V-I* and *I-V* droop-controlled converters, the output dynamic show resistive characteristic only in the low-frequency range. Moreover, the feasible range of such modeling method is too narrow to conduct generic stability analysis.

To solve this problem, an alternative solution is to use the converter's intrinsic admittance instead of virtual resistance to establish equivalent model of droop-controlled converters. For *V-I* droop-controlled converters, an equivalent circuit can be derived from (26) as shown in Fig. 8(a). The equivalent circuit of *I-V* droop-controlled converters can be derived from (27), as shown in Fig. 8(b). The inductance and resistance of additional virtual components (marked red in Fig. 8) are as follows:

$$\begin{cases} R_v^{V-I} = R_{vi} \\ L_{v1}^{V-I} = \dfrac{1}{K_{pvi}\omega_{clc}} \\ L_{v2}^{V-I} = \dfrac{\omega_{clc} - K_{ivi}/K_{pvi}}{K_{ivi}\omega_{clc}} \\ R_{Ld}^{V-I} = \dfrac{\omega_{clc} - K_{ivi}/K_{pvi}}{K_{pvi}\omega_{clc}} \end{cases} \qquad \begin{cases} R_v^{I-V} = R_{vi} \\ L_{v1}^{I-V} = \dfrac{R_{vi}}{\omega_{clc}} \end{cases} \tag{29}$$

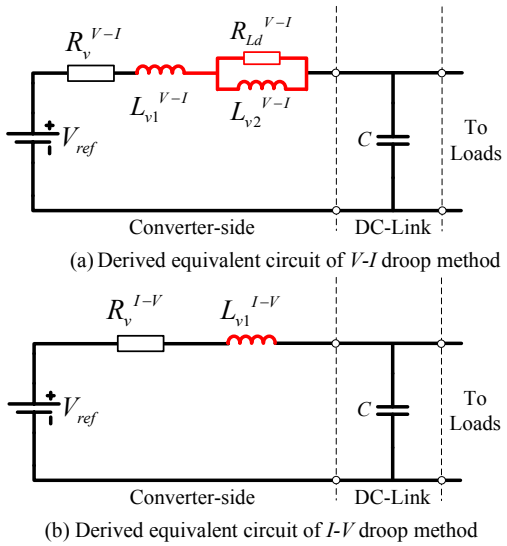

Fig. 8. Derived equivalent circuit models of droop-controlled converters.

It is noteworthy that the derived intrinsic admittance and equivalent circuit of *V-I* droop-controlled converter are both also applicable to analyze the behavior of more conventional voltage-controlled converter by simply set virtual resistance to be zero. It can be derived from (26) that *V-I* droop control scheme introduces a virtual resistor that connected in series to the voltage controlled converter's equivalent circuit, while the equivalent circuit itself is not affected by the additional feedback loop. The same conclusion can be also derived from (29) that the additional virtual components are all irrelevant to the virtual resistance.

As for the *I-V* droop method, a significant feature is its finite gain (which take the role of virtual resistance) in voltage control. Also for the same reason, the converter's intrinsic admittance is closely depending on the virtual resistance.

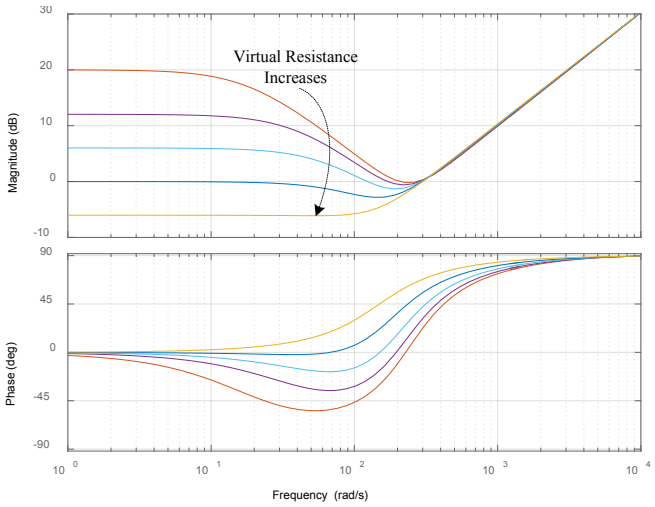

Fig. 9. Frequency response of dource-side output admittance with *V-I* droop-controlled converters under different virtual resistance (0.2Ω-4Ω) .

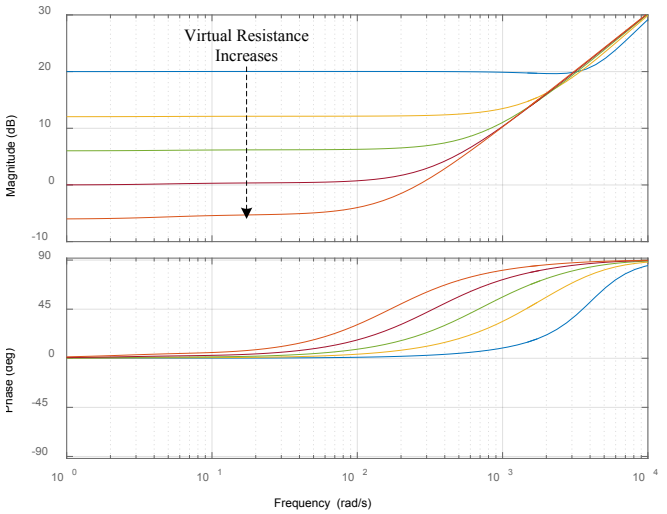

Fig. 10. Frequency response of source-side output admittance with *I-V* droop-controlled converters under different virtual resistance (0.2Ω-4Ω) .

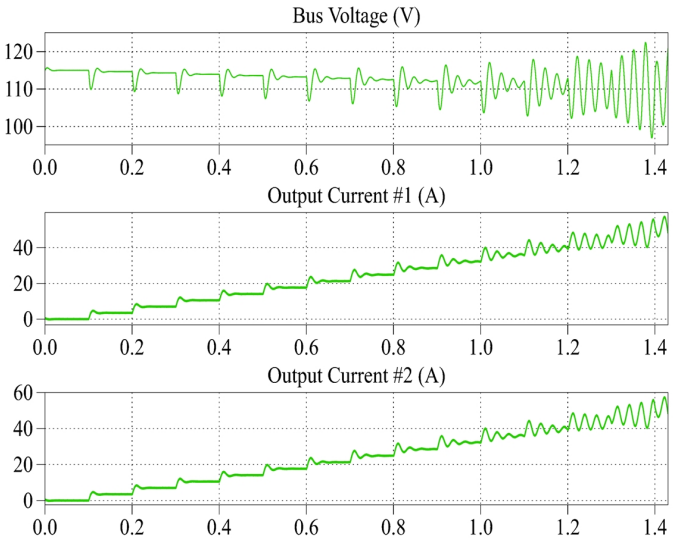

Fig. 11. Simulation results of *V-I* (R_v=0.1Ω) droop-controlled case feeding CPL.

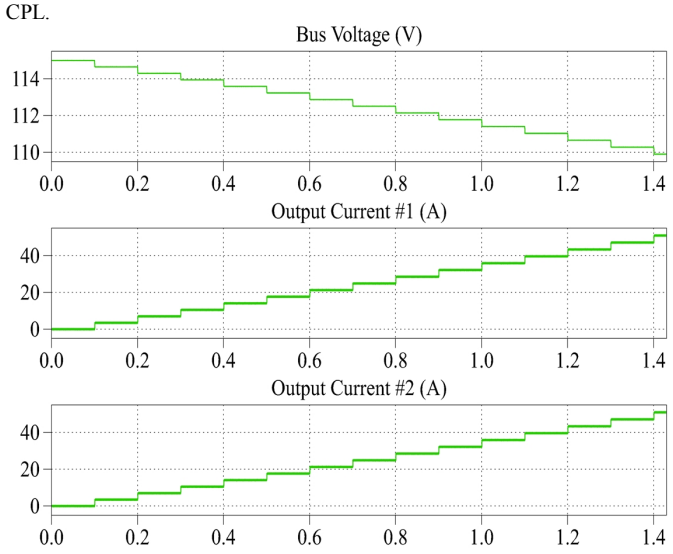

Fig. 12. Simulation results of *I-V* (Rv=0.1Ω) droop-controlled case feeding CPL.

Fig. 9 illustrates the source-side output admittance of *V-I* droop-controlled study case with different virtual resistance (i.e. each virtual resistance increases from 0.2Ω to 4Ω). Fig. 10 illustrates the source-side output admittance of *I-V* droop-controlled study case with the same virtual resistance settings. As a conclusion to the comparison, the *I-V* droop shows better stability margin, especially under small virtual resistances.

In Fig. 11 and Fig. 12, the simulation results of these two approaches feeding CPL is illustrated. The results show that the system damping of *V-I* droop-controlled DC MGs become poorer along with the increase of CPL. The system can be unstable if the CPL is too much. For the same load conditions, *I-V* droop can provide a much larger capability and stability margin when feeding CPL.

IV. Conclusion

In this paper, the output characteristics of both *V-I* and *I-V* droop-controlled converters are analyzed. For comparison, two detailed state-space based models are established for the study case. The proposed framework of state-space model can also be used to analyzed mixed *V-I* and *I-V* droop-controlled DC MG and can be extended to analyze *n*-converters MG. By deriving the transfer functions from the established models, the output admittance of droop controlled converters are obtained and compared. In addition, by fairly simplifying current loops as first-order delay with time constant derived by its control bandwidth, generalized analytical models are derived for other cases. From the generalized models, two modified Thévenin equivalents of both *V-I* and *I-V* droop-controlled converters are deduced. Simulations are carried out using PLECS and its impedance measurement function. The results validate the accuracy of proposed models and analytical results.

References

[1] R. H. Lasseter, "MicroGrids," 2002 IEEE Power Engineering Society Winter Meeting. Conference Proceedings (Cat. No.02CH37309), 2002, pp. 305-308 vol.1.

[2] J. J. Justo, F. Mwasilu, J. Lee, J. W. Jung, "AC-microgrids versus DC-microgrids with distributed energy resources: A review," Renewable and Sustainable Energy Reviews, 2013, 24, pp. 387-405.

[3] D. J. Becker and B. J. Sonnenberg, "DC microgrids in buildings and data centers," *2011 IEEE 33rd International Telecommunications Energy Conference (INTELEC)*, Amsterdam, 2011, pp. 1-7.

[4] H. Kakigano, Y. Miura and T. Ise, "Low-Voltage Bipolar-Type DC Microgrid for Super High Quality Distribution," in *IEEE Transactions on Power Electronics*, vol. 25, no. 12, pp. 3066-3075, Dec. 2010.

[5] J. M. Guerrero, J. C. Vasquez, J. Matas, L. G. de Vicuna and M. Castilla, "Hierarchical Control of Droop-Controlled AC and DC Microgrids—A General Approach Toward Standardization," in *IEEE Transactions on Industrial Electronics*, vol. 58, no. 1, pp. 158-172, Jan. 2011.

[6] J. M. Guerrero, M. Chandorkar, T. L. Lee and P. C. Loh, "Advanced Control Architectures for Intelligent Microgrids—Part I: Decentralized and Hierarchical Control," in *IEEE Transactions on Industrial Electronics*, vol. 60, no. 4, pp. 1254-1262, April 2013.

[7] I. Batarseh, K. Siri and H. Lee, "Investigation of the output droop characteristics of parallel-connected DC-DC converters," *Power Electronics Specialists Conference, PESC '94 Record., 25th Annual IEEE*, Taipei, 1994, pp. 1342-1351 vol.2.

[8] K. Siri and J. Banda, "Current distribution for parallel-connected DC power sources without remote sensing," *Proceedings of Intelec 94*, Vancouver, BC, 1994, pp. 196-203.

[9] Y. Wang, L. Zhang, H. Li, J. Liu, "Hierarchical coordinated control of wind turbine-based DC microgrid," *Proceedings of the Chinese Society of Electrical Engineering*, 2013, vol. 33, no.4, pp. 16-24.

[10] F. Chen, R. Burgos, and D. Boroyevich, "Output impedance comparison of different droop control realizations in DC systems," *2016 IEEE 17th Work. Control Model. Power Electron. COMPEL 2016*, 2016.

[11] F. Gao *et al*., "Comparative Stability Analysis of Droop Control Approaches in Voltage-Source-Converter-Based DC Microgrids," in *IEEE Transactions on Power Electronics*, vol. 32, no. 3, pp. 2395-2415, March 2017.

[12] A. Emadi, A. Khaligh, C. H. Rivetta and G. A. Williamson, "Constant power loads and negative impedance instability in automotive systems: definition, modeling, stability, and control of power electronic converters and motor drives," in *IEEE Transactions on Vehicular Technology*, vol. 55, no. 4, pp. 1112-1125, July 2006.

[13] R. D. Middlebrook, "Input Filter Considerations in Design and Application of Switching Regulators," presented at the *1976 IEEE IAS Annual Meeting (IAS'76)*, 1976.

[14] A. Riccobono and E. Santi, "Comprehensive Review of Stability Criteria for DC Power Distribution Systems," in *IEEE Transactions on Industry Applications*, vol. 50, no. 5, pp. 3525-3535, Sept.-Oct. 2014.

[15] S. D. Sudhoff and J. M. Crider, "Advancements in generalized immittance based stability analysis of DC power electronics based distribution systems," *2011 IEEE Electr. Sh. Technol. Symp. ESTS 2011*, pp. 207–212, 2011.

[16] R. Ahmadi and M. Ferdowsi, "Modeling closed-loop input and output impedances of DC-DC power converters operating inside dc distribution systems," *2014 IEEE Applied Power Electronics Conference and Exposition - APEC 2014*, Fort Worth, TX, 2014, pp. 1131-1138.

[17] Q. Xu et al., "Design and stability analysis for an autonomous DC microgrid with constant power load," 2016 IEEE Applied Power Electronics Conference and Exposition (APEC), Long Beach, CA, 2016, pp. 3409-3415.

[18] A. P. N. Tahim, D. J. Pagano, E. Lenz and V. Stramosk, "Modeling and Stability Analysis of Islanded DC Microgrids Under Droop Control," in *IEEE Transactions on Power Electronics*, vol. 30, no. 8, pp. 4597-4607, Aug. 2015.

PAPER C. Reference [59]

Constant Power Load Instability Mitigation in DC Shipboard Power Systems Using Negative Series Virtual Inductor Method

Zheming Jin, Lexuan Meng, and Josep M. Guerrero

The paper has been published in

IECON 2017 - 43rd Annual Conference of the IEEE Industrial Electronics Society, Beijing, 2017, pp. 6789-6794.

Constant Power Load Instability Mitigation in DC Shipboard Power Systems Using Negative Series Virtual Inductor Method

Zheming Jin, Lexuan Meng, Josep M. Guerrero
Department of Energy Technology
Aalborg University
Aalborg, Denmark
zhe@et.aau.dk

***Abstract*—DC distribution technology has become the new choice and the trending technology of shipboard power systems for its advancement over its AC counterpart. In DC shipboard power systems, the bus voltage stability is a critical issue. The presence of tightly controlled high-power constant power load can induce system-level voltage instability. To mitigate such a problem, a novel compensation method based on model-derived specially designed negative virtual inductance loop is proposed in this paper. The mechanism of the proposed method is presented in detail. In addition to that, the proposed compensation method is compliable with both voltage-controlled and droop-controlled converters. Simulations are carried out to validate the proposed method, and the results show enhanced stability margin and capability when feeding constant power loads.**

Keywords—All-electric ship; shipboard power system; constant power load; stability; virtual impedance.

I. INTRODUCTION

DC distribution technologies, especially in medium-voltage level (i.e. MVDC), have been considered as promising solution for future all-electric ships (AESs) [1-3]. While there are still advances in the AC solutions, DC distribution based solutions are expected to provide significant operational and economic benefits for future ships [2, 4, 5].

For DC shipboard power systems (SPSs), the system-level stability is a critical and challenging issue. As DC SPS is a typical example of power electronic based islanded power system, all the power generators and consumers are interfaced through power electronic converters (PECs). When acting as loads, the tightly controlled PECs have control bandwidth high enough to make the consumed power independent from the bus voltage variations, which is referenced as constant power load (CPL). When operating in DC systems, the CPLs will perform negative incremental resistance that decreases system damping, one step further, it can lead to bus voltage instability [6-7].

The study associated with CPL instability issue can be traced back to 1976, when the interaction among PECs and passive components was firstly analyzed in [8]. Extensive study of the CPL instability issue have been reported in [9-11]. At the same time, several approaches have been proposed to mitigate the CPL instability issue. In [12], passive damper design method is reported to mitigate CPL instability issue. In [13], active damping method is reported to solve the same problem. In [14] and [15] linearization via state feedback (LSF) method and corresponding parameter estimation method are introduced. In [16], loop-cancellation technique is reported to compensate CPL instability issue in automotive applications. At the same time, sliding mode control solution [17] and model predictive control solution [18] are also employed. However, considerable common problem of these non-linear methods is their sensitivity to the system parameter. It is also noteworthy that these methods are all designed for voltage control mode, droop control mode which is also a common grid-control method in MVDC SPS is not considered during their design procedure. In [19], linear quadratic regulator (LQR) is used to stabilize a droop-controlled system. In [20], more traditional virtual impedance method is implemented in droop-controlled DC microgrids with CPL instability issue. However, the virtual impedance based stabilizer presented in [20] is complex and it is divided into two branches connected in series to the output terminal and the DC capacitor, which require more efforts to implement in practical system.

In this paper, model-derived series virtual inductor method is proposed to mitigate CPL instability in DC SPSs. It differs from more conventional virtual impedance methods that the virtual inductor used in this paper is negative, instead of being positive, to cancel part of the intrinsic impedance of the PEC. The mechanism of CPL instability issue and proposed method are analyzed in the following parts of this paper. Simulations are carried out to validate the proposed method, the results show enhanced stability margin and capability of feeding CPLs.

II. CPL INSTABILITY ISSUE

A. Modeling Constant Power Load

For the constant power nature of tightly controlled PECs, the following expression will be satisfied within the control bandwidth of the controller:

$$i_{Load} = \frac{P_{Load}}{V_{dc}} \tag{1}$$

where V_{dc}, i_{Load}, and P_{Load} are the voltage, current and power of the CPL.

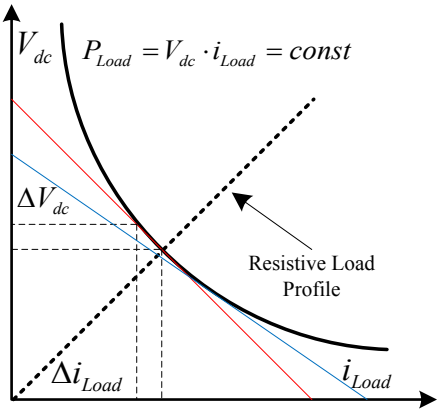

Fig. 1. Negative impedance behavior of CPLs.

As shown in Fig. 1, the incremental resistance of a CPL can be calculated by:

$$\frac{\partial V_{dc}}{\partial i_{Load}} = \frac{\partial}{\partial i_{Load}}\left(\frac{P_{Load}}{i_{Load}}\right) = -\frac{P_{Load}}{i^2_{Load}} = -\frac{V^2_{dc}}{P_{Load}} = R_{CPL} \qquad (2)$$

It indicates that the CPLs, although still consuming power, perform negative resistance in the system, which makes the system less damped and impacts the stability. A linearized equivalent circuit of a CPL can be derived from (2), which composed by the derived negative resistance and a controlled current source.

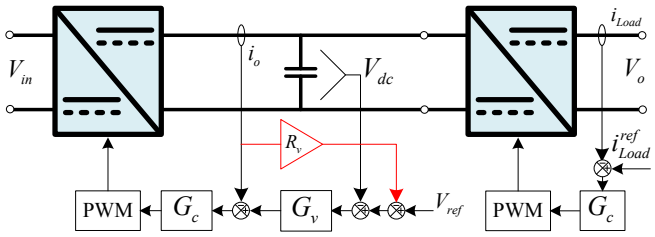

(a) Detailed control diagram

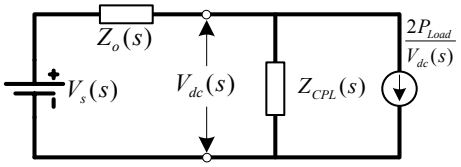

(b) Impedance based analytical diagram

Fig. 2. Analytical circuit of CPL instability issue.

In addition to the negative resistance shown in (2), the limited control bandwidth of controller will perform additional frequency-dependent negative impedance characteristic in the frequency range above the controller's control bandwidth. In Fig. 2, the linearized analytical circuit of CPL instability issue is presented, in which the bus voltage is determined by:

$$V_{dc}(s) = \frac{V_s(s)Z_{CPL}(s)}{Z_o(s)+Z_{CPL}(s)} = V_s(s)T_m(s), T_m(s) = \frac{1}{1+Z_o(s)/Z_{CPL}(s)} \qquad (3)$$

where $V_s(s)$, $Z_o(s)$ and $Z_{CPL}(s)$ stand for source voltage, source-side output impedance and negative impedance of CPLs, all presented in frequency-domain transfer functions. $T_m(s)$ is the minor loop gain of the system, which is critical to the system stability analysis [8-11].

The sufficient condition of system stability is that all the dominant poles of $T_m(s)$ locate in the stable region. It requires the source-side output impedance to have smaller magnitude than the negative impedance, or at least fulfill the marginal stability condition. In Fig. 3, a generalized scenario of CPL stability issue is illustrated by bode diagram. Detail analysis and discussion on the source-side output impedance will be given in the following part of this paper.

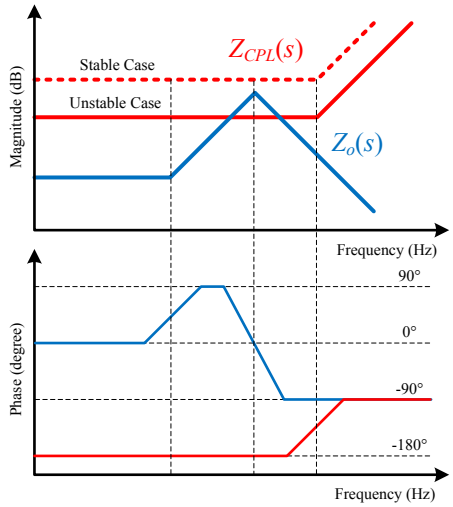

Fig. 3. Generalized frequency response of analytical circuit

B. *Source-side Output Impedance: Voltage Control Mode*

In Fig. 2(a), a generic control scheme for voltage control mode (VCM) and droop control mode (DCM) is illustrated. In this paper, conventional control architecture of PECs is used as the study case, in which PI controllers are used to regulate both voltage and current loops.

To analyzing the dynamic behavior of dual-loop controller, the inner current loop is commonly simplified as a first-order delay with a certain control bandwidth. Thus, the dynamic of DC-side output current in VCM can be descripted as:

$$I_o(s) = G_v(s)G_{clc}(s)\left[V_{ref}(s) - V_{dc}(s)\right] \qquad (4)$$

where $G_v(s)$ is the transfer function of voltage controller, $G_{clc}(s)$ is the simplified close-loop transfer function of the inner current loop.

Therefore, the source-side output impedance under VCM is calculated by:

$$Z_o(s) = Z_{con}(s) \| Z_c(s) = Z_{con}(s) \| \frac{1}{sC} \tag{5}$$

$$Z_{con}(s) = \frac{V_{ref}(s) - V_{dc}(s)}{I_o(s)} = \frac{1}{G_v(s)G_{clc}(s)} = \frac{1}{\frac{k(s+\alpha)}{s} \cdot \frac{\omega_c}{s+\omega_c}} \tag{6}$$

where $Z_{con}(s)$ stands for the inherent close-loop impedance of the PEC, C is the total capacitance in the DC bus. ω_c stands for the close-loop control bandwidth of the current loop, k is the proportional term of the voltage PI controller, and α presents the ratio of proportional and integral terms of the voltage PI controller.

From (5) and (6), an equivalent circuit can be derived to describe the dynamic of PEC, as shown in Fig. 4. Three virtual components are introduced, their parameters are shown as follow:

$$L_{d1} = \frac{1}{k\omega_c}, \quad L_{d2} = \frac{\omega_c - \alpha}{k\omega_c\alpha}, \quad R_d = \frac{\omega_c - \alpha}{k\omega_c}, \tag{7}$$

In Fig. 5, the derived frequency response of $Z_o(s)$, $Z_{con}(s)$, $Z_c(s)$ are illustrated. It can be seen from the bode diagram that the close-loop impedance $Z_{con}(s)$ under VCM is mostly inductive. When paralleled with DC capacitor, the output impedance $Z_o(s)$ got a peak near the intersection frequency.

C. *Source-side Output Impedance: Droop Control Mode*

From controller viewpoint, the main difference between DCM and VCM is the virtual resistance loop, which forms additional feedback loop to the controller. Similar to VCM, the dynamic of DCM controller can be descripted as:

$$I_o(s) = \frac{G_v(s)G_{clc}(s)}{1 + R_v G_v(s)G_{clc}(s)}\left[V_{ref}(s) - V_{dc}(s)\right] \tag{8}$$

where R_v stands for the virtual resistance, also named droop coefficient.

Thus, the close-loop impedance of converter under DCM will be:

$$Z_{con}(s) = \frac{1 + R_v G_v(s)G_{clc}(s)}{G_v(s)G_{clc}(s)} = R_v + \frac{1}{G_v(s)G_{clc}(s)} \tag{9}$$

It is seen from (9) that DCM have the same frequency-dependent impedance as VCM. In addition to that, the droop loop introduces an additional virtual resistor in series to the frequency-dependent impedance, as shown in Fig. 4(b).

In Fig. 6, the derived frequency response of $Z_o(s)$, $Z_{con}(s)$, $Z_c(s)$ are illustrated. Compared with the results shown in Fig.5, the close-loop impedance $Z_{con}(s)$ under DCM has resistive-inductive characteristic. Similar to the VCM case, the output impedance also has a peak near the intersection frequency. However, with the presence of virtual resistor, the peak value is more damped.

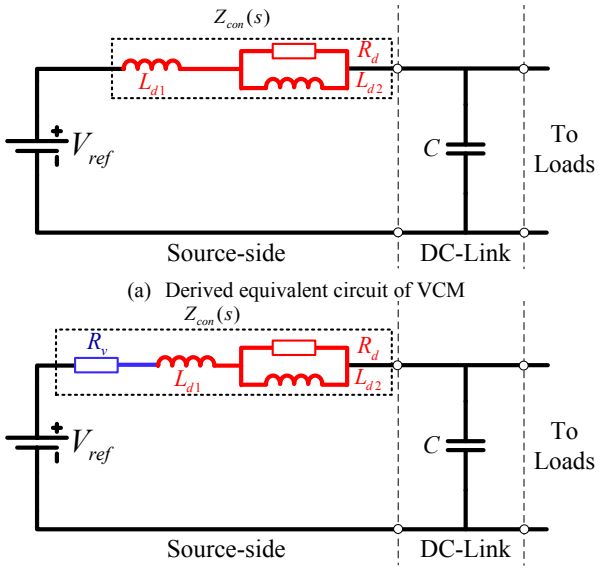

Fig. 4. Derived equivalent circuits of PEC with VCM and DCM controller.

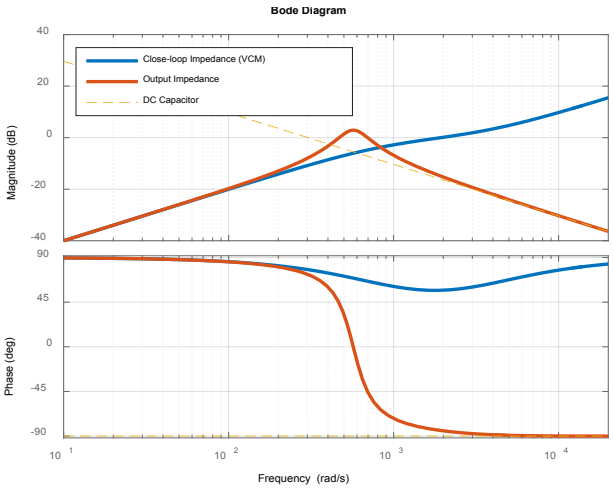

Fig. 5. Detailed frequency response of VCM controller .

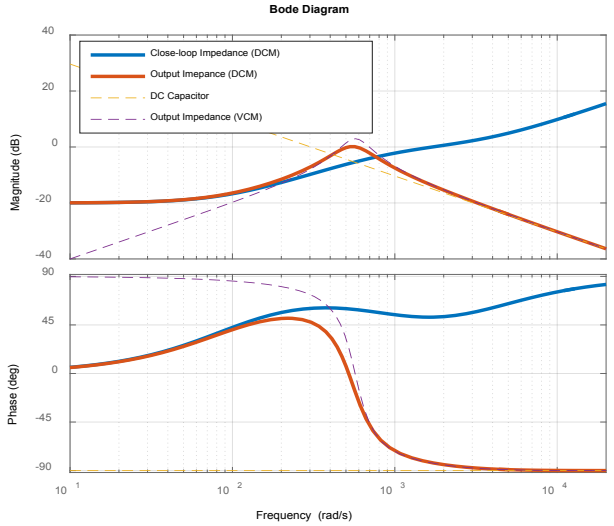

Fig. 6. Detailed frequency response of DCM controller.

III. PROPOSED METHOD

To mitigate the CPL instability issue discussed in the last section, a possible solution is to reduce the peak value of output impedance, therefore, the load-side performance will not be affected. It can be achieved by: (1) increase the series virtual resistance;(2) increase the capacitance of DC capacitor; (3) decrease the inductance of the equivalent circuit.

In case of DC SPS, the power ratings are considerably high, so that the virtual resistance must be much smaller than other applications. Otherwise, the voltage drop will exceed its operational limitation. At the same time, the increase of DC capacitance is costly in MVDC applications. In addition to that, it also results in more destructive DC-side short-circuit fault, which is critical to the system design. For these reasons, in this paper, a negative series virtual inductor method is proposed to refine the source-side output impedance, thus mitigating the CPL instability issue in DC SPS.

A. Mechanism of Negative Seires Virtual Inductor Method

As conclusions of the analysis in the last section, several key features of the converter's close-loop impedance can be summarized as following:

- The dual-loop controller itself performs an inductor in series to a paralleled *RL* branch, as shown in Fig. 4.
- The feedback loop used in droop method will perform additional component (marked blue) in series to the virtual components introduced by dual-loop controller (marked red).
- From (8) and (9), the droop resistor is irrelevant to the intrinsic impedance of dual-loop controller. According to the feature of feedback control, the same feature is equally applicable to other virtual impedance design.

With these remarks, a negative series virtual inductor can be introduced to partially cancel the inductance of the instinct impedance, thus decreasing the peak value of the source-side output impedance.

To form a series virtual inductor, the similar feedback loop that used in droop method is feasible. Derivation controller with well-designed parameter will be added, instead of using simplest gain to form virtual resistor. In Fig. 7 the control diagram of the proposed method is shown. It is noteworthy that the designed negative virtual inductor is to cancel the virtual component L_{d1}, so that the following design rules must be fulfill to ensure the controller is individually stable:

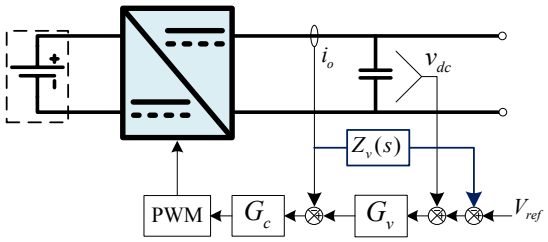

Fig. 7. Control diagram of the proposed method.

$$Z_v(s) = R_v - sL_v, \qquad (0 \le L_v \le L_{d1}) \tag{10}$$

In Fig. 8, the frequency response of output impedance using proposed method with different parameter settings (L_v=0~1.2L_{d1}) are shown. In Fig. 9, the poles and zeros of minor loop gain $T_m(s)$ is shown. Although the peak magnitude will continuously decreases with larger negative virtual inductor design, the bus voltage got unstable once the stability boundary shown in (10) is exceeded.

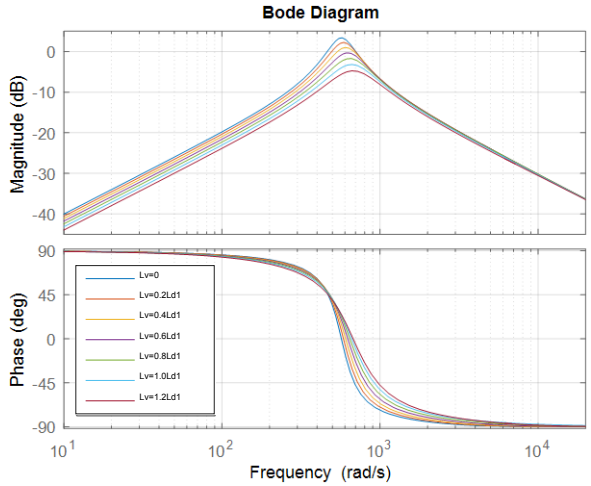

Fig. 8. Frequency response of output impedance (VCM as example) with proposed method.

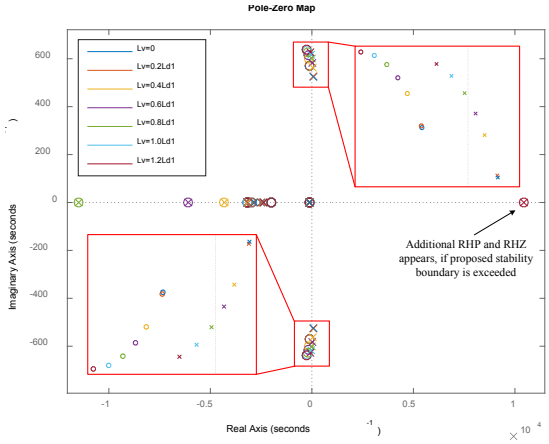

Fig. 9. Poles and zeros of $T_m(s)$ with proposed method. (P_{CPL}=6.5MW)

IV. SIMULATION VERIFICATION

To validate the proposed negative series virtual inductor method, simulations are carried out with a simplified DC SPS composed by two source converters and controllable CPLs. Similar study cases have been presented in [14] and [15]. The simulations are carried out with detailed switching model established by using PLECS. The parameters used in the simulations are given in Table I. In Fig. 9, the simulation results of the system under VCM operation are shown. In Fig. 10, the simulation results of the system under DCM operation are shown. It can be seen from the simulation results that the system's stability margin and capability of feeding CPL is enhanced with the proposed method.

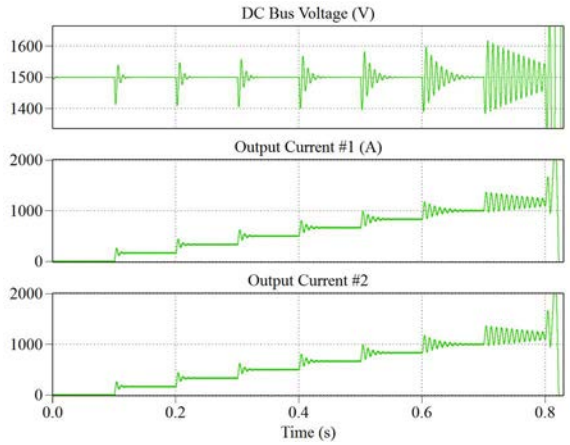

(a) Simulation results using only VCM controller

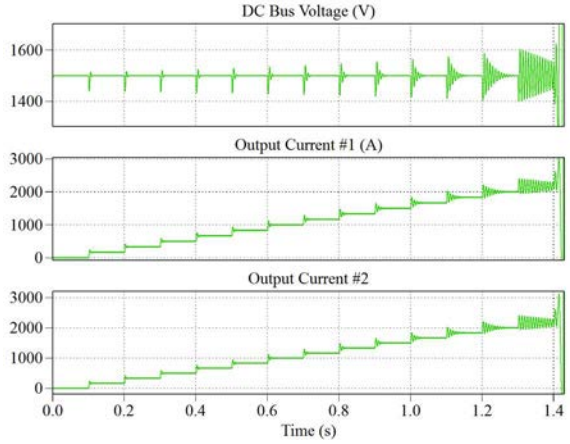

(b) Simulation results using VCM controller and proposed method

Fig. 10. Simulation results of VCM controller with/without proposed method.

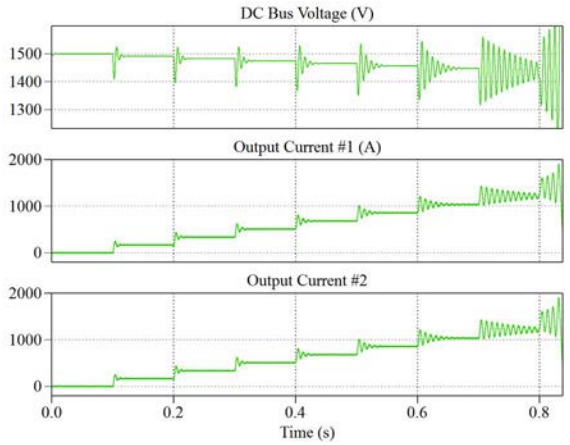

(a) Simulation results using only DCM controller

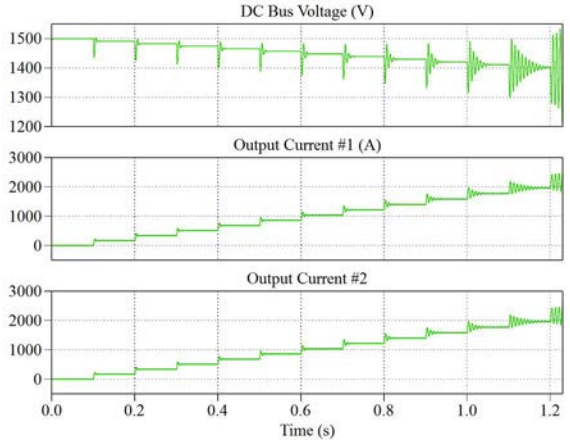

(b) Simulation results using DCM controller and proposed method

Fig. 11. Simulation results of DCM controller with/without proposed method.

TABLE I. PARAMETERS OF SIMULATED STUDY CASE

Description of the Parameter	***Symbol***	***Value***
Voltage Reference	V_{ref}	1500 V
Source Voltage	E_1, E_2	3000 V, 3000 V,
Inductance of Buck Converters	L_1, L_2	8 mH, 8 mH
Stary Resistance of inductors,	r_1, r_2	0.1 Ω, 0.1 Ω
Switching Frequency	f_{sw}	2 kHz
Total Capacitance in DC Bus	C	3.3 mF
Proportion Term of Voltage Controller	K_{pv1}, K_{pv2}	1, 1
Integral Term of Voltage Controller	K_{iv1}, K_{iv2}	1000, 1000
Proportion Term of Current Controller	K_{pc1}, K_{pc2}	0.009, 0.009
Integral Term of Current Controller	K_{ic1}, K_{ic2}	0.1, 0.1
Virtual Resistances for Droop Control	R_{v1}, R_{v2}	0.05 Ω, 0.05 Ω,
CPL Control Bandwidth	ω_{CPL}	2000 rad/s
Load Profile	P_{Load}	500 kW/step 10 steps/s
Inductance of Negative Series Virtual Inductor	L_{v1}, L_{v2}	-0.243mH, -0.243mH, ($\approx -0.8L_{d1}$)

It can be seen from the simulation results that when using the proposed method, the system's capability of feeding CPL are improved. When operating in VCM, the maximum capable power of CPL is increased from 3.5 MW to 6.5 MW. As for operation under DCM control, the maximum capable power of CPL is increased from 3.5 MW to 5.5 MW.

It is noteworthy that theoretically DCM controller has a lower peak value of output impedance. However, the voltage drop will result in increased negative impedance of the same amount of CPL. Conversely, the capability of feeding CPL may decrease, when compared with VCM.

V. CONCLUSIONS

In this paper, model-derived negative series virtual inductor is presented as a compensating method to mitigate the CPL instability issue in DC SPSs. It differs from conventional virtual resistance or virtual impedance methods that specially designed negative virtual inductor is used to modify system stability when feeding CPL. The mechanism of CPL instability and the proposed method are briefly introduced. The output impedance characteristic of VCM and DCM controllers are analyzed. Simulation results are carried out to validate the proposed method, the results show enhanced stability and capability of feeding CPL.

REFERENCES

[1] IEEE Recommended Practice for 1 kV to 35 kV Medium-Voltage DC Power Systems on Ships. IEEE Standard 1709, 2010.

[2] J. F. Hansen and F. Wendt, "History and State of the Art in Commercial Electric Ship Propulsion, Integrated Power Systems, and Future Trends," *Proc. IEEE*, vol. 103, no. 12, pp. 2229–2242, Dec. 2015.

[3] Z. Jin, G. Sulligoi, R. Cuzner, L. Meng, J. C. Vasquez and J. M. Guerrero, "Next-Generation Shipboard DC Power System: Introduction Smart Grid and dc Microgrid Technologies into Maritime Electrical Netowrks," in *IEEE Electrification Magazine*, vol. 4, no. 2, pp. 45-57, June 2016.

[4] R. Soman, M. M. Steurer, T. A. Toshon, M. O. Faruque and R. M. Cuzner, "Size and Weight Computation of MVDC Power Equipment in Architectures Developed Using the Smart Ship Systems Design Environment," in *IEEE Journal of Emerging and Selected Topics in Power Electronics*, vol. 5, no. 1, pp. 40-50, March 2017.

[5] S. Rao K., P. J. Chauhan, S. K. Panda, G. Wilson, Xiong Liu and A. K. Gupta, "An exercise to qualify LVAC and LVDC power system architectures for a Platform Supply Vessel," *2016 IEEE Transportation Electrification Conference and Expo*, Asia-Pacific (ITEC Asia-Pacific), Busan, 2016, pp. 332-337.

[6] C. Rivetta, G. A. Williamson and A. Emadi, "Constant power loads and negative impedance instability in sea and undersea vehicles: statement of the problem and comprehensive large-signal solution," *IEEE Electric Ship Technologies Symposium,* 2005., Philadelphia, PA, 2005, pp. 313-320.

[7] M. Cupelli, L. Zhu and A. Monti, "Why Ideal Constant Power Loads Are Not the Worst Case Condition From a Control Standpoint," in *IEEE Transactions on Smart Grid*, vol. 6, no. 6, pp. 2596-2606, Nov. 2015.

[8] R. D. Middlebrook, "Input Filter Considerations in Design and Application of Switching Regulators," presented at the *1976 IEEE IAS Annual Meeting (IAS'76)*, 1976.

[9] A. Emadi, A. Khaligh, C. H. Rivetta and G. A. Williamson, "Constant power loads and negative impedance instability in automotive systems: definition, modeling, stability, and control of power electronic converters and motor drives," in *IEEE Transactions on Vehicular Technology,* vol. 55, no. 4, pp. 1112-1125, July 2006.

[10] A. Kwasinski, C. N. Onwuchekwa, "Dynamic behavior and stabilization of DC microgrids with instantaneous constant-power loads", *IEEE Trans. Power Electron.*, vol. 26, no. 3, pp. 822–834, Mar. 2011.

[11] D. Marx, P. Magne, B. Nahid-Mobarakeh, S. Pierfederici and B. Davat, "Large Signal Stability Analysis Tools in DC Power Systems With Constant Power Loads and Variable Power Loads—A Review," in *IEEE Transactions on Power Electronics*, vol. 27, no. 4, pp. 1773-1787, April 2012.

[12] M. Cespedes, L. Xing and J. Sun, "Constant-Power Load System Stabilization by Passive Damping," in *IEEE Transactions on Power Electronics*, vol. 26, no. 7, pp. 1832-1836, July 2011.

[13] A. M. Rahimi and A. Emadi, "Active damping in DC/DC power electronic converters: a novel method to overcome the problems of constant power loads", *IEEE Transactions on Industrial Electronics*, vol. 56, no. 5, pp. 1428–1439, May 2009.

[14] G. Sulligoi, D. Bosich, G. Giadrossi, L. Zhu, M. Cupelli and A. Monti, "Multi-Converter Medium Voltage DC Power Systems on Ships: Constant-Power Loads Instability Solution using Linearization via State Feedback Control", *IEEE Transactions on Smart Grid*, accepted for publication.

[15] D. Bosich; G. Sulligoi; E. Mocanu; M. Gibescu, "Medium Voltage DC Power Systems on Ships: an Off-line Parameter Estimation for Tuning the Controllers' Linearizing Function," in *IEEE Transactions on Energy Conversion* , vol.PP, no.99, pp.1-1.

[16] A. M. Rahimi, G. A. Williamson and A. Emadi, "Loop-Cancellation Technique: A Novel Nonlinear Feedback to Overcome the Destabilizing Effect of Constant-Power Loads," in *IEEE Transactions on Vehicular Technology*, vol. 59, no. 2, pp. 650-661, Feb. 2010.

[17] A. Agarwal, K. Deekshitha, S. Singh and D. Fulwani, "Sliding mode control of a bidirectional DC/DC converter with constant power load," *2015 IEEE First International Conference on DC Microgrids (ICDCM)*, Atlanta, GA, 2015, pp. 287-292.

[18] X. Zhang, D. M. Vilathgamuwa, K. J. Tseng, B. S. Bhangu and C. J. Gajanayake, "Power Buffer With Model Predictive Control for Stability of Vehicular Power Systems With Constant Power Loads," in *IEEE Transactions on Power Electronics*, vol. 28, no. 12, pp. 5804-5812, Dec. 2013.

[19] L. Zhu, J. Liu, M. Cupelli and A. Monti, "Decentralized Linear Quadratic Gaussian control of multi-generator MVDC shipboard power system with Constant Power Loads," *2013 IEEE Electric Ship Technologies Symposium (ESTS)*, Arlington, VA, 2013, pp. 308-313.

[20] X. Lu, K. Sun, J. M. Guerrero, J. C. Vasquez, L. Huang and J. Wang, "Stability Enhancement Based on Virtual Impedance for DC Microgrids With Constant Power Loads," in *IEEE Transactions on Smart Grid*, vol. 6, no. 6, pp. 2770-2783, Nov. 2015.

PAPER D. Reference [60]

Admittance-type RC-mode Droop Control to Introduce Virtual Inertia in DC Microgrids

Zheming Jin, Lexuan Meng, Renke Han, Josep M. Guerrero, and Juan C. Vasquez

The paper has been published in

2017 IEEE Energy Conversion Congress and Exposition (ECCE), Cincinnati, OH, 2017, pp. 4107-4112.

Admittance-type RC-mode Droop Control to Introduce Virtual Inertia in DC Microgrids

Zheming Jin, Lexuan Meng, Renke Han, Josep M. Guerrero, Juan C. Vasquez
Department of Energy Technology
Aalborg University
Aalborg, Denmark
zhe@et.aau.dk

***Abstract*— One of the major feature of DC microgrids is its high penetration of power electronic converters, as a result, the system inertia becomes a problem. In this paper, an admittance-type droop control with additional capability of introducing virtual inertia to the system. With the proposed method, each energy source will also contribute virtual inertia to the system, thus improving transient response and stability of the entire DC microgrid. The inertia issue of droop control is firstly analyzed. A comparative study is carried out between conventional method (i.e. impedance-type droop control method) and the new proposal in terms of their different control principles, characteristics of equivalent output admittance/impedance, and effectiveness in achieving desired virtual inertia introduction. Ultimately, simulations and experiments are carried out to verify proposed control methods. The results show improved system inertia and enhanced performance.**

Keywords—DC microgrids, droop control, virtual inertia, stability, transient response.

I. INTRODUCTION

DC microgrids (MGs) are drawing great attention due to their convenience and high efficiency in integrating renewable energy sources, energy storage systems and modern electronic loads, especially in off-grid or islanded applications [1]-[2]. Power electronic converters are the key components, as well as the enabling technology, in the DC MGs, providing necessary interface between energy sources and the common DC buses. However, the high penetration of PECs will also result in a low-inertia system, the stability and the dynamic performance of which can be easily affected [3]. Therefore, virtual inertia is a promising and effective way to solve the problem without introducing additional cost or loss. Heretofore, virtual inertia control of PECs mainly focus on the active power support to the utility grid or AC MG in transient response. A representative virtual inertia control method is to operate inverters as virtual synchronous generators [4]. However, the research of virtual inertia control in the field of DC MG is barely reported.

Droop control is the common control method in both AC and DC MGs to regulate the frequency/voltage at the common buses (i.e. point of common coupling) and to share the loads properly among all the power sources [5]. In case of DC MGs, the most frequently used droop method is the V-I droop, also namely virtual resistance control, the control diagram of which is illustrated in Fig. 1(a) (using Buck converter as example). In several recent studies [6], the I-V droop, as known as reverse droop, is introduced to achieve the similar control effect, the control diagram of which is shown in Fig. 1(b). It can be seen from the control diagrams that a virtual resistance is used in the feedback loop of V-I droop method, meanwhile, its reciprocal (physically the conductance) is used in the I-V droop method. For this reason, these two methods and their derivatives can be categorized into impedance-type and admittance-type methods to realize droop control. However, with conventional droop design (i.e. using only virtual resistance/conductance), neither V-I droop method nor I-V droop method will introduce additional inertia to the DC MGs.

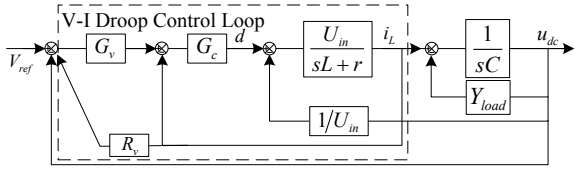

(a) Control diagram of *V-I* droop method

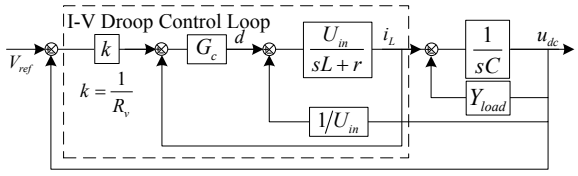

(b) Control diagram of *I-V* droop method

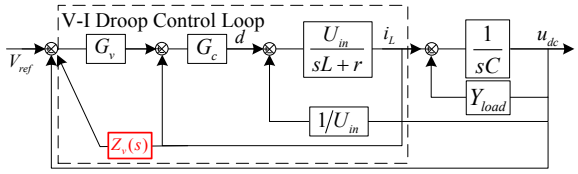

(c) Generalized diagram of impedance-type droop method

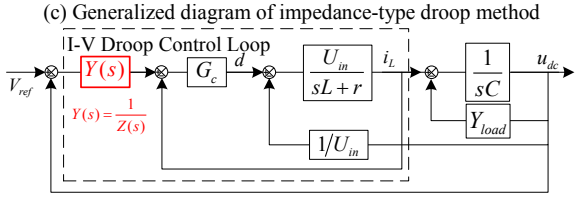

(d) Generalized diagram of admittance-type droop method

Fig. 1. Illustration of different droop control methods

In this paper, an admittance-type RC-mode droop control method is proposed to introduce virtual inertia into DC MGs. The major contributions can be summarized as: (1) analysis of the inertia issue and mechanism of virtual inertia is carried out; (2) a comparison of different realization methods of droop control is carried out to address their different characteristics, especially considering complex virtual impedance/admittance; (3) propose a decentralized virtual inertia control method for inertia enhancement in DC MGs. Simulations and experiments are carried out with the proposed method and the results show enhanced system inertia and improved transient response.

II. System Inertia of DC MG

In general, inertia of a power system behaves as to prevent sudden change in critical variable spontaneously by releasing its stored energy, and thereby allowing the power sources to rebuild equilibrium timely. For AC power systems, the inertia behaves as to prevent sudden change in systemic frequency, and the active power is regulated to rebuild equilibrium, as detailed in rotation equation of synchronous machine [4]:

$$P_{set} - P_o - D_p(\omega - \omega_n) = J\omega\frac{d\omega}{dt} = P_{vi} \tag{1}$$

where P_{set}, P_o, P_{vi}, ω, ω_n, D_p, J are the active power reference, the output power, released power of inertial behavior, the real-time angular frequency, the rated angular frequency, the damping coefficient, and the moment of inertia, respectively.

When setting $J=0$, the equation (1) can be rewritten as:

$$\omega = \omega_{no} - mP_o \quad \text{where} \quad \omega_{no} = \omega_n + P_{set}/D_p; \quad m = 1/D_p; \tag{2}$$

which is the widely-used ω-P droop equation in the field of AC MGs [5]. In other words, the ω-P droop characteristic is actually emulating the behavior of a synchronous machine without inertia.

Similarly, in DC MGs, the inertia behaves as to prevent sudden change in DC bus voltage, and the output power of converters will be regulated to rebuild equilibrium, as detailed in the following power balancing equation:

$$P_{set} - P_o - D_p(u - u_n) = C_v u\frac{du}{dt} = P_{vi} \tag{3}$$

where u, u_n, C_v are the DC bus voltage, the rated DC bus voltage and the inertia coefficient (physically as a capacitance).

When setting $C_v=0$, the equation (3) can be rewritten as:

$$u = u_{no} - mP_o \quad \text{where} \quad u_{no} = u_n + P_{set}/D_p; \quad m = 1/D_p; \tag{4}$$

where i_v represents the desired current injection, u_{no} is the no-load bus voltage of DC droop control, m presents the droop coefficient of the power source.

From (1) and (3), it can be derived that the virtual inertia control is essentially modification to the droop method with additional power injection to support the system in transient-states. In addition to that, when substitute the basic power equation into (3), the desired current injection of virtual inertia control can be derived as:

$$i_{vi} = -\frac{kP_{vi}}{u} = -kC_v\frac{du}{dt} = C_v'\frac{d(u_{no} - u)}{dt} \tag{5}$$

where the injected power of virtual inertia control is k times of the system's original inertial behavior, the negative sign is to present that power is injecting to the system, $C_v'=kC_v$ which is the virtual inertia coefficient introduced to the system.

The equation (5) can be also transformed into:

$$u(s) = u_{no} - \frac{1}{sC_v'}i_{vi}(s) \tag{6}$$

$$i_{vi}(s) = sC_v'\left(u_{no} - u(s)\right) \tag{7}$$

The equation (6) and (7) show that the desired virtual inertia control can be achieved using droop control framework by adding capacitive virtual impedance/admittance in addition to the conventional virtual resistance/conductance. It is also noteworthy that the proposed component shall be equivalently parallel connected to the original virtual component. Therefore, the modified droop control function become:

$$u(s) = u_{no} - \left(\frac{1}{sC_v'} \| R_d\right)i_{vi}(s) = u_{no} - Z_d(s)i_o(s) \tag{8}$$

$$i_o(s) = \left(\frac{1}{R_d} + sC_v'\right)\left(u_{no} - u(s)\right) = Y_d(s)\left(u_{no} - u(s)\right) \tag{9}$$

In this case, each participant of droop based voltage regulation will be able to contribute both power support and virtual inertia support to the DC MG. Meanwhile, the virtual inertia become additional degree of freedom for the system design and management.

III. Impact of Different Realizations

In the last section, the inertia issue and the control principle of the proposed virtual inertia control method is analyzed. However, in the previous analysis, the dynamic behavior of controllers and the impact of using different control diagrams (i.e. impedance-type or admittance-type droop methods as shown in Fig. 1) is completely neglected. To address this problem, the impact of different realization of the proposed method is analyzed in this section.

To analyze the impact of using different realization, an admittance based analysis is carried out to address and compare the effectiveness of impedance-type and admittance-type droop methods when realizing the proposed virtual inertia control. In Fig. 2 the admittance based analysis is illustrated.

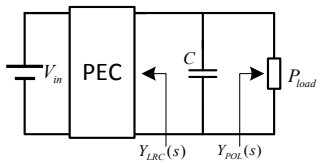

Fig. 2. Illustration of different droop control methods

In order to analyze the behavior of dual-loop control system, a common method is to assume the inner current loop is well-designed with a control bandwidth of ω_c, and simplified as a first order transfer function [6]. In this paper, the general-case controller (PI based voltage/current control loop) is considered, therefore, the transfer function of voltage controller and close-loop transfer function of current loop are considered as:

$$G_v(s) = k_p + \frac{k_i}{s} = k_p \frac{s+\alpha}{s}; \quad G_{clc}(s) = \frac{\omega_c}{s+\omega_c}; \tag{10}$$

In [7], the detailed state-space model of the two basic droop control methods has been established. From which, the detailed close-loop transfer function of current loop and simplified case are shown in Fig. 3, it shows that the approximation is still accurate enough for further analysis.

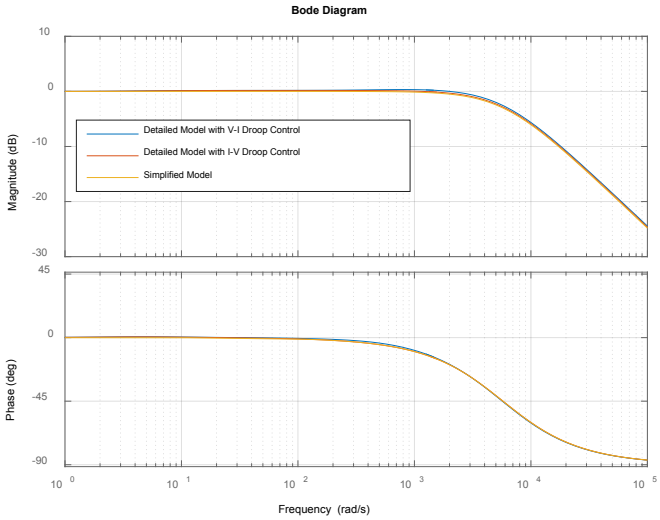

Fig. 3. Frequency response of detailed close-loop current control

In equation (8) and (9), the ideal droop control principle has been shown. However, when considering the non-ideal control behavior of the practical controllers, the variables shown in (8) and (9) are actually the reference of inner-loop controllers. By analyzing the control diagrams shown in Fig. 1, the behaviors of impedance-type and admittance-type droop controller can be descripted as following equations:

$$I_o^{V-I}(s) = \frac{G_v(s)G_{clc}(s)}{1+Z_d(s)G_v(s)G_{clc}(s)}(u_{no} - u(s)) \tag{11}$$

$$I_o^{I-V}(s) = Y_d(s)G_{clc}(s)(u_{no} - u(s)) \tag{12}$$

In this case, the output admittance/impedance of droop-controlled converters can be derived by:

$$\begin{cases} Y_o^{V-I}(s) = \dfrac{I_o^{V-I}(s)}{u_{no} - u(s)} = \dfrac{G_v(s)G_{clc}(s)}{1+Z_d(s)G_v(s)G_{clc}(s)} \\ Z_o^{V-I}(s) = \dfrac{1}{Y_o^{V-I}(s)} = Z_d(s) + \dfrac{1}{G_v(s)G_{clc}(s)} \end{cases} \tag{13}$$

$$\begin{cases} Y_o^{I-V}(s) = \dfrac{I_o^{I-V}(s)}{u_{no} - u(s)} = Y_d(s)G_{clc}(s) \\ Z_o^{I-V}(s) = \dfrac{1}{Y_o^{I-V}(s)} = \dfrac{Z_d(s)}{G_{clc}(s)} = Z_d(s) + \dfrac{s}{\omega_c}Z_d(s) \end{cases} \tag{14}$$

From these equations, several very important remarks can be derived:

- The output admittance/impedance of impedance-type realization is performed by desired virtual impedance and an irrelevant component connected in series. The additional component is determined by the parameters of the dual-loop controller, which can be treat as the intrinsic impedance of the controller.
- The output admittance/impedance of admittance-type realization is performed by desired virtual admittance and a higher-order term of the virtual admittance. The additional component is determined by both the virtual admittance design and control bandwidth of the system.

By substitute (10) into (13), the intrinsic impedance can be descripted as:

$$\begin{aligned} Z_{con}^{V-I}(s) &= \frac{1}{G_v(s)G_{clc}(s)} = \frac{1}{k_p\omega_c}\frac{s(s+\omega_c)}{s+\alpha} \\ &= s\frac{1}{k_p\omega_c} + s\frac{\omega_c-\alpha}{k_p\omega_c\alpha} \| \frac{\omega_c-\alpha}{k_p\omega_c} \\ &= sL_1 + sL_2 \| R_1 \end{aligned} \tag{15}$$

In Fig. 4, the derived output admittance/impedance are presented by equivalent circuits. It is important to notice that the intrinsic impedance of the dual-loop controlled converter (including both voltage mode control and impedance-type droop control) is mainly inductive. The presence of inductive intrinsic impedance will make impedance-type method less effective when achieving proposed virtual inertia control.

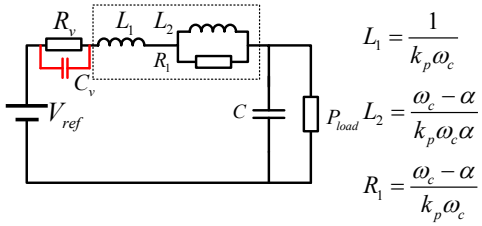

(a) Derived equivalent circuit of impedance-type droop method

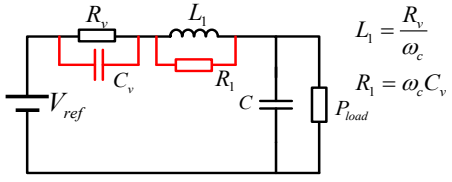

(b) Derived equivalent circuit of admittance-type droop method

Fig. 4. Equivalent circuits of different droop approaches with proposed virtual inertia control. (virtual components introduced by proposed virtual inertia method is marked red)

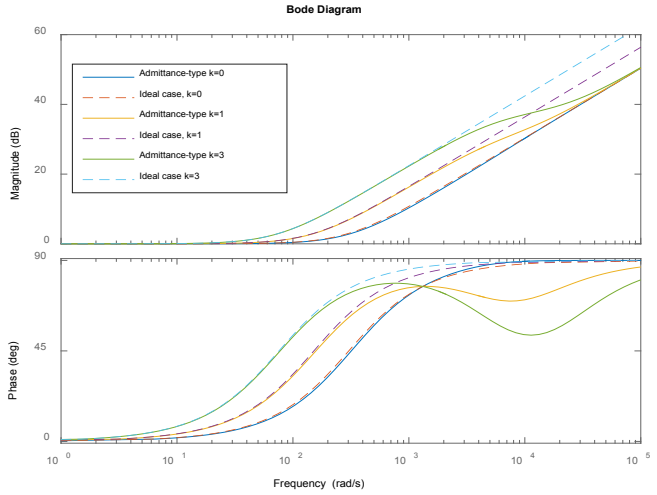

(a) Source-side admittance of the system using admittance-type droop method with different settings of virtual inertia

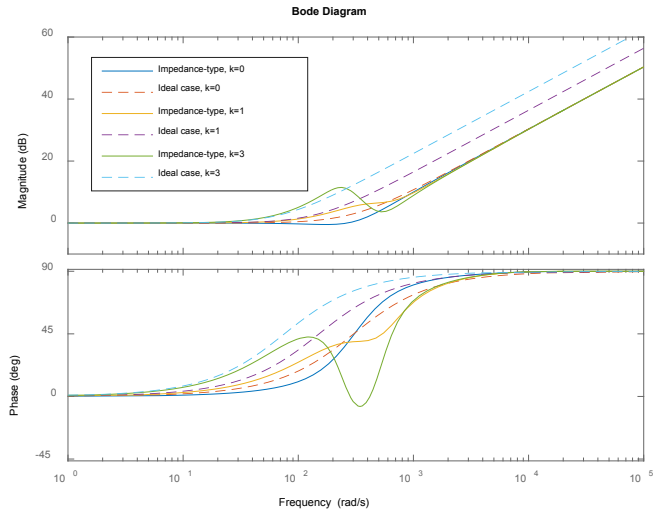

(b) Source-side admittance of the system using impedance-type droop method with different settings of virtual inertia

Fig. 5. Derived source-side admittance of the system using different droop approaches together with different settings of virtual inertia.

In Fig. 5, the frequency-response of source-side admittance with different settings of virtual inertia ($k=0,1,3$). In order to compare the effectiveness (or suitableness) of different droop approaches, the ideal cases which is derived by assuming the output admittance of droop-controlled converters are exactly as desired design (i.e. $Y_o=1/R_d+sC_v'=1/R_d+ksC_v$).

From Fig. 5(a), it can be found that the system behavior within the control bandwidth of current loop is following the ideal case very well when using admittance-type realization of proposed virtual inertia control. Beyond the control bandwidth limitation, the virtual inertia will gradually degrade.

As for impedance-type realization, the output admittance of the system does not follow the ideal case very well, which means the system behavior will not meet the expectation. In addition to that, the interaction between the intrinsic impedance and desired virtual capacitance is significant. The interaction shows resonant behavior and it will further reduce the effective range of the impedance-type realization.

Based on these analytical results, the admittance-type droop method is chosen as the realization method for proposed virtual inertia control.

IV. Simulation Validation of Proposed Method

In order to validate the proposed virtual inertia control method, simulations are carried out using PLECS. The study case DC MG used in the simulation has the same parameters of experimental setup. In the simulation, two droop-controlled converters are connected in parallel, feeding a resistive load. The system parameters are listed in Table I.

In Fig. 6 the simulation results are shown. In Fig. 6(a), the simulation results of basic admittance-type realization without virtual inertia control (i.e. $k=0$). In Fig. 6(b), the simulation results of using proposed virtual inertia control are shown.

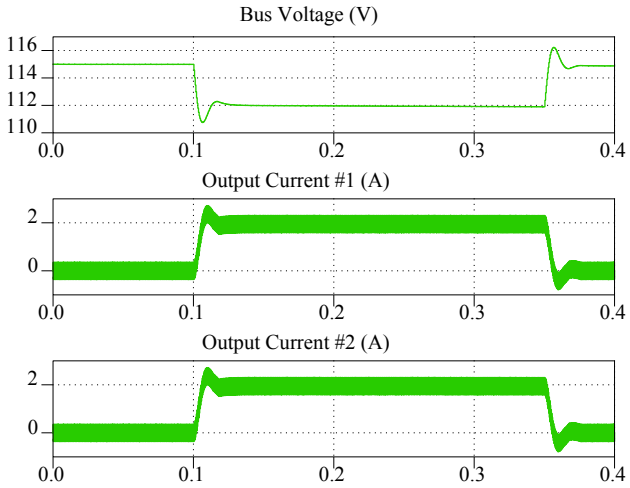

(a) Simulation results of load changing without proposed virtual inertia control

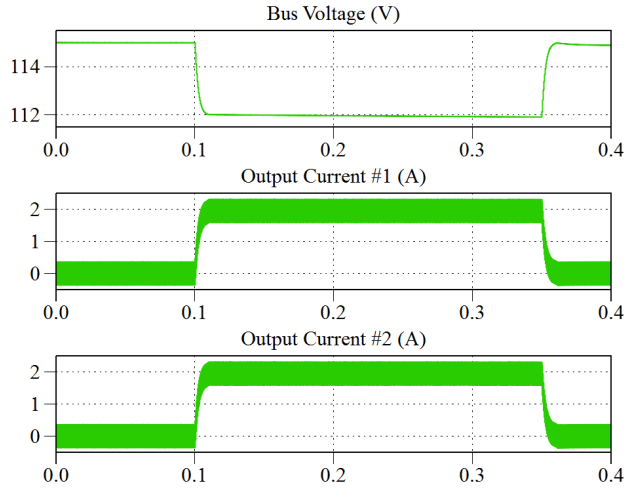

(b) Simulation results of load changing with proposed virtual inertia control

Fig. 6. Simulation results of load changing with and without proposed virtual inertia control.

TABLE II. PARAMETERS OF SIMULATED STUDY CASE

Description of the Parameter	*Symbol*	*Value*
Global No-load Voltage Reference	V_{ref}	115 V
Source Voltage	E_1, E_2	230 V, 230 V
Inductance of Buck Converters	L_1, L_2	8 mH, 8 mH
Stary Resistance of inductors,	r_1, r_2	0.1 Ω, 0.1 Ω
Switching Frequency	f_{sw}	10 kHz
Virtual Resistances for Droop Control	R_{v1}, R_{v2}	1.5 Ω, 1.5 Ω
Total Capacitance in DC Bus	C	3.3 mF
Proportion Term of Current Controller	K_{pc1}, K_{pc2}	0.02, 0.02
Integral Term of Current Controller	K_{ic1}, K_{ic2}	0.1, 0.1
Resistive Load	R_{Load}	28.75 Ω

The simulation results show that with proposed virtual inertia control, the dynamic response of DC bus voltage will have reduced overshoot and smoother transient when load changing occurs in the system.

V. EXPERIMENTAL VALIDATION OF PROPOSED METHOD

In order to verify the proposed virtual inertia control methods, especially its performance under noised real-world DC MGs, experiments are also carried out using a LVDC MG setup with four DC/DC converters. The parameters of the

TABLE I. PARAMETERS OF EXPERIMENTAL TESTBED

Description of the Parameter	*Symbol*	*Value*
Global No-load Voltage Reference	V_{ref}	120 V
Source Voltage	E_i	240 V, 240 V
Inductance of Buck Converters	L_i	8.6 mH, 8.6 mH
Stary Resistance of inductors,	r_i	0.1 Ω, 0.1 Ω
Switching Frequency	f_{sw}	10 kHz
Virtual Resistances for Droop Control	R_{vi}	4 Ω, 4 Ω
Virtual Capacitance for Virtual Inertia	C_{vi}	2mF
Total Capacitance in DC Bus	C	3.3 mF
Proportion Term of Current Controller	K_{pci}	0.02, 0.02
Integral Term of Current Controller	K_{ici}	0.1, 0.1
Resistive Load	R_{Load}	17 Ω

LVDC MG setup are shown in Table II. The real-time control and data acquisition are done by dSpace RTI 1006 platform. The experimental results are shown in Fig. 7 and Fig. 8.

By comparing the experimental results shown in Fig. 7 and Fig. 8, it can be found that the inertial behavior of the system is strengthened after adopting proposed virtual inertia control method. It is performed by the improved bus voltage transient,

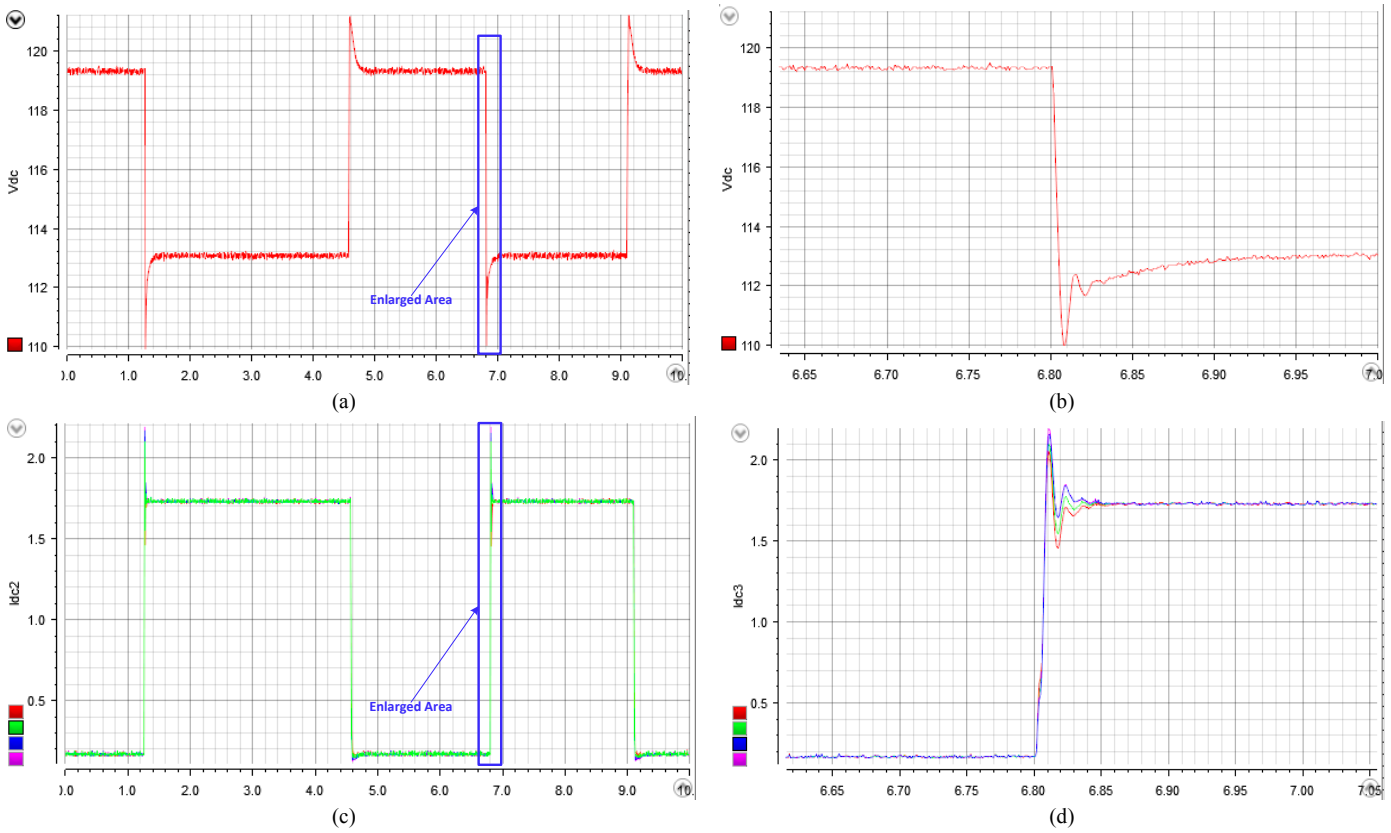

Fig. 7. Experimental results of load changing with basic admittance-type droop (without proposed virtual inertia control design) : (a) DC bus voltage response; (b) Transient response of DC bus voltage; (c) Output currents of converters; (d) transient response of output currrent.

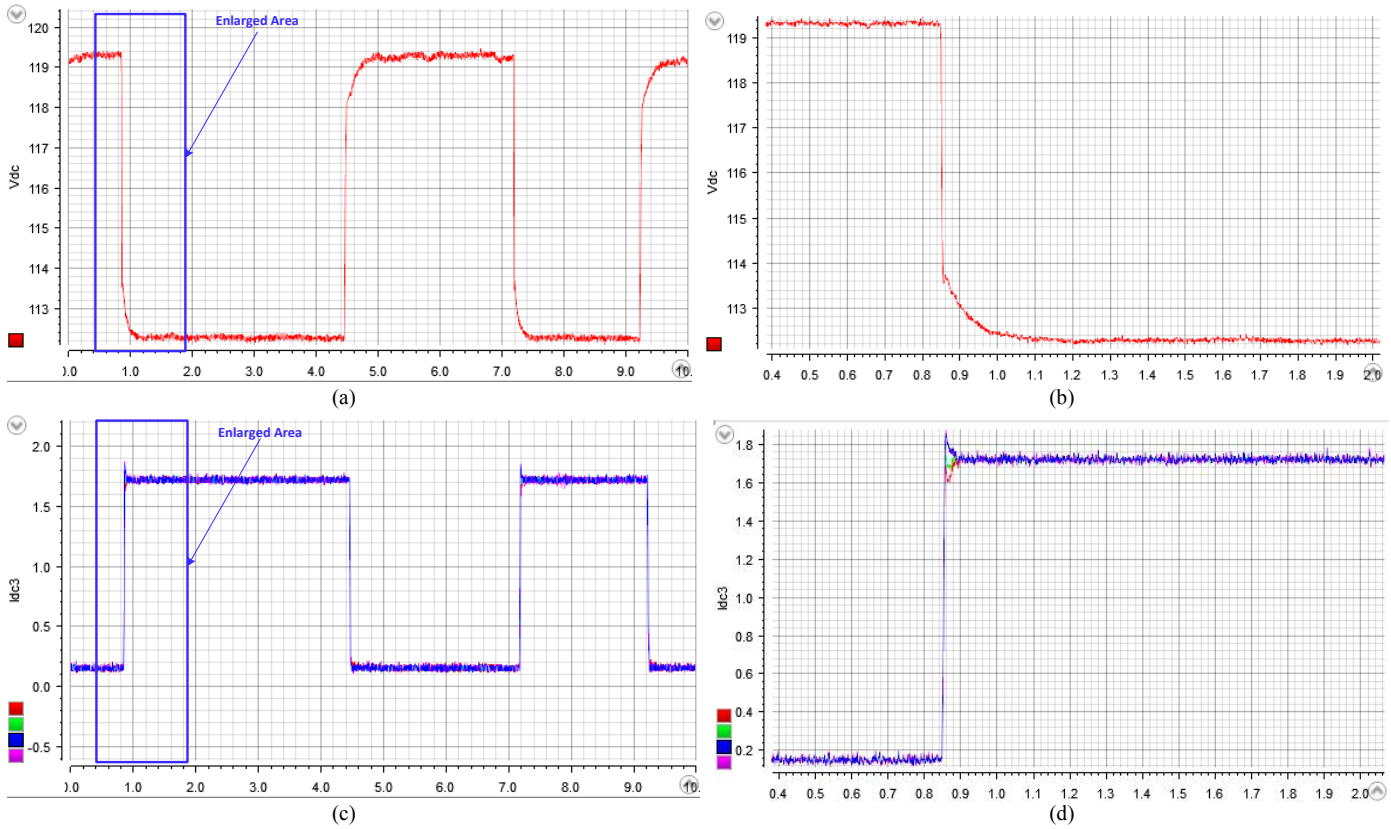

Fig. 8. Experimental results with proposed virtual inertia control realized by admittance-type droop method (R_v=4Ω, C_v=2mF): (a) DC bus voltage response; (b) Transient response of DC bus voltage; (c) Output currents of converters; (d) transient response of output currents.

significantly reduced overshoots, faster response of output voltage, and the increased time constant of the system when load increases. It is also noteworthy that the proper power sharing effect of droop control is not affected by the proposed virtual inertia control.

The experimental results show that with proposed virtual inertia control method, the inertia of the entire DC MG can be improved, and thus being able to mitigate the low-inertia issue of DC MG.

VI. Conclusion

In this paper, an admittance-type RC-mode droop control method is proposed to introduce virtual inertia into DC MGs. The inertia issue and the mechanism of virtual inertia in DC MGs are analyzed. A comparative study is carried out to address the impact of using different realization methods of droop control, especially considering complex design of the virtual impedance/admittance. The analytical results indicate that admittance-type realization method has advantages when achieving proposed virtual inertia control. Based on the analytical results, simulations and experiments are carried out to validate the proposed control methods. The results show effective improvement in the system-level inertial behavior and transient response. Meanwhile, the desired proportional power sharing effect of droop control is not affected. To the author's knowledge, with enhanced system inertia, DC MG will have (1) improved stability margin when feeding constant power loads; (2) enhanced 'Plug & Play' capability and better scalability.

References

[1] B. T. Patterson, "DC, Come Home: DC Microgrids and the Birth of the "Enernet"," in *IEEE Power and Energy Magazine*, vol. 10, no. 6, pp. 60-69, Nov.-Dec. 2012.

[2] M. Liserre, T. Sauter, and, Y. Hung John, "Future energy systems Integrating renewable energy sources into the smart power grid through industrial electronics," *IEEE Ind. Electron. Mag.*, vol. 4, no. 1, pp. 18-37, Mar. 2010.

[3] X. Lu, K. Sun, J. M. Guerrero, J. C. Vasquez, L. Huang, and J. Wang, "Stability Enhancement Based on Virtual Impedance for DC Microgrids With Constant Power Loads," *IEEE Trans. Smart Grid*, vol. 6, no. 6, pp. 2770-2783, Aug. 2015.

[4] H. P. Beck and R. Hesse, "Virtual synchronous machine," *2007 9th International Conference on Electrical Power Quality and Utilisation*, Barcelona, 2007, pp. 1-6.

[5] J. M. Guerrero, J. C. Vasquez, J. Matas, L. G. De Vicuña, and M. Castilla, "Hierarchical control of droop-controlled AC and DC microgrids - A general approach toward standardization," *IEEE Trans. Ind. Electron.*, vol. 58, no. 1, pp. 158–172, 2011.

[6] F. Gao *et al*., "Comparative Stability Analysis of Droop Control Approaches in Voltage-Source-Converter-Based DC Microgrids," in *IEEE Transactions on Power Electronics*, vol. 32, no. 3, pp. 2395-2415, March 2017.

[7] Z. Jin, L. Meng, J. M. Guerrero. "Comparative Admittance-based Analysis for Different Droop Control Approaches in DC Microgrids," *Proceedings of 2nd International Conference on DC Microgrids, IEEE, 2017,* pp1-6.

ISSN (online): 2446-1636
ISBN (online): 978-87-7210-322-8

AALBORG UNIVERSITY PRESS